Pisias, N.G., Mayer, L.A., Janecek, T.R., Palmer-Julson, A., and van Andel, T.H. (Eds.), 1995
Proceedings of the Ocean Drilling Program, Scientific Results, Vol. 138

6. A NEW LATE NEOGENE TIME SCALE: APPLICATION TO LEG 138 SITES[1]

N.J. Shackleton,[2] S. Crowhurst,[2] T. Hagelberg,[3] N.G. Pisias,[3] and D.A. Schneider[4]

ABSTRACT

The sediments recovered during Leg 138 provide a remarkable opportunity to improve the geological time scale of the late Neogene. We have developed new time scales in the following steps. First, we constructed age models on the basis of shipboard magnetostratigraphy and biostratigraphy, using the time scale of Berggren, Kent, and Flynn (1985). Second, we refined these age models using shipboard GRAPE density measurements to provide more accurate correlation points. Third, we calibrated a time scale for the past 6 m.y. by matching the high-frequency GRAPE density variations to the orbital insolation record of Berger and Loutre (1991); we also took into account $\delta^{18}O$ records, where they were available. Fourth, we generated a new seafloor anomaly time scale using our astronomical calibration of C3A.n (t) at 5.875 Ma and an age of 9.639 Ma for C5n.1n (t) that is based on a new radiometric calibration (Baksi, 1992). Fifth, we recalibrated the records older than 6 Ma to this new scale. Finally, we reconsidered the 6- to 10-Ma interval and found that this could also be partially tuned astronomically.

INTRODUCTION

In geology, the phrase "time scale" denotes the formal framework that is used to assign ages to geological deposits or to events in the geological record. It is often hard for a nongeologist to appreciate either the importance of the development of geological time scales or the difficulties that arise in generating and applying them. In this chapter, we focus on three types of "time scale." First, we have a time scale for variations in the geometry of the Earth-sun orbital system. We have used that published by Berger and Loutre (1991). Berger (1988) reviewed the history of studies of the Milankovitch theory in relation to climate in the geological past, and Berger and Loutre (1992) reviewed the accuracy of recent computations. Second, we generate a time scale for variations in sediment density (reflecting changes in the ratio of opal to calcite) that is based primarily on Sites 849, 850, and 851, with records from Sites 846 and 847 providing important information; this time scale will probably be applicable to a large area of the equatorial Pacific Ocean. Third, we use this to recalibrate a section of the magnetic polarity time scale that is used globally to assign ages to rock sequences for recording an identified sequence of magnetic field reversals.

In another chapter (Shackleton et al., this volume), we use the time scale of this study to calibrate part of the oxygen isotope time scale (Shackleton and Opdyke, 1973; Imbrie et al., 1984). Finally, we apply our new time scale to the extensive series of biostratigraphic datums, determined by our colleagues, to refine the Neogene biostratigraphic time scale (Shackleton et al., biostratigraphic summary, this volume). The results of major synthetic studies on the geological time scale (Berggren, Kent, and Flynn [1985] and Berggren, Kent, and Van Couvering [1985]; Harland et al. [1990]) are usually presented in terms of age calibration of chronostratigraphic boundaries defined in stratotype sections. The geological literature is muddled by the fact that the word "age" has a specialized meaning: "*sensu stricto* the chronostratic division of rank between epoch and chron. . ." (quoted from the glossary in Harland, 1978) that we do not make use of here. In this chapter, we are concerned with the numerical ages expressed in an astronomical unit (years) and calibrated through slower astronomical cycles.

The first statistically convincing demonstration that the imprint of variations in Earth's orbital geometry can be detected in deep-sea sediment records of climatic variability was that of Hays et al. (1976). The major advance that led to this work was the application of a reliable initial time scale through the simultaneous application of magnetostratigraphy and oxygen isotope stratigraphy in equatorial Pacific Ocean Core V28-238 (Shackleton and Opdyke, 1973), and indeed, preliminary spectral analysis indicated that the validation of the Milankovitch hypothesis was imminent. The advantage of the cores examined by Hays et al. (1976) was the relatively high sedimentation rate of about 4 cm/k.y., which ensured that the evidence for precession could be detected. By contrast, Core V28-238, having a sedimentation rate of less than 2 cm/k.y., barely preserves a precession signal.

Imbrie et al. (1984) published a time scale for the past 800 k.y. on the basis of a stack of oxygen isotope records from a number of cores. The major part of this calibration has held up to subsequent scrutiny, but the lowest part, which was dependent on two cores having low sedimentation rates, has undergone major revision (Shackleton et al., 1990; henceforth, SBP90). This revision was only possible because the Ocean Drilling Program (ODP) visited DSDP Site 504 again and resampled it as Site 677 using the advanced piston corer (APC). Site 677 has a consistent sedimentation rate of about 4 cm/k.y. There is little doubt that sedimentation rate is the chief limitation on the reliable detection of orbital signals in deep-sea sequences. Leg 138 was planned so as to core a number of sites in the high productivity area of the eastern equatorial Pacific Ocean, where scientists already knew that high sedimentation rates could be anticipated, and where pervasive evidence of lithological cyclicity was also known (van Andel et al., 1975). Thus, an excellent opportunity was presented for extending the astronomical time scale.

PAST RESEARCH

The first steps toward astronomical calibration of the pre-Brunhes time scale were those of Pisias and Moore (1981), who had access to only relatively low-resolution data from a piston core. A major advance was made by Ruddiman et al. (1986) and Raymo et al. (1989), while working on DSDP Site 607 in the North Atlantic Ocean. These scientists showed that a long interval, now known to extend at least to 3 Ma, existed during which climatic variability was concentrated at the frequency of changes in obliquity (period 41 k.y.). Making only minor adjustments to the time scale based on linear interpolation between observed magnetic reversals, and using published ages for the last few reversals of Earth's magnetic field, these researchers developed a time scale that extended to about 2.4 Ma. This major

[1] Pisias, N.G., Mayer, L.A., Janecek, T.R., Palmer-Julson, A., and van Andel, T.H. (Eds.), 1995. *Proc. ODP, Sci. Results,* 138: College Station, TX (Ocean Drilling Program).
[2] University of Cambridge, Godwin Laboratory, Free School Lane, Cambridge, CB2 3RS, United Kingdom.
[3] College of Oceanography, Oregon State University, Corvallis, OR 87331, U.S.A.
[4] Woods Hole Oceanographic Institution, Woods Hole, MA 02543, U.S.A.

achievement was possible because of the careful work that had been done to develop a complete and continuous section for Site 607 (Ruddiman, Kidd, Thomas, et al., 1987) and by the large amount of laboratory work that had been invested in that site.

Both Hilgen (1991a, henceforth H91) and SBP90 found evidence that this pioneering work, in fact, had led to incorrect conclusions. Hilgen's work was focused on the sequence of sapropels preserved in Pliocene rocks in southern Italy; he obtained an astronomically calibrated age for the Matuyama/Gauss boundary on the basis of matching these sequences with the astronomical eccentricity and precession signals. Soon after, Hilgen (1991b, henceforth H91) extended his calibration to the base of the Pliocene and gave ages for magnetic reversals back to Thvera Subchron (H91). SBP90 worked on planktonic and benthic $\delta^{18}O$ records from ODP Site 677 in the eastern equatorial Pacific Ocean, covering the past 2.6 m.y. These workers identified three points where Ruddiman et al. (1986) had interpreted as a single obliquity cycle a section of record that actually spanned two obliquity cycles. Other researchers subsequently have confirmed this interpretation by examining GRAPE density records from the Atlantic (Herbert et al., 1992) and through a new high-resolution $\delta^{18}O$ record from the Indian Ocean (Bassinot, pers. comm., 1992). Since that time, a number of scientists have provided new estimates of the age of the last few magnetic reversals (largely based on high precision $^{40}Ar/^{39}Ar$ dating) that support the new calibrations. For the Brunhes/Matuyama boundary, Izett and Obradovich (1991), Tauxe et al. (1992), Spell and McDougall (1992), Baksi et al. (1992), and Hall and Farrell (1993) all obtained ages supporting the new astronomically calibrated age of 0.78 Ma. For the Jaramillo Subchron, Glass et al. (1991), Spell and McDougall (1992), and Tauxe et al. (1992) found support for the new age (although Obradovich and Izett [1992] obtained values nearer the conventional age). Obradovich and Izett (1992) obtained age estimates for Cobb Mountain and for the base of the Olduvai to support the astronomical calibration. Walter et al. (1991) also obtained an age within the Olduvai Subchron at Olduvai Gorge to support the astronomical calibration of the base of the normal subchron. Walter et al. (1992) obtained ages in the Gauss that support the new calibration, and McDougall et al. (1992) showed that age determinations in the Gilbert (that had previously appeared anomalous), in fact, were in good agreement with the H91 time scale for the early Pliocene. Finally, Wilson (1993) demonstrated that if seafloor spreading rates are examined with high precision, they prove to be less variable when estimated using the astronomical time scale than when using other published time scales.

MAGNETOSTRATIGRAPHY OF LEG 138 SITES

The time scale used during Leg 138 was based on the version of the seafloor spreading magnetic anomaly time scale derived by Berggren, Kent, and Flynn (1985). In turn, this represented a new age calibration of the anomaly sequence created by LaBrecque et al. (1977), which was based on the classic South Atlantic profile of Heirtzler et al. (1968). Berggren, Kent, and Flynn (1985) used as age control points eight anomalies having ages that range from 3.40 to 84.0 m.y.; they assumed linear spreading on their profile between these controls. Recently, Cande and Kent (1992) (henceforth CK92) introduced three significant modifications to this time scale. First, they generated a more reliable baseline anomaly sequence by re-evaluating a suite of South Atlantic profiles, instead of relying on the single profile of Heirtzler et al. (1968). Second, they restacked high-resolution profiles from other areas onto this improved South Atlantic sequence. Third, they used a cubic-spline, instead of a linear interpolation, to estimate the ages of anomalies between their calibration points; this is important from a geophysical standpoint, because it avoids introducing artificial instantaneous plate accelerations at the control point ages. CK92 also documented some additional reversals that were not included in the scheme of LaBrecque et al. (1977). Finally, CK92 introduced a minor improvement to the nomenclature, which we use in this chapter, alongside the familiar Pliocene–Pleistocene terminology. We have used the standard South Atlantic Ocean profile of CK92 as our guide to the relative spatial and temporal spacing of reversals during the Neogene.

Among the 11 sites drilled during Leg 138, eight (844, 845, 848, 850, 851, 852, 853, and 854) provided segments of useful magnetostratigraphy. Taken together, these provide a complete coverage of the polarity transitions of the last 13 m.y. since C5AB.n (t). For the purpose of calibration, reversals located in sediments having a higher sedimentation rate are more valuable. In this sense, Site 851 is particularly valuable for events between the present and C3n.1n (the Cochiti Subchron). Site 852 preserves a good record to the top of C5.2n, except for the interval between C3A.n1 and C4A.n1, where we rely on Site 853. Site 848 also preserves a record to the base of C5r.1n. For the oldest part of the record, we rely primarily on Site 845, which extends to C5AB.n (t). The depths of the reversals in each site are given in the appropriate site chapter, with a few exceptions. Schneider (this volume) has reinterpreted the data for Core 138-844C-6H; we have accepted this new version. Schneider (this volume) has also improved the data from Site 845 by analyzing discrete samples. Again, we have used this revised data set. We accept the Gauss/Gilbert boundary in Hole 850B (plotted in error, p. 841, Fig. 22 of Mayer, Pisias, Janecek, et al., 1992). Data for Hole 851D are provided by Meynadier et al. (this volume).

BIOSTRATIGRAPHY

Remarkably high resolution was achieved in the shipboard biostratigraphy for all the major microfossil groups. Initially, age models were developed on the basis of the compilation given in the "Explanatory Notes" chapter (Shipboard Scientific Party, 1992). A small number of datum levels were redated (within the framework of the Berggren, Kent, and Flynn [1985] time scale) on the basis of the excellent magnetostratigraphy in Sites 844 and 845. This more-or-less self-consistent set of datum levels provided the basis for the age models developed in the site chapters and in Shackleton et al. (1992).

The objective of this chapter is to develop a more accurate time scale than has hitherto been available, by using the obvious cyclic character of the GRAPE density records as a monitor of the response of the fertile equatorial circulation system to forcing by variations in Earth's orbital geometry. The gamma-ray attenuation porosity evaluator (GRAPE) density tool is used aboard *JOIDES Resolution* to obtain automatic high-resolution records of sediment density; these data are discussed in Hagelberg et al. (this volume). In this region, sediment density varies with carbonate content, which in turn is closely linked to surface productivity. Since it was obvious at an early stage that this study would entail significant changes to the time scale used aboard *JOIDES Resolution*, biostratigraphic datum levels were used mainly to maintain the stratigraphic correlation between sites as the "tuning" was performed. Procedurally, this was done by recalculating the age for each datum level as the ages of the magnetostratigraphic boundaries were estimated again. Subsequently (Shackleton et al., this volume), we created a new set of best estimates for the ages of all useful biostratigraphic datums, based on the combined evidence of all the Leg 138 sites. Here, it is appropriate to remark that published estimates for a good proportion of the datums used were based on sparse data. This means that it is difficult to evaluate an age model for many of the sites because of apparent conflicts among age estimates suggested by data from different fossil groups. Ultimately, the most rigorous test of our age models will come, on the one hand, from the statistical evaluation of the patterns of density variability that they predict (Hagelberg et al., this volume) and, on the other, from further radiometric dating of the magnetic reversal sequence.

OXYGEN ISOTOPE STRATIGRAPHY

To maintain internal consistency in this study, we have attempted to develop a time scale that is based almost entirely on characteristic events in the GRAPE density records. We have not directly used the standard $\delta^{18}O$ chronology in the upper part. As these data emerged, we have had access to the benthic $\delta^{18}O$ records of Sites 846 and 849 (Mix et al., this volume) and to the planktonic $\delta^{18}O$ records of Sites 847 (Farrell et al., this volume) and 851 (Ravelo et al., this volume) for the Pleistocene, as well as to the benthic $\delta^{18}O$ record of Site 846 (Shackleton et al., this volume) for the Pliocene. Our aim has been to generate a GRAPE-based time scale for the Pleistocene that would not be in conflict with a $\delta^{18}O$-based time scale, where that is available. Thus, we have used as control points features that are visible in the GRAPE density records. Initially, we utilized the same procedure throughout, correlating GRAPE density maxima to insolation maxima and GRAPE density minima to insolation minima. However, Farrell et al. (this volume) show that in the Pleistocene section of Site 847, age differences between our time scale based on GRAPE density and one based on $\delta^{18}O$ stratigraphy do arise, although they seldom exceed a few thousand years. Thus, we have in addition developed modified time scales for the past million years in which the ages for GRAPE density events have been shifted away from the ages of insolation maxima and minima to generate time scales that are closer to those suggested by the $\delta^{18}O$ data.

In Tables 1 to 11, we present age models that are probably close to a true $\delta^{18}O$ time scale through the past million years; we also present (Table 12) the alternative age models for the upper part that were developed independent of the $\delta^{18}O$ data. These may be regarded as viable alternative age models. Although age models based solely on GRAPE density might be expected to be less reliable than those based on $\delta^{18}O$ stratigraphy, one cannot assume that the current $\delta^{18}O$ time scale is perfect in every detail.

Table 1. Age model for Site 844.

Age (Ma)	Depth (mcd)	Age (Ma)	Depth (mcd)
0.000	0.00	4.981	29.90
0.088	0.58	5.232	31.30
0.127	1.48	5.875	35.10
0.140	1.63	6.122	36.85
0.174	2.07	6.256	37.85
0.184	2.35	6.554	38.70
0.247	3.27	6.919	41.00
0.354	4.39	7.072	41.80
0.479	6.43	7.406	43.15
0.509	6.78	7.533	44.40
0.579	7.76	7.618	44.95
0.614	8.43	8.027	49.95
0.628	8.50	8.631	53.72
0.659	8.80	8.945	56.75
0.717	9.31	9.142	58.00
0.737	9.60	9.218	58.90
0.783	10.09	9.482	60.60
0.990	11.83	9.543	61.95
1.070	12.63	9.639	62.40
1.770	18.10	10.022	67.13
1.950	19.15	10.548	73.01
2.600	22.20	10.693	75.27
3.053	23.75	10.991	81.74
3.131	23.95	11.373	93.65
3.224	24.40	11.988	116.77
3.337	24.50	12.636	134.68
3.611	25.45	12.929	148.04
4.192	26.95	13.252	160.48
4.322	27.40	14.070	189.45
4.478	27.90	14.950	219.98
4.604	28.40	15.830	258.05
4.784	29.05	17.060	308.30
4.878	29.35		

Table 2. Age model for Site 845.

Age (Ma)	Depth (mcd)	Age (Ma)	Depth (mcd)
0.000	0.00	8.205	120.82
0.410	12.32	8.631	129.71
1.961	43.03	8.945	136.74
3.053	53.88	9.142	140.01
3.131	54.98	9.218	141.43
3.224	55.98	9.482	145.08
3.337	57.38	9.543	146.70
3.611	59.88	9.639	147.74
4.192	65.56	9.775	150.34
4.322	66.62	9.815	150.78
4.478	68.51	10.839	164.94
4.604	69.76	10.943	166.03
4.784	71.59	10.991	166.78
4.878	72.04	11.373	174.17
4.981	73.29	11.428	175.78
5.232	75.97	11.841	183.65
5.875	87.49	11.988	187.06
6.122	90.22	12.605	204.91
6.256	93.00	12.637	206.26
6.555	96.31	12.705	208.13
6.919	101.44	12.752	209.57
7.072	103.18	12.929	215.54
7.406	108.04	13.083	220.07
7.533	110.12	13.252	226.07
7.618	111.02	15.830	275.23
8.027	119.29	16.450	309.10
8.174	120.53		

TUNING METHODS

It was a strength of the investigation by Hays et al. (1976) that they were able to document variance in the bandwidth of each of the three orbital variables (eccentricity, obliquity, and precession) in three independent paleoclimate proxies ($\delta^{18}O$, radiolarian-based sea-surface temperature, and percentage *Cycladophora davisiana*) using an age model for their cores that was entirely independently generated. In general, this is difficult to achieve, especially in a situation such as the eastern equatorial Pacific Ocean, where sedimentation rate clearly varies with climate, perhaps over a wide range. Thus, we have not attempted to demonstrate independently for each segment of time in each site that a statistical likelihood exists for the variability observed to be associated with orbital forcing. However, spectra on untuned sections of GRAPE density record consistently suggest concentration of power at orbital frequencies.

In a similar manner, Imbrie et al. (1984) did not attempt to demonstrate in advance that each of the records they used in their compilation contained the orbital imprint. Instead, they reasoned that the time scale that they generated gave rise to a sufficiently high coherency between $\delta^{18}O$ and orbital insolation that the time scale was probably largely correct. Procedurally, Imbrie et al. (1984) used a strategy based on digital filters. To do this, one must develop an initial time scale, filter one orbital bandwidth (for example, obliquity), and note such small changes in the age model as may be needed to maintain a constant phase relationship between the filtered signal and the calculated obliquity record. The disadvantage of the method is that it is difficult to apply if sedimentation rates are extremely variable. In the case of the Leg 138 sites, it was already clear that this is so (Shackleton et al., 1992). For this reason, we chose to work entirely in the time domain, comparing GRAPE density with a target record derived from the orbital data.

This was also the strategy used by SBP90 for Site 677 (indeed the same strategy also had its place in the study of Imbrie et al. [1984] as considerable uncertainty regarding the appropriate "first guess" chronology existed when that work started). However, in the case of the work on Site 677, a reasonable tuning target already existed; SBP90 used the simple ice sheet model of Imbrie and Imbrie (1980) to produce a target record that embodied the same time constants relating ice volume and summer insolation at 65°N that have been documented for the late Pleistocene. In the case of GRAPE density (or the underlying variable, the ratio of calcite to biogenic opal), we do not have a model linking the forcing and the response. Therefore, we have simply used the calculated record of summer insolation at 65°N as the tuning target. We have throughout assumed that no phase lag existed between insolation and GRAPE density and that high density (high percentage of $CaCO_3$) is associated with high Northern Hemisphere summer insolation. This phase relationship may be approximately valid for the most recent past; in the Pacific Ocean, a low percentage

Table 3. Age Model for Site 846.

Age (Ma)	Depth (mcd)	Age (Ma)	Depth (mcd)	Age (Ma)	Depth (mcd)	Age (Ma)	Depth (mcd)
0.000	0.00	2.023	74.88	4.154	161.02	6.404	262.79
0.039	1.80	2.086	79.00	4.182	161.78	6.423	263.59
0.088	3.70	2.097	79.50	4.204	162.34	6.443	263.91
0.127	5.96	2.118	80.06	4.225	163.00	6.501	265.35
0.148	6.76	2.140	80.74	4.246	163.60	6.535	266.61
0.171	7.38	2.190	82.60	4.272	164.74	6.540	266.73
0.184	7.94	2.211	83.88	4.296	165.50	7.080	280.34
0.220	8.76	2.233	84.54	4.319	166.04	7.090	281.16
0.240	9.60	2.255	85.56	4.339	167.08	7.117	282.60
0.247	9.94	2.278	86.48	4.361	167.74	7.163	284.86
0.278	11.04	2.305	87.48	4.412	169.66	7.204	286.98
0.290	11.26	2.348	89.26	4.451	170.88	7.225	287.75
0.310	11.84	2.377	90.16	4.491	172.02	7.315	290.05
0.326	12.36	2.411	91.62	4.537	174.22	7.370	292.70
0.333	12.66	2.422	92.22	4.562	175.26	7.404	294.54
0.354	13.44	2.438	92.64	4.595	177.24	7.474	296.84
0.388	15.04	2.477	94.94	4.629	179.20	7.496	297.34
0.405	15.70	2.490	95.54	4.653	180.12	7.740	301.84
0.422	16.26	2.521	96.52	4.676	181.26	7.878	304.84
0.446	17.06	2.534	97.68	4.698	182.82	7.921	305.74
0.479	18.78	2.547	98.78	4.722	183.78	7.946	306.39
0.509	19.90	2.569	99.56	4.744	184.96	8.013	307.49
0.515	20.14	2.592	100.36	4.770	186.64	8.080	308.74
0.523	20.38	2.637	102.43	4.812	187.88	8.301	310.54
0.544	20.96	2.683	104.43	4.866	190.14	8.312	310.79
0.579	22.12	2.707	105.37	4.896	191.40	8.322	311.19
0.614	22.88	2.741	107.27	4.919	192.38	8.373	312.24
0.628	23.38	2.754	108.27	4.940	193.46	8.414	312.94
0.659	24.42	2.776	109.39	4.984	194.64	8.434	313.29
0.681	25.38	2.798	110.13	5.011	195.26	8.470	313.79
0.692	25.72	2.835	111.61	5.033	195.73	8.547	314.59
0.717	26.26	2.853	112.53	5.077	196.87	8.639	315.69
0.737	26.92	2.876	113.63	5.101	197.41	8.682	316.29
0.772	28.16	2.904	115.21	5.127	198.31	8.732	317.59
0.783	28.74	2.926	115.83	5.148	199.41	8.776	318.29
0.863	32.18	2.949	117.61	5.170	200.77	8.786	318.49
0.884	33.26	2.994	119.57	5.224	202.53	8.833	318.64
0.908	34.34	3.042	121.71	5.264	204.65	8.926	320.94
0.936	35.14	3.063	122.55	5.300	206.79	8.990	322.65
0.978	35.98	3.085	123.81	5.342	208.41	9.084	324.30
0.999	36.56	3.135	125.49	5.392	210.07	9.133	325.10
1.029	37.46	3.156	126.37	5.414	211.71	9.155	325.40
1.050	37.92	3.177	127.05	5.435	212.57	9.199	326.60
1.092	39.80	3.198	127.75	5.457	213.43	9.291	328.05
1.114	40.80	3.231	128.49	5.507	215.83	9.420	330.15
1.136	42.12	3.288	129.91	5.528	216.57	9.465	330.65
1.215	44.68	3.328	131.39	5.549	217.97	9.489	331.05
1.243	45.14	3.371	133.51	5.569	218.93	9.511	331.40
1.317	47.12	3.401	134.51	5.587	220.21	9.535	331.75
1.337	47.74	3.422	135.51	5.624	223.25	9.557	332.10
1.358	48.86	3.464	138.05	5.643	224.15	9.626	333.00
1.379	49.54	3.496	139.13	5.661	225.05	9.662	333.40
1.400	50.64	3.516	139.59	5.680	226.03	9.704	333.85
1.431	52.14	3.526	140.01	5.700	226.89	9.735	334.45
1.473	53.06	3.578	142.99	5.721	227.23	9.754	334.70
1.493	53.58	3.614	144.03	5.752	229.01	9.798	335.40
1.513	54.58	3.654	145.27	5.772	230.79	9.822	335.90
1.528	54.92	3.680	145.79	5.794	232.05	9.847	336.25
1.547	55.22	3.709	146.69	5.815	235.61	9.892	336.74
1.567	55.80	3.730	147.51	5.864	237.49	9.913	336.99
1.606	57.24	3.751	147.99	5.887	238.31	9.985	338.29
1.645	58.28	3.781	148.93	5.981	242.07	10.372	343.29
1.664	59.18	3.802	149.48	6.060	247.42	10.693	346.54
1.697	60.96	3.824	150.14	6.099	249.76	10.987	353.39
1.708	61.72	3.867	151.32	6.174	252.88	11.212	357.04
1.782	64.02	3.918	152.70	6.215	253.38	11.377	359.94
1.832	65.88	3.960	154.30	6.267	255.14	13.326	394.97
1.875	67.72	4.014	156.88	6.289	255.50	13.480	400.00
1.926	70.24	4.034	157.46	6.309	255.92	15.835	423.80
1.947	71.20	4.089	159.02	6.330	258.80	18.067	460.00
1.968	72.36	4.110	159.52	6.349	260.12		
1.986	73.62	4.131	160.22	6.383	262.35		

of $CaCO_3$ is associated with interglacial-to-glacial transitions and good carbonate preservation with glacial-to-interglacial transitions (e.g., Ninkovich and Shackleton, 1975; Keir and Berger, 1985; Le and Shackleton, 1992). Whether this phase relationship is appropriate to the equatorial high productivity belt in the eastern Pacific Ocean, and whether the same phase relationship is appropriate for the older part of the record, is not yet known. Although the uncertain phase contributes a significant source of potential error in our time scale, it only entails, at a maximum, a few thousand years of systematic error in the uncertainty of the age estimates.

Table 4. Age model for Site 847.

Age (Ma)	Depth (mcd)	Age (Ma)	Depth (mcd)	Age (Ma)	Depth (mcd)
0.000	0.00	2.211	73.33	4.110	129.10
0.039	1.79	2.233	74.03	4.131	129.54
0.088	3.01	2.255	74.99	4.154	130.14
0.116	3.81	2.278	75.51	4.182	130.70
0.127	4.11	2.305	76.13	4.204	131.28
0.148	4.75	2.348	77.43	4.225	131.94
0.171	5.99	2.390	78.91	4.246	132.52
0.184	6.73	2.422	79.69	4.296	133.82
0.220	7.45	2.438	80.39	4.319	134.40
0.240	8.17	2.477	82.39	4.339	135.42
0.247	8.83	2.521	83.57	4.361	136.00
0.278	9.49	2.547	84.49	4.376	136.80
0.290	9.79	2.569	84.85	4.412	137.76
0.308	10.29	2.592	85.91	4.433	138.02
0.326	10.77	2.614	86.77	4.491	139.88
0.333	11.13	2.637	87.25	4.537	141.86
0.349	11.81	2.683	88.83	4.562	143.44
0.388	13.19	2.707	89.47	4.583	144.26
0.405	13.77	2.729	89.89	4.606	146.68
0.422	14.05	2.754	91.11	4.629	148.70
0.446	14.51	2.776	91.47	4.653	151.60
0.463	15.19	2.786	91.79	4.698	155.60
0.479	15.71	2.798	92.45	4.722	156.70
0.484	16.05	2.835	93.93	4.744	157.30
0.509	16.69	2.876	94.83	4.770	158.70
0.544	17.45	2.904	95.41	4.821	159.90
0.579	18.23	2.926	96.33	4.847	161.80
0.614	19.09	2.937	96.97	4.866	163.50
0.636	19.59	2.949	97.23	4.896	166.20
0.659	20.33	2.969	97.75	4.919	167.20
0.681	21.27	2.994	98.31	4.940	167.80
0.692	21.47	3.019	99.07	4.962	168.30
0.717	22-23	3.030	99.41	4.984	169.00
0.737	22.69	3.041	99.69	5.033	170.80
0.772	23.39	3.063	100.11	5.055	171.30
0.783	24.29	3.085	100.63	5.077	172.50
0.824	25.15	3.111	101.29	5.101	173.80
0.908	28.15	3.135	102.12	5.107	174.10
0.978	29.61	3.156	102.82	5.148	174.50
1.000	30.43	3.177	103.42	5.170	176.60
1.050	31.53	3.198	103.92	5.224	178.30
1.072	32.67	3.231	104.66	5.245	179.30
1.205	37.51	3.252	105.72	5.264	180.20
1.215	38.15	3.271	106.28	5.300	181.70
1.243	39.09	3.288	106.68	5.320	182.60
1.272	39.77	3.308	107.48	5.342	183.70
1.283	40.51	3.328	107.94	5.392	185.30
1.307	41.07	3.348	108.68	5.414	185.90
1.327	41.73	3.359	108.96	5.435	186.90
1.337	42.41	3.391	109.72	5.507	189.50
1.379	43.81	3.401	110.06	5.528	190.30
1.400	44.75	3.422	110.80	5.549	191.10
1.431	45.57	3.443	111.44	5.569	192.20
1.493	47.55	3.464	111.84	5.587	192.80
1.528	48.59	3.496	112.62	5.603	193.80
1.567	49.83	3.516	113.10	5.624	194.60
1.606	50.89	3.578	114.94	5.643	196.20
1.697	53.09	3.604	115.74	5.680	198.50
1.718	55.15	3.633	116.84	5.721	199.30
1.750	55.87	3.654	117.38	5.752	200.10
1.811	57.65	3.689	118.28	5.772	201.50
1.832	58.79	3.720	119.40	5.783	202.00
1.875	61.25	3.750	120.00	5.794	202.20
1.904	61.93	3.824	122.14	5.815	204.10
1.947	63.71	3.867	123.32	5.836	205.20
1.958	64.67	3.896	124.10	5.864	206.00
2.003	66.15	3.918	124.60	5.887	206.70
2.023	66.83	3.939	125.06	5.909	207.50
2.042	68.15	3.960	125.72	5.929	208.90
2.052	68.59	4.014	126.84	6.003	211.00
2.097	70.07	4.034	127.26	6.300	230.21
2.118	70.55	4.055	127.98	6.700	251.01
2.129	70.83	4.072	128.26		
2.140	71.17	4.089	128.62		

Procedurally, the process of tuning the GRAPE density data may be idealized as follows. We must, however, emphasize that in reality a considerable number of iterations exist for each step. The work was performed on three-dimensional LOTUS 1-2-3 spreadsheets. For each site, the starting point was the composite section of continuous GRAPE density record generated by splicing segments of data from among the holes available and shown by Hagelberg et al. (1992; Chapter 5, Fig. 6) and by Shackleton et al. (1992; Chapter 6, Fig. 1).

Table 5. Age model for Site 848.

Age (Ma)	Depth (mcd)	Age (Ma)	Depth (mcd)
0.000	0.00	2.614	31.18
0.039	0.68	2.637	31.34
0.056	1.02	2.695	31.74
0.088	1.44	2.766	32.36
0.127	1.76	2.864	32.90
0.171	2.46	2.892	33.18
0.184	2.64	2.937	33.40
0.247	3.12	2.969	33.60
0.278	3.68	2.994	33.68
0.290	3.80	3.030	33.86
0.326	4.16	3.054	33.92
0.349	4.70	3.231	34.52
0.372	5.20	3.252	34.66
0.388	5.52	3.318	34.96
0.405	5.64	3.359	35.24
0.422	5.96	3.433	35.64
0.446	6.52	3.440	35.70
0.479	7.20	3.475	35.82
0.504	7.64	3.516	35.92
0.526	7.88	3.537	36.02
0.579	8.98	3.578	36.38
0.614	9.30	3.654	36.80
0.628	9.64	3.689	37.00
0.659	10.36	3.730	37.16
0.681	10.80	3.781	37.38
0.717	11.34	3.867	37.64
0.737	11.70	3.918	37.92
0.772	12.20	4.110	38.68
0.783	12.46	4.154	38.84
0.863	13.80	4.204	39.12
0.908	14.86	4.334	39.64
0.925	15.16	4.361	39.84
0.978	15.76	4.491	40.70
0.999	16.02	4.537	41.04
1.061	16.96	4.583	41.48
1.092	17.84	4.606	42.08
1.215	19.66	4.744	44.28
1.272	20.60	4.770	44.80
1.307	21.04	4.821	45.28
1.347	21.48	4.847	45.70
1.379	21.86	4.880	46.20
1.400	22.44	5.004	47.64
1.431	22.88	5.170	49.44
1.493	23.50	5.224	50.40
1.528	23.82	5.342	52.95
1.567	24.28	5.528	56.45
1.606	24.44	5.549	57.15
1.664	24.96	5.680	59.85
1.718	25.52	6.099	65.05
1.750	25.70	6.330	67.65
1.799	26.28	6.575	70.85
1.821	26.50	7.406	81.05
1.875	27.00	7.533	82.00
1.916	27.30	7.618	82.25
1.958	27.50	8.027	84.40
2.003	27.74	8.174	84.70
2.052	28.08	8.631	87.60
2.086	28.42	8.945	89.70
2.097	28.60	9.142	91.00
2.140	28.76	9.218	91.95
2.245	29.20	9.482	94.20
2.293	29.32	9.543	94.60
2.325	29.44	9.639	94.75
2.377	29.82	9.775	95.20
2.411	30.06	9.815	95.40
2.438	30.14	10.839	102.80
2.490	30.44	10.943	103.35
2.500	30.52	10.991	103.65
2.534	30.70	11.270	105.60
2.604	31.08		

For Sites 846 to 852, this was later replaced by the stacked record, generated by Hagelberg et al. (this volume). This stacked record is based on the same depth scale as the original spliced record, with data from all the other holes at the site stacked onto it and averaged to provide a record having a higher signal-to-noise ratio. This GRAPE density record was placed first on a low-resolution time scale. This time scale was based on the age models in Shackleton et al. (1992) modified on the basis of a smooth conversion to the CK92 magnetostratigraphic time scale. The GRAPE density time series then was compared on the same age scale with the orbital insolation record.

Table 6. Age model for Site 849.

Age (Ma)	Depth (mcd)	Age (Ma)	Depth (mcd)	Age (Ma)	Depth (mcd)	Age (Ma)	Depth (mcd)
0.000	0.02	2.521	71.10	4.513	126.32	6.554	261.41
0.039	1.16	2.534	71.72	4.537	127.62	6.575	263.50
0.088	2.76	2.547	71.98	4.562	129.62	6.596	265.60
0.116	3.60	2.569	72.30	4.595	132.42	6.621	271.55
0.127	4.02	2.592	73.04	4.641	135.22	6.647	273.75
0.148	4.74	2.614	73.50	4.653	135.62	6.669	275.25
0.171	5.58	2.637	74.08	4.698	137.52	6.690	275.75
0.184	6.12	2.650	74.54	4.722	140.62	6.711	276.20
0.220	7.22	2.683	74.94	4.744	143.02	6.742	276.95
0.240	8.02	2.707	75.80	4.770	145.12	6.762	277.40
0.247	8.34	2.729	76.44	4.788	145.82	6.784	277.70
0.278	9.00	2.741	76.64	4.812	146.52	6.803	278.25
0.290	9.34	2.754	77.12	4.821	146.92	6.880	280.75
0.308	9.72	2.776	77.98	4.847	147.72	6.912	281.50
0.326	10.10	2.798	78.32	4.866	148.22	6.933	282.00
0.349	11.30	2.823	78.80	4.896	149.02	6.954	283.05
0.388	12.46	2.853	79.58	4.919	149.92	6.976	284.65
0.405	12.98	2.876	80.16	4.940	150.45	6.999	285.30
0.422	13.22	2.904	80.78	4.962	151.40	7.026	285.84
0.446	13.90	2.926	81.38	4.984	152.50	7.070	286.69
0.463	14.34	2.937	81.84	5.011	154.80	7.117	288.64
0.479	14.82	2.949	81.96	5.033	155.60	7.141	290.44
0.526	16.48	2.969	82.50	5.055	156.80	7.163	291.24
0.579	17.50	2.994	83.12	5.077	157.80	7.204	293.64
0.636	18.76	3.019	83.68	5.101	158.60	7.280	295.14
0.681	20.24	3.030	84.16	5.127	160.10	7.315	296.49
0.737	21.92	3.041	84.46	5.148	160.40	7.357	298.34
0.783	23.00	3.063	85.02	5.170	162.00	7.404	300.64
0.805	23.24	3.085	85.58	5.190	162.80	7.449	302.24
0.853	24.56	3.135	86.76	5.224	164.05	7.474	302.99
0.874	25.28	3.156	87.42	5.264	166.60	7.496	303.44
0.908	26.16	3.177	87.96	5.282	167.50	7.623	306.34
0.936	26.86	3.198	88.66	5.300	168.45	7.774	306.39
0.957	27.36	3.252	90.36	5.320	171.85	7.784	306.74
0.978	27.62	3.271	90.88	5.342	174.00	7.807	307.89
0.999	28.26	3.288	91.36	5.392	177.20	7.830	308.44
1.050	29.44	3.298	91.72	5.414	179.45	7.878	309.94
1.072	30.54	3.318	92.14	5.435	180.65	7.928	311.54
1.092	30.92	3.348	92.92	5.457	181.35	7.946	312.29
1.114	31.56	3.359	93.34	5.479	182.75	7.972	312.94
1.136	32.06	3.370	93.62	5.507	183.55	7.993	313.39
1.187	33.20	3.391	93.98	5.528	184.75	8.032	314.09
1.215	33.76	3.401	94.52	5.549	185.70	8.144	316.14
1.263	35.32	3.422	95.00	5.587	188.45	8.164	316.39
1.283	36.20	3.443	95.46	5.603	190.25	8.186	317.09
1.337	37.94	3.464	95.94	5.624	191.45	8.208	318.19
1.369	39.50	3.496	97.12	5.643	193.00	8.235	318.99
1.389	39.90	3.537	98.04	5.661	193.90	8.258	320.34
1.400	40.08	3.567	98.76	5.680	195.45	8.279	320.89
1.431	40.56	3.587	99.66	5.721	197.50	8.301	321.84
1.463	41.28	3.595	99.96	5.752	199.70	8.322	322.79
1.493	41.78	3.614	100.28	5.772	201.75	8.351	324.29
1.528	42.72	3.633	100.78	5.794	204.40	8.434	325.64
1.567	43.82	3.654	101.32	5.815	209.45	8.470	326.64
1.586	44.30	3.689	102.53	5.836	211.10	8.489	326.93
1.606	44.88	3.709	103.05	5.864	214.80	8.508	327.28
1.645	45.62	3.730	103.73	5.887	215.75	8.547	327.93
1.664	46.22	3.751	103.91	5.909	216.45	8.588	328.83
1.697	46.68	3.781	104.81	5.929	216.75	8.600	329.43
1.718	47.88	3.802	105.85	5.951	217.25	8.661	330.23
1.739	48.28	3.824	106.23	5.981	218.05	8.682	330.68
1.760	48.90	3.845	106.95	6.043	223.40	8.732	331.43
1.782	49.24	3.867	107.51	6.060	225.95	8.796	332.73
1.811	50.18	3.896	108.17	6.080	228.15	8.816	333.33
1.832	50.66	3.918	108.75	6.099	229.45	8.926	335.13
1.854	51.54	3.939	109.35	6.121	230.30	8.947	335.48
1.916	53.92	3.960	109.87	6.138	231.05	8.968	335.83
1.947	54.48	4.014	111.39	6.154	232.56	8.990	336.33
1.958	55.38	4.034	111.83	6.174	234.31	9.062	337.88
2.003	57.22	4.055	112.47	6.195	235.11	9.155	339.73
2.023	57.94	4.072	112.85	6.215	237.16	9.199	340.53
2.052	59.24	4.089	113.43	6.239	238.16	9.218	341.28
2.097	60.88	4.110	113.99	6.267	240.06	9.397	344.13
2.129	61.42	4.131	114.49	6.289	240.96	9.465	345.23
2.140	61.82	4.154	115.21	6.309	241.61	9.511	346.08
2.211	63.20	4.204	116.59	6.330	243.06	9.583	347.48
2.233	63.68	4.215	116.99	6.349	243.86	9.682	348.63
2.278	64.72	4.246	117.81	6.383	245.56	9.704	348.98
2.305	65.58	4.272	118.67	6.404	246.21	9.815	350.08
2.325	65.92	4.296	119.39	6.423	247.26	10.548	360.98
2.348	66.56	4.319	120.03	6.443	248.51	10.693	364.33
2.367	66.88	4.339	121.05	6.461	249.71	11.212	379.07
2.388	67.46	4.412	123.25	6.480	250.91	11.420	384.72
2.428	68.44	4.451	124.02	6.501	254.21	11.600	387.42
2.462	69.68	4.491	125.42	6.535	259.21		

Table 7. Age model for Site 850.

Age (Ma)	Depth (mcd)	Age (Ma)	Depth (mcd)	Age (Ma)	Depth (mcd)	Age (Ma)	Depth (mcd)	Age (Ma)	Depth (mcd)
0.000	0.00	2.023	40.09	3.614	75.31	5.643	146.20	8.186	277.70
0.039	0.75	2.052	40.73	3.633	75.71	5.661	146.80	8.188	277.80
0.056	1.03	2.097	41.69	3.654	76.17	5.680	148.10	8.197	277.10
0.088	1.65	2.118	41.97	3.689	76.99	5.700	148.90	8.258	279.60
0.127	2.31	2.129	42.15	3.709	77.49	5.721	150.20	8.301	281.50
0.148	3.21	2.140	42.45	3.730	78.17	5.752	152.00	8.322	282.60
0.171	3.89	2.190	43.29	3.751	78.43	5.762	155.20	8.373	285.40
0.220	4.77	2.201	43.45	3.781	79.05	5.794	158.00	8.434	287.90
0.240	5.11	2.211	43.71	3.802	79.63	5.815	159.30	8.470	289.20
0.247	5.45	2.222	43.93	3.824	80.15	5.836	160.50	8.489	289.80
0.278	5.87	2.233	44.05	3.835	80.49	5.864	161.40	8.508	290.70
0.290	5.99	2.255	44.65	3.855	80.71	5.893	163.10	8.525	291.20
0.308	6.53	2.278	45.09	3.867	81.01	5.909	164.30	8.547	291.80
0.326	6.69	2.305	45.75	3.896	81.59	5.929	165.10	8.567	292.30
0.333	6.95	2.316	46.17	3.918	82.13	5.951	166.50	8.588	293.00
0.349	7.43	2.325	46.45	3.939	82.61	5.981	168.00	8.661	296.00
0.372	7.85	2.336	46.75	3.960	83.15	6.003	170.60	8.682	296.80
0.388	8.33	2.377	48.27	4.034	84.47	6.022	172.20	8.685	296.90
0.405	8.67	2.390	48.59	4.055	84.87	6.023	172.80	8.755	297.40
0.422	8.91	2.411	49.41	4.072	85.15	6.059	175.50	8.776	297.80
0.446	9.41	2.422	49.65	4.089	85.65	6.121	178.70	8.796	298.80
0.463	9.71	2.438	49.89	4.110	86.03	6.174	181.80	8.833	300.30
0.479	10.29	2.477	50.31	4.131	86.39	6.190	182.40	8.851	301.10
0.504	10.51	2.490	50.63	4.154	86.79	6.195	182.50	8.872	302.10
0.526	10.85	2.534	51.29	4.204	87.39	6.215	184.90	8.890	303.40
0.579	11.59	2.558	51.81	4.225	87.41	6.267	188.50	8.926	304.90
0.628	12.53	2.580	52.43	4.246	87.77	6.289	189.40	8.990	306.20
0.659	13.69	2.604	52.91	4.272	88.45	6.309	190.40	9.002	306.70
0.681	14.11	2.625	53.39	4.296	88.93	6.330	191.10	9.031	307.00
0.692	14.31	2.650	53.93	4.319	89.32	6.336	191.30	9.107	310.30
0.717	14.73	2.661	54.21	4.339	90.22	6.373	191.60	9.133	310.80
0.737	15.09	2.683	54.49	4.361	91.32	6.383	192.10	9.155	311.40
0.749	15.37	2.707	55.19	4.412	92.23	6.404	193.10	9.199	312.31
0.772	15.63	2.729	55.47	4.451	93.15	6.501	198.50	9.221	312.91
0.805	16.27	2.754	56.33	4.470	93.54	6.575	210.50	9.251	313.61
0.824	16.61	2.798	57.33	4.490	94.46	6.647	220.91	9.269	314.11
0.863	17.57	2.835	58.05	4.513	94.93	6.690	225.11	9.291	314.81
0.884	17.99	2.853	58.55	4.537	96.06	6.711	226.01	9.305	315.41
0.908	18.51	2.864	58.79	4.562	97.24	6.762	227.11	9.315	315.71
0.978	19.65	2.876	58.95	4.583	97.82	6.803	228.11	9.381	316.71
0.999	19.93	2.926	60.23	4.606	99.97	6.954	233.21	9.397	317.21
1.029	20.53	2.937	60.59	4.629	101.09	6.999	235.11	9.420	318.01
1.050	20.87	2.949	60.79	4.653	102.50	7.026	236.41	9.443	318.71
1.072	21.81	2.969	61.25	4.698	106.10	7.070	237.50	9.465	319.51
1.092	22.19	2.981	61.61	4.744	107.20	7.110	239.40	9.489	320.11
1.136	23.17	2.994	61.73	4.770	108.90	7.120	239.90	9.511	321.01
1.166	23.69	3.019	62.23	4.812	110.30	7.141	240.70	9.535	322.11
1.187	23.97	3.041	62.81	4.866	112.20	7.163	242.00	9.626	324.51
1.205	24.19	3.063	63.05	4.900	114.30	7.204	245.80	9.662	326.21
1.224	24.57	3.085	63.53	5.011	115.30	7.238	246.70	9.677	326.41
1.243	24.91	3.111	64.11	5.055	116.70	7.257	247.60	9.682	326.81
1.263	25.07	3.135	64.65	5.101	118.30	7.280	248.80	9.735	328.01
1.283	25.45	3.156	65.41	5.127	119.70	7.315	250.20	9.777	329.71
1.317	26.29	3.177	66.01	5.159	120.60	7.380	253.00	9.798	330.21
1.337	26.81	3.198	66.25	5.170	121.10	7.404	253.90	9.869	332.21
1.358	27.31	3.214	66.53	5.224	122.60	7.428	255.20	9.963	334.91
1.379	27.55	3.231	66.79	5.264	124.40	7.449	256.20	9.985	335.81
1.400	27.97	3.252	67.23	5.270	124.90	7.474	257.30	10.070	336.01
1.463	29.25	3.262	67.45	5.282	125.30	7.496	258.00	10.270	345.51
1.473	29.37	3.271	67.67	5.300	126.70	7.525	258.90	10.370	345.71
1.493	29.51	3.288	68.01	5.310	128.80	7.645	259.00	10.400	347.01
1.504	29.89	3.328	68.85	5.320	129.10	7.650	259.20	10.490	350.61
1.528	30.37	3.338	69.01	5.342	131.50	7.740	262.40	10.510	351.41
1.547	30.85	3.348	69.15	5.363	133.80	7.763	263.50	10.520	355.31
1.567	31.17	3.359	69.41	5.370	134.20	7.808	265.60	10.693	363.51
1.606	31.91	3.391	69.91	5.410	134.70	7.830	266.30	10.725	364.71
1.697	33.29	3.401	70.13	5.414	134.80	7.855	266.90	10.757	364.91
1.739	34.55	3.422	70.61	5.435	136.30	7.878	268.10	10.843	368.11
1.750	34.73	3.433	71.03	5.457	137.40	7.955	268.20	11.154	382.71
1.811	35.91	3.443	71.15	5.479	138.70	7.955	268.50	11.413	393.51
1.832	36.35	3.464	71.61	5.507	139.80	7.972	269.10	11.547	393.91
1.904	37.73	3.496	72.49	5.549	141.10	7.993	270.40	11.950	407.31
1.916	38.19	3.516	72.87	5.569	142.30	8.032	271.60		
1.958	38.93	3.537	73.29	5.587	143.90	8.069	273.10		
1.986	39.31	3.567	74.19	5.614	144.20	8.090	273.90		
2.003	39.69	3.595	74.89	5.624	144.70	8.144	275.60		

Age control points then were added so as to align prominent groups of density maxima with groups of insolation peaks. We found that sections having about 0.8-m.y. duration were conveniently viewed. Each of the sites containing orbital scale variability over a chosen time interval was first tuned in this fashion independently. Next, records were compared with each other and, if necessary, with other lower-resolution sites containing magnetostratigraphic data. Because aboard the ship we had observed close similarities among the GRAPE density records of sites even when widely separated, we have assumed throughout this exercise that changes in percentage carbonate (as reflected in the GRAPE density records) in reality did occur synchronously over wide areas of the Pacific Basin. Many previous studies have been based successfully on this hypothesis (Arrhenius, 1952; Hays et al., 1969; Vincent, 1981; Farrell and Prell, 1991).

Table 8. Age model for Site 851.

Age (Ma)	Depth (mcd)	Age (Ma)	Depth (mcd)	Age (Ma)	Depth (mcd)	Age (Ma)	Depth (mcd)	Age (Ma)	Depth (mcd)
0.000	0.00	1.916	35.48	3.391	63.80	5.435	111.29	7.541	209.85
0.039	0.82	1.947	35.80	3.401	64.20	5.457	111.81	7.565	210.40
0.065	1.44	1.958	36.14	3.422	64.56	5.479	112.98	7.592	211.85
0.088	1.84	2.003	36.80	3.443	65.16	5.507	114.37	7.611	212.65
0.127	2.48	2.023	37.28	3.464	65.36	5.528	115.07	7.650	214.35
0.148	2.78	2.041	37.84	3.475	65.76	5.549	116.16	7.691	216.60
0.171	2.98	2.052	38.06	3.496	66.08	5.587	118.36	7.740	218.30
0.184	3.16	2.097	38.74	3.516	66.48	5.603	119.03	7.763	219.35
0.220	3.84	2.118	39.00	3.537	66.78	5.624	119.88	7.784	220.50
0.240	4.00	2.129	39.12	3.567	67.32	5.643	120.45	7.807	221.50
0.247	4.26	2.140	39.54	3.604	67.94	5.661	121.38	7.830	222.15
0.278	4.66	2.190	40.24	3.623	68.56	5.680	122.42	7.855	223.10
0.308	4.88	2.211	40.58	3.654	69.08	5.700	122.88	7.878	223.95
0.326	5.22	2.233	40.94	3.689	69.72	5.721	123.73	7.899	225.55
0.349	5.72	2.278	42.04	3.720	70.26	5.752	124.64	7.921	226.00
0.388	6.52	2.293	42.22	3.764	70.84	5.772	125.99	7.972	228.30
0.405	6.70	2.305	42.36	3.781	71.02	5.794	127.88	7.993	229.50
0.422	6.90	2.316	42.48	3.792	71.30	5.815	129.07	8.069	231.46
0.446	7.50	2.325	42.68	3.813	71.50	5.836	130.91	8.144	233.81
0.479	8.26	2.336	42.96	3.824	71.64	5.864	131.85	8.186	234.86
0.479	9.66	2.377	44.74	3.835	71.90	5.887	132.47	8.208	235.36
0.510	10.28	2.390	45.12	3.845	72.08	5.909	133.27	8.235	235.91
0.523	10.54	2.411	45.58	3.867	72.26	5.929	133.80	8.247	236.16
0.544	10.82	2.438	46.00	3.884	72.58	5.951	134.38	8.301	236.26
0.579	11.30	2.465	46.42	3.896	72.74	5.966	134.87	8.351	238.46
0.614	11.62	2.477	46.60	3.918	73.04	5.981	135.28	8.373	239.26
0.628	11.80	2.490	46.92	3.939	73.38	6.003	135.78	8.394	239.91
0.636	12.00	2.534	47.56	3.960	73.70	6.043	136.89	8.434	242.11
0.659	12.66	2.547	47.80	4.004	74.38	6.060	137.69	8.470	243.91
0.681	13.18	2.569	48.02	4.034	74.72	6.121	139.84	8.508	244.51
0.717	14.24	2.592	48.52	4.110	75.80	6.215	146.86	8.547	245.96
0.737	14.54	2.614	49.00	4.154	77.08	6.267	149.76	8.661	249.11
0.783	15.30	2.637	49.26	4.204	77.50	6.289	150.67	8.682	249.46
0.805	15.70	2.650	49.60	4.225	77.96	6.309	151.28	8.704	249.81
0.824	15.90	2.661	49.84	4.246	78.44	6.383	153.76	8.755	251.26
0.863	16.60	2.684	50.04	4.272	79.08	6.404	154.41	8.776	252.61
0.884	16.92	2.707	50.36	4.319	79.92	6.423	155.18	8.816	254.41
0.908	17.60	2.718	50.62	4.339	80.56	6.461	157.49	8.833	255.31
0.925	17.90	2.729	51.00	4.361	81.36	6.501	158.94	8.872	258.01
0.978	18.80	2.754	51.82	4.412	82.28	6.518	160.55	8.890	258.76
0.999	19.12	2.766	52.24	4.451	83.04	6.535	163.85	8.907	259.41
1.050	19.80	2.776	52.44	4.491	84.08	6.554	165.30	8.926	260.06
1.072	20.30	2.798	52.72	4.513	84.64	6.575	167.00	8.947	260.81
1.092	20.98	2.835	53.36	4.537	84.96	6.596	168.20	8.990	262.30
1.114	21.54	2.853	53.80	4.562	85.62	6.621	174.65	9.018	263.20
1.136	21.88	2.904	54.68	4.583	85.84	6.640	177.20	9.062	265.25
1.166	22.40	2.926	55.24	4.595	86.42	6.669	178.85	9.084	265.85
1.205	23.10	2.937	55.68	4.641	87.72	6.690	179.65	9.199	269.50
1.215	23.32	2.949	55.84	4.665	88.74	6.711	180.75	9.269	271.50
1.243	23.56	2.969	56.14	4.698	89.63	6.742	181.45	9.280	271.80
1.263	24.14	2.994	56.50	4.722	90.18	6.803	183.40	9.348	272.00
1.283	24.60	3.019	56.98	4.744	90.68	6.822	183.95	9.397	273.35
1.317	25.18	3.030	57.44	4.770	91.64	6.839	184.85	9.420	274.00
1.337	25.60	3.041	57.58	4.812	92.49	6.880	186.20	9.443	274.55
1.379	26.32	3.063	57.94	4.835	93.12	6.954	188.25	9.465	275.20
1.400	26.94	3.085	58.42	4.866	93.93	6.976	189.70	9.489	275.75
1.431	27.46	3.095	58.48	4.878	94.59	6.999	190.25	9.511	276.50
1.463	27.96	3.111	58.64	4.919	95.41	7.070	193.50	9.626	279.70
1.493	28.78	3.135	59.08	4.940	96.00	7.117	195.45	9.682	282.50
1.567	29.82	3.156	59.58	4.962	96.84	7.141	196.70	9.735	284.30
1.595	30.22	3.177	59.90	4.997	98.08	7.163	197.55	9.798	286.25
1.606	30.42	3.198	60.28	5.043	99.38	7.204	199.05	9.847	287.65
1.645	30.96	3.231	60.80	5.087	100.94	7.238	199.90	9.892	289.10
1.664	31.32	3.252	61.20	5.115	101.86	7.257	200.35	9.913	289.70
1.697	31.64	3.271	61.66	5.159	102.81	7.280	200.90	9.939	290.35
1.718	31.80	3.288	61.86	5.170	103.21	7.333	202.75	9.963	291.40
1.750	32.84	3.308	62.38	5.190	103.56	7.380	203.95	10.022	293.05
1.811	33.70	3.318	62.62	5.224	104.13	7.404	204.90	10.693	323.54
1.832	34.00	3.328	62.90	5.320	107.41	7.449	205.75	11.212	346.08
1.854	34.34	3.348	63.12	5.342	107.93	7.474	206.90	11.420	353.48
1.875	34.70	3.359	63.32	5.392	109.09	7.496	207.45	12.000	370.63
1.904	35.00	3.370	63.50	5.414	110.67	7.519	208.85		

Mayer (1991) showed how one may calculate a record of percentage carbonate from a GRAPE density record, and Hagelberg et al. (this volume) show carbonate records derived by this method for the Leg 138 sites. We chose to work with untransformed GRAPE density data because analytical uncertainty (and, hence, any measure of significance) is uniform across the density range, whereas it is not uniform across the percentage range. For logistical reasons, we initially worked with the spliced records as displayed in Hagelberg et al. (1992; Fig. 5); when a stacked record for a site (Hagelberg et al., this volume) became available, this was used instead. Consequently, not all the records were worked on at the same degree of smoothing. In general, working with the stacked and smoothed records was easier. For the plots that are shown in this chapter as Figures 1A through 1F, all the GRAPE density data were smoothed in the time domain.

RESULTS

In this section, we discuss the results of tuning the Leg 138 sites in 1-m.y. sections, starting from the most recent increment. The outcome is reported in the series of Tables 1 through 11 that lists depth-

Table 9. Age model for Site 852.

Age (Ma)	Depth (mcd)	Age (Ma)	Depth (mcd)	Age (Ma)	Depth (mcd)
0.000	0.00	2.637	30.15	4.919	56.37
0.039	0.53	2.683	30.57	4.940	56.71
0.056	0.73	2.718	30.95	4.984	57.47
0.088	1.11	2.729	31.15	4.997	57.61
0.127	1.65	2.766	31.95	5.055	58.57
0.171	2.17	2.798	32.25	5.087	59.15
0.184	2.23	2.835	32.61	5.115	59.75
0.220	2.37	2.853	33.03	5.159	60.81
0.240	2.57	2.864	33.15	5.200	61.25
0.247	2.65	2.876	33.25	5.224	61.55
0.278	2.93	2.892	33.41	5.264	62.15
0.308	3.11	2.904	33.63	5.320	63.21
0.326	3.23	2.915	33.81	5.342	63.77
0.349	3.61	2.926	33.91	5.363	64.11
0.388	4.05	2.949	34.35	5.392	64.33
0.422	4.37	2.969	34.45	5.435	65.13
0.446	4.61	2.994	34.73	5.457	65.39
0.479	5.11	3.019	34.85	5.479	65.81
0.510	5.65	3.041	35.29	5.507	66.17
0.579	6.31	3.063	35.47	5.528	66.47
0.614	6.49	3.111	36.09	5.549	66.93
0.628	6.77	3.131	36.25	5.587	67.37
0.659	6.95	3.146	36.51	5.643	68.11
0.681	7.51	3.198	37.11	5.680	68.59
0.712	8.09	3.231	37.35	5.721	69.35
0.717	8.17	3.252	37.53	5.732	69.53
0.772	8.85	3.262	37.59	5.752	70.15
0.783	9.05	3.271	37.77	5.783	70.49
0.824	9.49	3.318	38.23	5.825	71.07
0.863	10.09	3.333	38.39	5.864	71.69
0.908	10.65	3.338	38.45	5.909	72.41
0.957	11.17	3.348	38.57	5.951	72.97
0.978	11.29	3.370	38.79	5.981	73.59
1.050	12.17	3.391	38.91	6.003	74.07
1.092	12.97	3.401	39.11	6.060	75.37
1.114	13.25	3.411	39.25	6.080	75.81
1.166	13.97	3.422	39.39	6.122	76.27
1.205	14.25	3.443	39.69	6.195	77.91
1.243	14.75	3.475	40.05	6.215	78.23
1.283	15.35	3.496	40.21	6.239	78.67
1.337	15.91	3.516	40.35	6.289	79.47
1.379	16.57	3.537	40.51	6.383	80.53
1.400	16.87	3.548	40.71	6.404	80.85
1.431	17.21	3.567	40.83	6.480	81.67
1.493	17.87	3.614	41.23	6.501	81.97
1.528	18.19	3.680	41.65	6.621	83.91
1.567	18.61	3.751	42.09	6.669	84.41
1.606	19.17	3.781	42.55	6.742	85.21
1.645	19.59	3.802	42.79	6.933	89.83
1.664	19.79	3.824	42.95	7.404	95.53
1.750	20.73	3.884	43.65	7.474	96.05
1.811	21.39	3.918	43.93	7.519	96.75
1.832	21.57	3.960	44.53	7.740	99.49
1.854	21.71	4.034	45.15	7.763	99.95
1.875	21.91	4.141	46.07	7.807	100.85
1.947	22.51	4.204	46.51	7.855	101.71
1.958	22.65	4.225	46.75	7.899	102.59
1.986	22.93	4.246	46.97	7.921	103.17
2.023	23.35	4.319	47.77	7.946	103.51
2.042	23.57	4.339	48.31	8.027	105.02
2.075	24.09	4.412	49.21	8.144	107.66
2.097	24.45	4.451	49.81	8.164	107.96
2.140	24.81	4.470	50.03	8.174	108.32
2.190	25.33	4.491	50.33	8.635	114.36
2.233	25.69	4.537	50.77	8.945	116.60
2.278	25.99	4.583	51.31	9.142	117.30
2.305	26.43	4.606	51.79	9.218	118.10
2.336	26.73	4.629	51.87	9.482	119.04
2.377	27.25	4.676	52.55	9.543	119.40
2.390	27.43	4.698	53.11	9.639	119.64
2.438	27.85	4.744	53.67	9.775	120.34
2.477	28.37	4.758	54.11	9.815	120.50
2.534	29.17	4.770	54.33	10.022	122.40
2.558	29.37	4.812	54.87	10.548	127.60
2.592	29.67	4.835	55.17	10.576	127.86
2.604	29.75	4.878	55.87	10.830	128.30

age pairs for recognizable GRAPE events at each site. Figures 1A to 1F show GRAPE density for Sites 846 to 854 vs. age for each age interval; each panel covers 2 m.y. For each site, vertical lines show the positions of all age control points. To aid in comparison, all the GRAPE density data for Figure 1 were interpolated at 1-k.y. intervals and smoothed in the time domain using a Gaussian filter having a total width of 5.9 k.y. Where the reconstructed sedimentation rate falls below about 5 m/m.y., as it does at several points in Site 848, the data are further smoothed; these intervals are not useful for tuning.

We show the results of tuning sections of individual holes from Sites 850, 851, and 852 in Figures 2 to 8 for two reasons. First, it is only by referring to the individual holes that one can assess the exact relationship between the GRAPE density and paleomagnetic stratigraphies. Second, these figures display the strengths and limitations of our tuning approach more clearly than Figure 1 does.

The interval from zero to 2 Ma (Fig. 1A) was surprisingly difficult to tune, considering the amount of work that has been devoted to the study of Pleistocene climate. Examination of Figure 1A shows a convincing degree of correlation among the sites, but the relationship with the orbital data is not at all obvious. Here, we do not quantify the correlation among sites, but note that Hagelberg et al. (this volume) demonstrate by empirical orthogonal function (EOF) analysis that a high proportion of the variability in all the sites is explained by the first EOF.

Figure 2 shows the data for the interval 0 to 1 Ma from Holes 851B, 851C, 851D, and 851E separately, tuned with GRAPE density extremes correlated to insolation extremes. In this interval, the match between GRAPE density and the orbital record is fairly poor. As regards tuning to the orbital record is concerned, we emphasize again that in this interval we have been guided by the objective of creating a time scale based on features in the GRAPE density record that is not grossly inconsistent with a $\delta^{18}O$-based time scale. By contrast, in Figure 1, the GRAPE density data for Site 851 are shown using the control points in Table 8, so that for the past million years the GRAPE density extremes are no longer all exactly aligned with insolation

Table 10. Age model for Site 853.

Age (Ma)	Depth (mcd)	Age (Ma)	Depth (mcd)
0.000	0.22	4.885	28.15
0.473	1.77	5.004	28.96
0.681	2.47	5.240	31.50
0.780	2.95	5.875	38.57
0.990	3.85	6.256	43.55
1.070	4.19	6.554	46.52
1.770	7.80	7.072	54.16
1.950	8.57	7.318	55.56
2.600	12.18	7.351	56.31
3.054	15.23	7.406	56.55
3.127	15.74	7.533	58.30
3.221	16.33	7.618	59.04
3.325	16.89	8.027	65.60
3.612	18.82	8.173	68.40
4.188	22.30	8.205	69.00
4.320	23.53	8.635	75.06
4.452	25.24	8.645	75.20
4.621	26.08		
4.801	27.41		

Table 11. Age model for Site 854.

Age (Ma)	Depth (mcd)	Age (Ma)	Depth (mcd)
0.000	0.00	6.919	25.27
0.780	4.08	7.072	27.57
0.990	5.35	7.406	30.72
1.070	5.82	7.533	32.69
1.770	10.61	7.618	33.23
1.950	11.48	8.027	39.78
2.600	16.68	8.174	41.75
3.053	17.68	8.205	42.30
3.131	17.82	8.631	43.78
3.224	17.95	8.945	45.40
3.337	18.15	9.142	46.55
3.611	19.08	9.218	47.33
3.740	19.50	9.482	48.85
5.875	19.93	9.543	49.48
6.122	21.11	9.639	49.80
6.256	21.91		
6.555	23.03		

Table 12. Age-depth control points for the interval 0 to 1Ma derived by correlating GRAPE density and orbitally controlled insolation without regard to the established $\delta^{18}O$ time scale.

Age (Ma)	Depth (mcd)
Site 844	
0.000	0.00
0.780	10.04
0.990	11.83
1.070	12.36
Site 845	
0.000	0.00
3.610	59.88
Site 846	
0.000	0.00
0.033	1.82
0.056	3.04
0.126	5.98
0.148	6.76
0.173	7.38
0.218	8.52
0.241	9.06
0.262	9.94
0.290	11.84
0.311	12.06
0.333	12.66
0.354	13.44
0.386	14.70
0.408	15.98
0.462	17.72
0.473	18.78
0.484	19.44
0.504	19.90
0.515	20.14
0.528	20.38
0.577	22.12
0.598	22.32
0.620	23.38
0.648	24.42
0.692	25.72
0.712	26.06
0.787	28.74
0.863	32.18
0.884	33.26
0.908	34.34
0.936	35.14
0.978	35.98
0.999	36.56
Site 847	
0.000	0.00
0.056	1.11
0.082	2.73
0.103	3.47
0.126	4.11
0.219	7.65
0.262	8.83
0.290	9.79
0.311	10.29
0.333	11.13
0.354	11.81
0.372	12.23
0.408	13.77
0.462	15.19
0.484	16.05
0.528	17.45
0.577	18.23
0.648	20.33
0.692	21.47
0.712	21.71
0.749	22.69
0.787	24.29
0.824	25.15
0.908	28.15
0.978	29.61
1.000	30.43
Site 848	
0.000	0.00
0.056	0.68
0.082	1.02
0.114	1.44
0.148	2.14
0.173	2.46
0.218	2.80
0.241	3.12
0.262	3.44
0.311	4.10
0.354	4.70
0.408	5.64
0.462	6.52
0.484	7.42
0.528	7.88
0.565	8.68
0.609	9.30
0.648	10.08
0.681	10.80
0.710	11.08
0.749	11.86
0.787	12.70
0.863	13.80
0.908	14.86
0.925	15.16
0.978	15.76
0.999	16.02
Site 849	
0.000	0.02
0.056	1.58
0.070	2.76
0.082	3.18
0.126	4.02
0.148	5.10
0.173	5.58
0.218	7.04
0.241	8.34
0.277	8.92
0.290	9.72
0.333	10.46
0.354	11.30
0.386	12.06
0.397	12.46
0.408	12.98
0.462	13.90
0.484	15.22
0.528	16.54
0.565	17.10
0.577	17.50
0.631	18.76
0.681	20.24
0.692	20.38
0.749	21.92
0.787	23.00
0.805	23.24
0.853	24.56
0.874	25.28
0.908	26.16
0.936	26.86
0.957	27.36
0.978	27.62
0.999	28.26
1.050	29.44
Site 850	
0.000	0.00
0.056	1.03
0.082	1.39
0.126	2.31
0.148	3.21
0.173	3.89
0.218	4.53
0.262	5.45
0.290	6.01
0.333	6.95
0.354	7.43
0.372	7.85
0.408	8.67
0.425	9.07
0.445	9.41
0.462	9.71
0.484	10.39
0.504	10.51
0.528	10.85
0.577	11.59
0.598	12.11
0.631	12.79
0.681	14.11
0.692	14.31
0.712	14.81
0.749	15.09
0.805	16.27
0.824	16.61
0.863	17.57
0.884	17.99
0.908	18.51
0.978	19.65
0.999	19.93
1.029	20.53
Site 851	
0.000	0.00
0.056	1.16
0.082	1.62
0.103	1.98
0.126	2.48
0.148	2.78
0.173	2.98
0.218	3.76
0.262	4.26
0.290	4.88
0.333	5.36
0.354	5.70
0.372	6.06
0.408	6.70
0.425	7.02
0.462	7.50
0.484	8.48
0.504	9.02
0.528	9.28
0.555	9.50
0.577	9.94
0.648	12.66
0.692	13.50
0.712	14.14
0.749	14.54
0.787	15.30
0.805	15.70
0.824	15.90
0.863	16.60
0.884	16.92
0.908	17.60
0.925	17.90
0.978	18.80
0.999	19.12
Site 852	
0.000	0.00
0.056	0.73
0.126	1.65
0.196	2.31
0.262	2.63
0.290	3.03
0.354	3.61
0.408	4.21
0.462	4.67
0.484	5.49
0.577	6.31
0.648	6.95
0.692	7.85
0.749	8.49
0.787	9.05
0.824	9.49
0.863	10.09
0.908	10.65
0.957	11.17
0.978	11.29
Site 853	
0.00	0.22
0.78	2.95
0.99	3.85
Site 854	
0.00	0.00
0.78	4.08
0.99	5.35

Table 13. Coherency between June insolation at 65° N (Berger and Loutre, 1991) and stacked GRAPE density for sites 849, 850 and 851 estimated over 1 m.y. intervals (Fig. 9).

Interval (Ma)	COH 41 k.y.	COH 23 k.y.	COH 19 k.y.
0–1[a]	0.87	0.63	0.38
0–1[b]	0.89	0.91	0.78
1–2	0.78	0.96	0.94
2–3	0.89	0.96	0.90
3–4	0.86	0.97	0.97
4–5	0.74	0.92	0.91
5–6	0.61	0.94	0.92
6–7	0.42	0.90	0.91

[a] ^{18}O-based time scale from Tables 6, 7, and 8.
[b] GRAPE-based time scale from Table 12.

extremes. From a statistical standpoint, the tuning illustrated in Figure 2 leads to an acceptable coherency between GRAPE density and orbital insolation, whereas the tuning illustrated in Figure 1 does not (Table 13). The fact that neither version of the time scale for the interval from 0 to 1 Ma leads to high coherency for both GRAPE density and $\delta^{18}O$ has the unfortunate consequence that we cannot obtain statistically useful information on the phase relationship between these two parameters.

Between 1 and 2 Ma, the situation is slightly clearer (Fig. 3). In this time interval, $\delta^{18}O$ records are dominated by 40-k.y. obliquity cycles (Pisias and Moore, 1981; Ruddiman et al., 1986). Several segments of GRAPE density variability show evidence of 40-k.y. cycles over this interval; see, for example, Sites 847 and 852 in Figure 1A. The individual holes of Site 851 do not show the 40-k.y. cycles so clearly (Fig. 3), and it would not have been possible to develop the time scale on the basis of only this site.

Moving to the interval between 2 and 4 Ma shown in Figure 1B, the tuning operation became easier. For intervals between 2.0 and 2.6 Ma, we have been guided by the $\delta^{18}O$ record of Site 846 (Shackleton et al., this volume). Correlating this record to that of Site 677 (SBP90) implies a strong obliquity signal in the GRAPE density, especially between 2.4 and 2.6 Ma. In some sites, the precession cycles between 2.1 and 2.3 Ma are recognizable. The good magnetostratigraphic record for Site 851 (Fig. 4) provides a tie to the astronomical calibration of SBP90 in Site 677, and it is only for the section older than 2.6 Ma that we are seeking a tuning that is independent of previous work. Thus, the marked similarity between GRAPE density variations and the orbital record between 2.5 and 3.0 Ma in several sites, as well as the conspicuous precession cycles in the interval from 3.0 and 3.2 Ma and between 3.7 and 4.0 Ma, are particularly important for carrying the tuning operation back through the Gauss. It is appropriate to remark that our starting point was the assumption that since the time scale developed by Cande and Kent (1992) was calibrated astronomically at 2.6 Ma, it would prove to be nearly correct. We were aware that this time scale diverges from H91 in the Gilbert Chron, but imagined (wrongly, as it turns out) that this disagreement would be resolved in favor of smooth seafloor spreading and, hence, in favor of the time scale of Cande and Kent (1992). The data for the individual holes of Sites 850 and 851 for the interval 3 to 4 Ma are shown in Figures 5 and 6. From 3.0 to 3.5 Ma, the tuning is exceptionally clear; however, with the data from several sites to work with, the tuning to 4 Ma also is reliable.

The interval from 4.0 to 6.0 Ma is shown in Figure 1C. Again, the precession signal is well recorded in several of the sites. Between 4.0 and 4.4 Ma, Site 846 shows a clear precession signal, and both Sites 846 and 847 appear to record the interval between 4.6 and 5.0 Ma, during which the insolation record shows strong precession cycles flanking an interval dominated by obliquity. Of course, this pattern is a reflection of eccentricity maxima flanking a broad interval of low eccentricity. The significance of this is that although uncertainties in the astronomical calculations mean that the exact temporal relation-

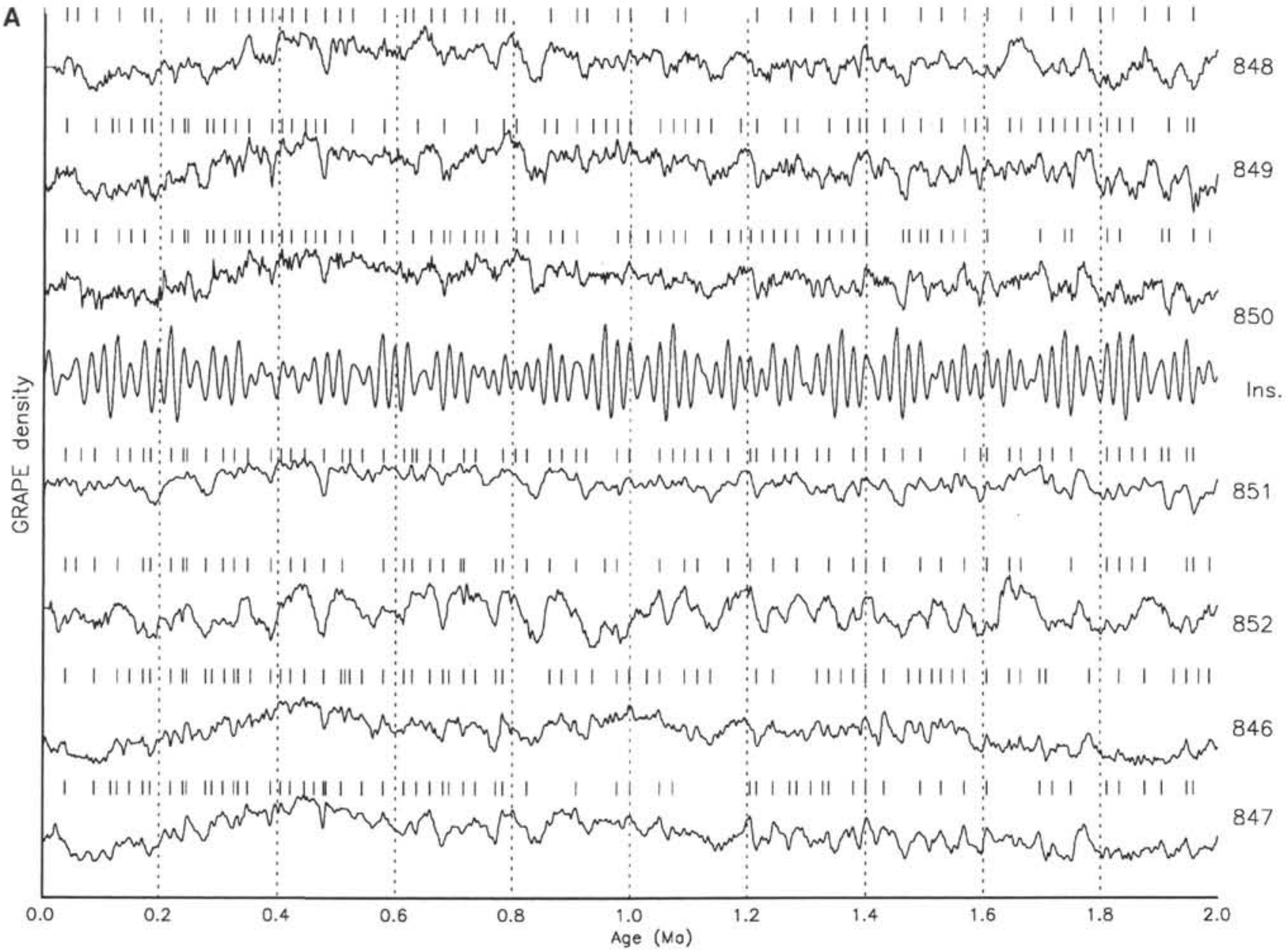

Figure 1. **A.** GRAPE density vs. age for Sites 846, 847, 848, 849, 850, 851, and 852, 0 to 2 Ma. For each site, the upper part has been constructed from the stacked records, making use of data from all holes at the site, while the older parts of the sections have been based on the shipboard splice. Vertical lines above the data for each site show the age control points from Tables 1 to 11. For this figure, all data sets have been smoothed in the time domain with the same filter (see text). **B.** GRAPE density vs. age for Sites 846, 847, 848, 849, 850, 851, and 852, 2 to 4 Ma. **C.** GRAPE density vs. age for Sites 846, 847, 848, 849, 850, 851, and 852, 4 to 6 Ma. **D.** GRAPE density vs. age for Sites 846, 847, 848, 849, 850, 851, and 852, 6 to 8 Ma. **E.** GRAPE density vs. age for Sites 846, 847, 848, 849, 850, 851, and 852, 8 to 10 Ma. **F.** GRAPE density vs. age for Sites 846, 847, 848, 849, 850, 851, and 852, 10 to 12 Ma.

ship between a particular precession peak and a particular obliquity maximum may be unknown, the timing of the eccentricity record is probably reliable (Berger et al., 1992).

Between 5 and 6 Ma, GRAPE density variations are more erratic, but even so, there appear to be intervals having large-amplitude variations associated with precession. These large jumps in mean density value adversely affect the results of bandpass filtering of the data. Their origin is partly the episodes during which laminated sediments accumulated (Kemp and Baldauf, 1993). It is difficult to put bounds on possible sedimentation rate excursions associated with these events and, in some details, the tuning is speculative in those parts of the record associated with accumulation of laminated sediments. At about 5.8 Ma, we were assisted in correlating sites by features in the bulk sediment $\delta^{13}C$ record that could be correlated among sites (Shackleton and Hall, this volume).

STATISTICAL EVALUATION

To present a straightforward statistical evaluation of the time scales that have been generated, we constructed a synthetic western transect record by simply averaging the GRAPE density estimate at each 0.001-Ma age increment at Sites 849, 850, and 851. Figure 9 shows cross-spectral analyses of this record vs. the 65°N insolation record of Berger and Loutre (1991) in million-year segments. It is apparent from Figure 9 that tuning has resulted in coherency estimates in the precession band of more than 0.9 in every time interval except 0 to 1 Ma. Coherency estimates are given in Table 13. In every time interval, coherency with precession is greater than coherency with obliquity; coherency with obliquity ranges from a low of 0.61 in the 5- to 6-Ma interval to 0.89 in the 2- to 3-Ma interval. Phase plots are not shown because we tuned by assuming a zero phase lag between insolation and GRAPE density; however, note that in no case are the phase estimates for either precession or obliquity significantly different from zero, other than the phase against obliquity in the range of from 3 to 4 Ma, where GRAPE density lags insolation by $50 \pm 20°$ (6 ± 2 k.y.) in the obliquity band. In the interval from 0 to 1 Ma, coherency is acceptable for the age models in which GRAPE density extremes are exactly aligned with insolation extremes (Table 12), but not for the $\delta^{18}O$ age models given in the upper parts of Tables 1 to 11.

Coherency between the geological data and the orbital target in the precession band is the fundamental method by which a time scale may be evaluated. There are two reasons for this. First, the modulation on the precession signal is very much stronger than that on the obliquity signal, so that the test of coherency is more valuable. Second, the modulation on the precession signal arises directly from the orbital eccentricity record for which the calculations are the most robust (Berger et

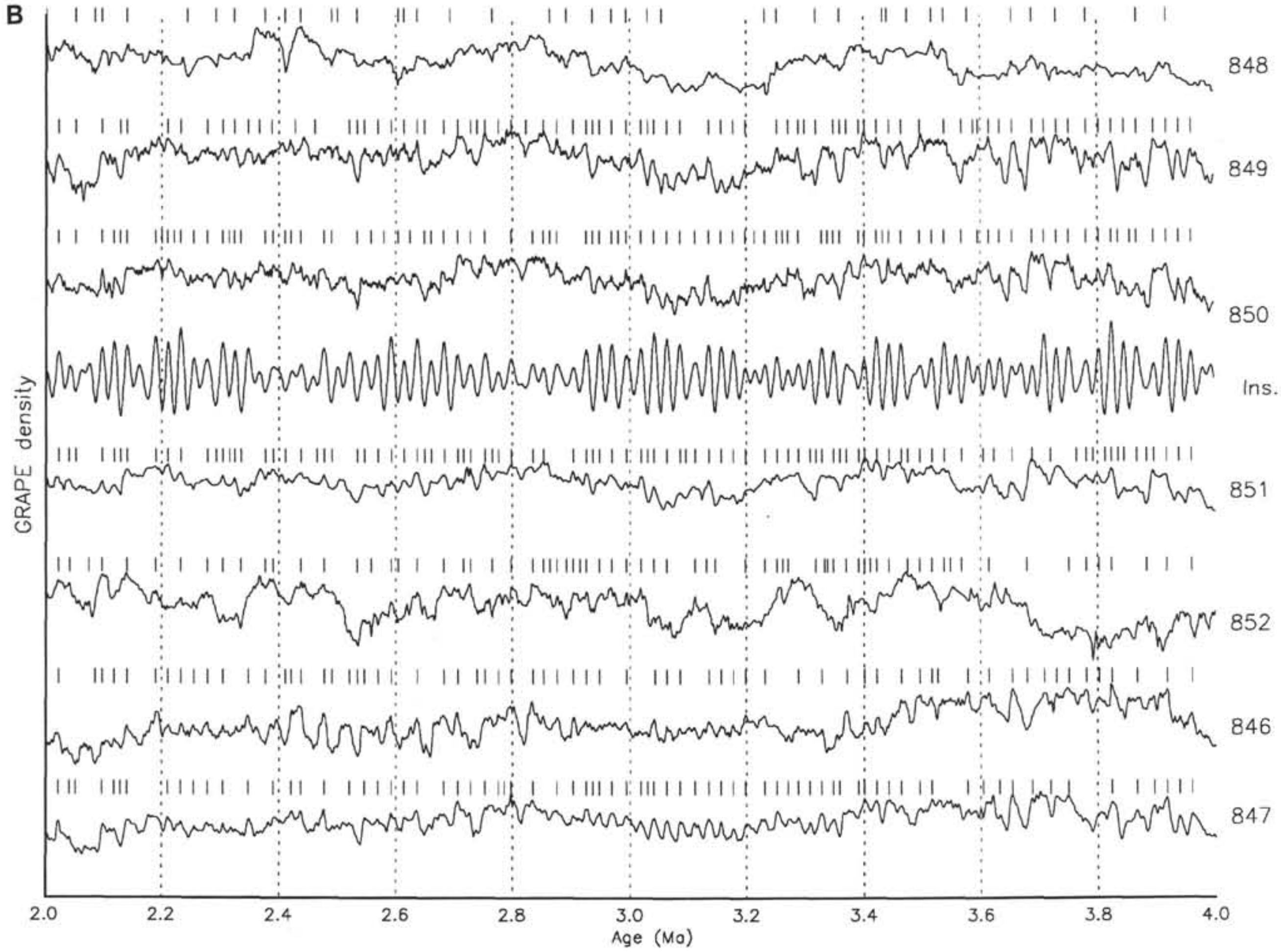

Figure 1 (continued).

al., 1992), whereas the modulation on the obliquity signal (1) does not have a clearly defined and independent origin, (2) appears in the series expansion through the interference between several terms with periods close to 41 k.y. (Berger and Loutre, 1991; Table 7), and (3) thus is sensitive to extremely small errors in their estimation.

Two studies (Pisias, 1983, and Brüggemann, 1992) showed that high coherencies cannot be generated by "tuning" a randomly varying time series to the orbital signal (although Neeman [in press] reached a different conclusion). Thus, it seems unlikely that the very high coherencies shown in Figure 9 could have been obtained had there not been a close coupling between changing solar insolation and East Pacific Ocean paleoceanography. Moreover, Hagelberg (1993) showed that, although estimated coherency is reasonably robust with respect to small errors in time scale, the reduction in coherency resulting from time-scale error is frequency dependent, with the coherency at precession frequencies showing the highest degradation. Thus, the very high coherencies in the precession band shown in Figure 9 constitute strong evidence that our time scale is close to correct. It must be pointed out that the high coherencies shown by Imbrie et al. (1984) for a stacked $\delta^{18}O$ record covering the past 0.78 Ma did also imply that the chronology was close to correct; this remains true, despite the fact that we now think that it was correct only over 75% of the interval covered (SBP90).

The high coherencies shown in Figure 9 also indicate that the physical linkage between changing solar insolation and paleoceanography has remained strong through the whole Pliocene, suggesting that it may be amenable to modeling. On the other hand, it must be said that it is important in the future to test the validity of the calibrations that we have obtained beyond the range of overlapping with H91 in an area that experienced less violent fluctuations in sedimentation rate. The reason is that one property of a convincing age model is that it should not generate physically unreasonable changes in sedimentation rate; one of the findings of Leg 138 was that in the eastern equatorial Pacific, sedimentation rates are extremely variable so that it is difficult to specify what is, in fact, a physically unreasonable change. In addition, the hole-to-hole comparisons made by Hagelberg et al. (this volume) show that a significant proportion of the apparent variability in sedimentation rate either persists over only small distances on the seafloor or else is an artifact of distortion during coring.

It is a striking feature of both the records from the Mediterranean Basin, studied by Hilgen (1991a, 1991b), and those from the eastern Atlantic Ocean, studied by Tiedemann (1992), that good evidence can be seen for a 100-k.y. eccentricity cycle in their data. Indeed, the ground-breaking study by Hilgen (1991a) was possible only because he was able to place his records in the context of the 400- and 100-k.y. eccentricity cycles and so could to develop an astronomically calibrated time scale without working systematically back from the present. It is evident from Figures 1 and 9 that this approach is not possible in the GRAPE density records recovered during Leg 138. No consistent 100-k.y. signal is present, and coherency between insolation and GRAPE density is only marginally significant in the eccentricity fre- quency band. Figure 1 shows that there is considerable low-frequency variability in GRAPE density; presumably, this masks any eccentricity signal that might otherwise have been present.

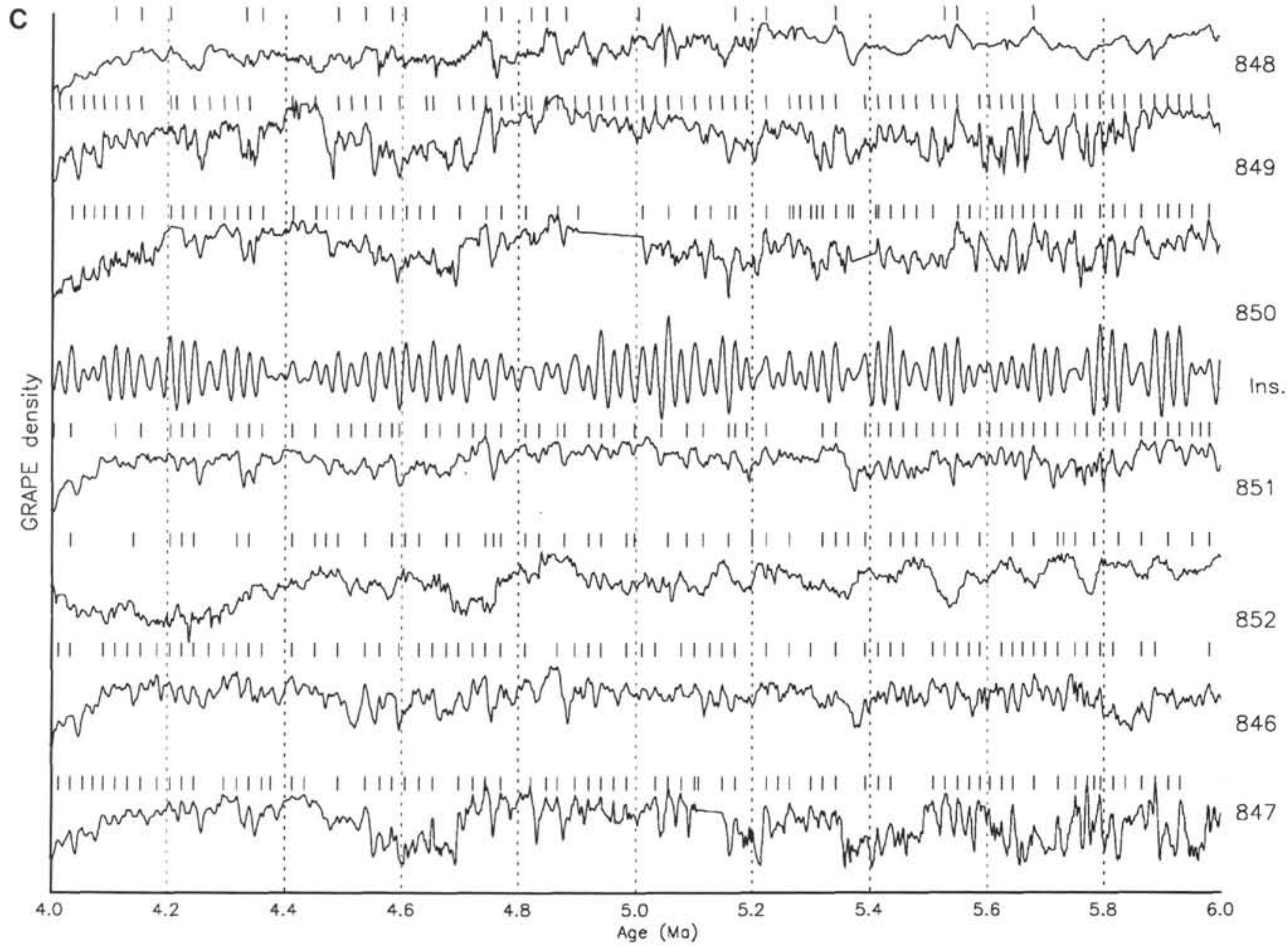

Figure 1 (continued).

DISCUSSION: CALIBRATIONS OF THE MAGNETIC POLARITY TIME SCALE FROM 0 TO 6 M.Y.

To obtain the most reliable ages for Pliocene magnetostratigraphy, we examined the critical intervals hole by hole. This enabled us to evaluate the quality of each estimate. In Figures 2 to 5, we show the magnetic declination and tuned GRAPE density vs. age for each hole in Sites 850 and 851 over the interval from 3 to 4 Ma. For the Kaena and Mammoth subchrons, the boundaries are clearly related to the GRAPE stratigraphy, and the estimates are consistent (Table 14). Initially, we were unable to obtain a clear calibration for the base of the Gauss, but careful examination of the data for Holes 850A and 850B (Fig. 5) shows clear precession cycles; by correlating the holes of Site 851 to those of Site 850, we obtain a consistent calibration.

In the Gilbert interval, Site 852 provides the vehicle for transferring our time scale to the paleomagnetic record; in addition, a record of the Cochiti occurs in Site 851. Figures 7 and 8 show the GRAPE density and magnetic declination data for the individual holes of Site 852 over the intervals from 4 to 5 Ma and from 5 to 6 Ma. In these records, the age control points derive from correlation to Sites 849, 850, and 851, rather than direct correlation to the orbital record; for this reason, we show in Figures 7 and 8 the stacked GRAPE density records of Sites 849, 850, and 851, as well as the orbital insolation, so that the tuning process may be followed. The interpolated ages of each of the reversals in each hole are given in Table 15.

The top of the Nunivak is a problematic area because the 65°N orbital signature is structureless where the GRAPE data show evident structure; here, we may have difficulties with the accuracy of the astronomical solution. If this is the correct explanation, we would be led to conclude that the eccentricity values were not so low as those given in the calculations of Berger and Loutre (1992). Such a conclusion would not necessarily be in conflict with the observation that the main eccentricity periods are known rather accurately so that the timing of eccentricity maxima is reliably known at ages where the timing of obliquity maxima is less well known.

Table 16 provides mean estimates for the ages of the magnetic reversals in Sites 850, 851, and 852 that arise from the tuning discussed above. These estimates are compared (1) with those that, until recently, have been regarded as "standard" (Berggren, Kent, and Flynn (1985) and Berggren, Kent, and Van Couvering (1985); (2) with those given by CK92; and (3) with the earlier tuned ages of SBP90 and H91.

It is apparent from Table 16 that ages for the Kaena and Mammoth intervals agree well with both Hilgen's estimates and those of CK92. At the base of the Gauss, our estimate agrees with that of Hilgen (1991a); both estimates are significantly older than those of CK92. The age obtained here, 3.594 Ma, is a little younger than that reported by Shackleton et al. (1992). The reason is that we reevaluated the GRAPE density record of Site 850, which has the higher sedimentation rate across this interval, and identified the complete sequence of precession cycles in this critical interval. We then mapped the Site 851 holes into this record. The result (Figs. 5 and 6) is convincing.

On average, our age estimates are a few thousand years greater than those given by Hilgen (1991a). Hilgen's estimates were based on an assumed lag of 4 k.y. between precession extremes and the midpoints of the equivalent lithological bed, whereas we have not assumed any lag between insolation and GRAPE density extremes.

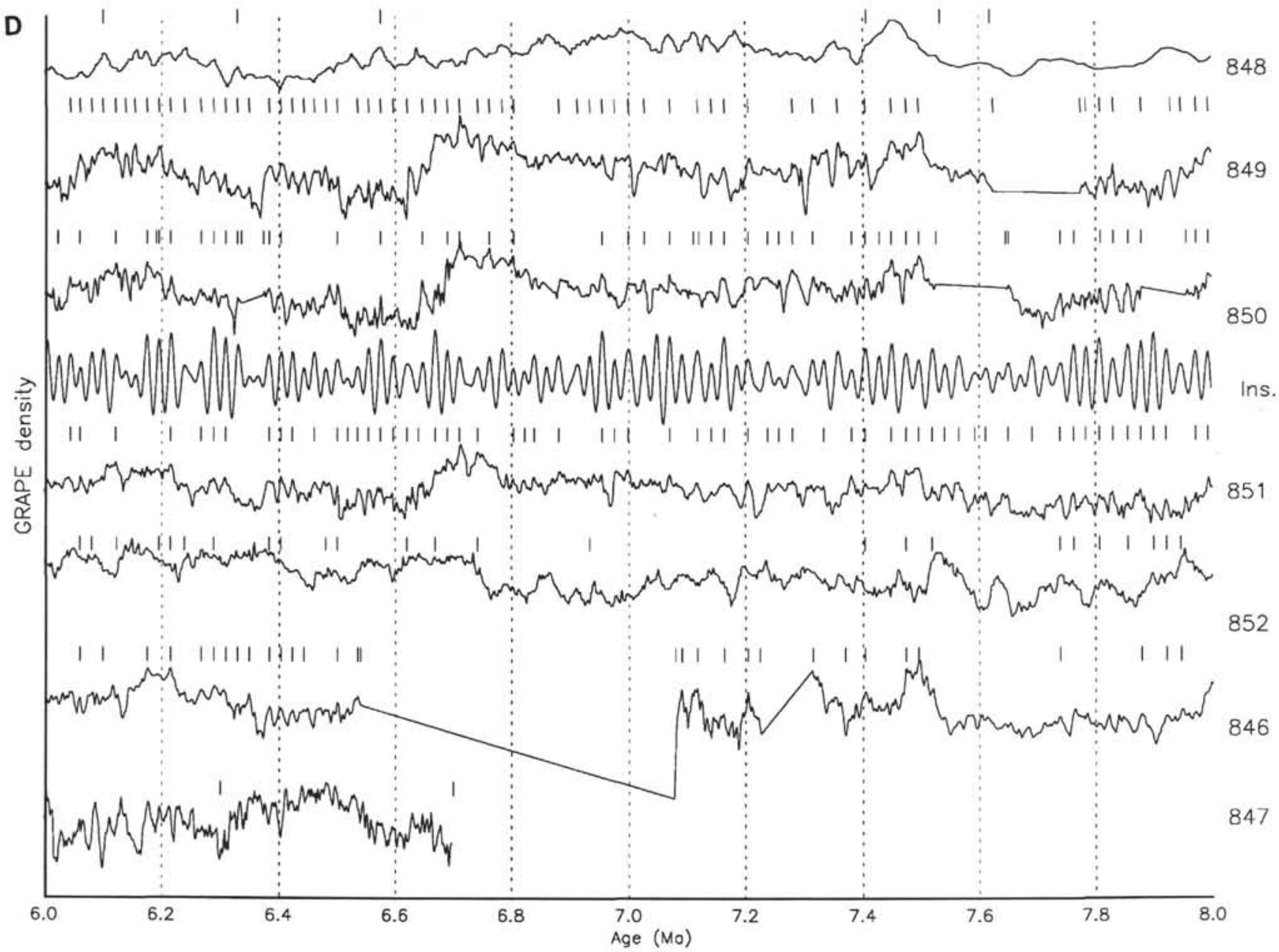

Figure 1 (continued).

Pending a more sophisticated evaluation of the response of the respective paleoceanographic systems to orbital forcing, we conclude that differences between our estimates and H91 are negligible. From the Cochiti to the base of the Thvera subchrons, our estimates also are near those given by Hilgen (1991b), although, because they were calibrated in more slowly accumulating sediment, our estimates for the ages of these reversals are not so precise as those for the reversals in the Gauss. However, it is now clear that this time scale provides true accuracy through a sufficient amount of the Pliocene that one must recalibrate the magnetic anomaly time scale of CK92 to take into account the significant deviations that become evident by the base of the Gauss.

From the Thvera to C3A.1n (t), tuning was difficult as a result of the exceptionally wide ranges in sedimentation rate in several sites. However, we attempted it for two reasons. First, this is a key to extending the work of Hilgen (1991b) into the Miocene: it is necessary to cover the interval of the Messinian salinity crisis by working in extra-Mediterranean sediments. Second, the young side of C3A is widely used as a calibration point when developing time scales for the seafloor magnetic anomaly sequence. In the interval from 5 to 6 Ma, GRAPE density and orbital insolation are highly coherent in the precession band, but only weakly coherent in the obliquity band (Fig. 9F); moreover, in our solution, no discrete concentration of variance is observed in the 41-k.y. band. The $\delta^{18}O$ record developed for Site 846 does not show a strongly coherent 41-k.y. signal either; it remains possible that either a different tuning of the data investigated here or a record of different components of the climate system might lead to higher coherencies than those we have obtained here.

RECALIBRATING THE MIOCENE TIME SCALE

One will recall that CK92 calibrated the distance scale for the South Atlantic Ocean anomaly sequence on the basis of a control age at 2.6 Ma and another at 14.8 Ma (and of course others through the past 100 Ma). The age of 2.6 Ma for the Gauss/Matuyama boundary was based on astronomical calibration (SBP90), while the remaining have been based on radiometric age determinations. Clearly, for several years to come, there will be two sections to the anomaly time scale: an upper section that is calibrated in detail by astronomical tuning, and a lower section that is developed by interpolation between a limited number of control points that are based on radiometric dates. A possible procedure at this juncture would be to insert one new age control in the latest Miocene and retain the remaining points as used by CK92. However, when South Atlantic spreading rates are estimated on this basis, a geophysically unexpected oscillation in spreading rate is generated (Fig. 10). Therefore, we have inserted an additional control point on the basis of the new determination by Baksi (1992) for C5 (t), 9.66 ± 0.05 Ma. For ease of use, we have adopted the value of 9.64 Ma for this boundary, which is the closest age within the uncertainty limits that enables GRAPE density to be matched directly to the insolation record. We have used 5.875 Ma for C3A (t). Table 17 gives the ages of reversal boundaries estimated from Table 2 in CK92 by fitting a cubic-spline in the same manner as they adopted. If one uses these new figures for events younger than 14.8 Ma together with those given by CK92 for older events, this does not generate a significant discontinuity at 14.8 Ma; we suggest that this time scale is probably more nearly correct as regards its depiction of changes in spreading rate during the late

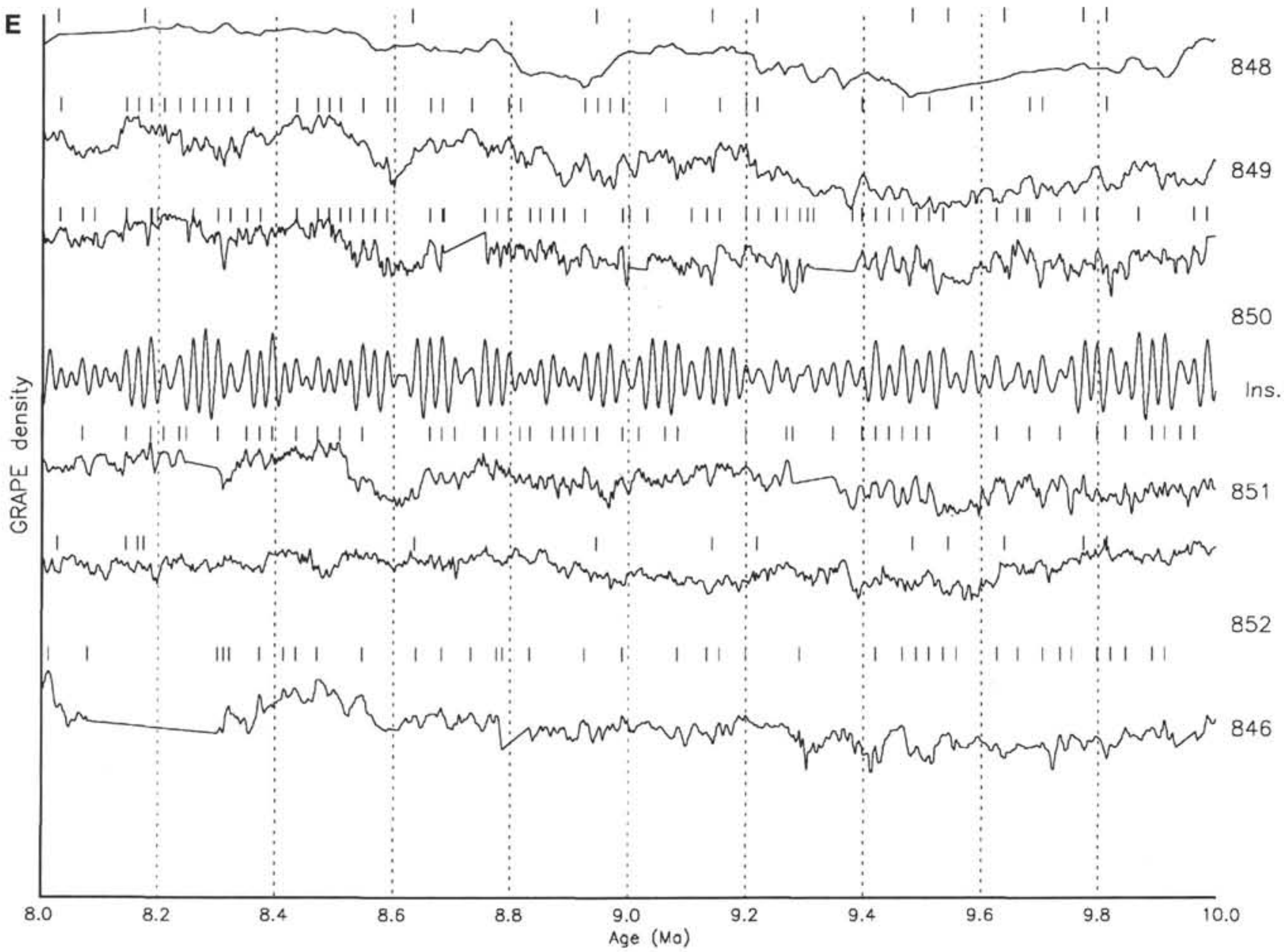

Figure 1 (continued).

Neogene (Fig. 10) than that of CK92. Because South Atlantic spreading rates clearly did change significantly during the late Miocene, it is highly likely that future tuning will modify this picture. These future modifications may undermine the basis for using a cubic-spline fit to predict the ages of the seafloor anomalies, but in the meantime, we recommend that the ages in Table 17, together with those in CK92, Table 6, for ages greater than 14.8 Ma, be used for Miocene calibrations. We are aware that the control age at 14.8 Ma may also be questioned (Baksi and Farrar, 1990) but prefer here to devise a solution that limits the adjustments recommended to that part of the time scale over which we have contributed new data.

DISCUSSION: MIOCENE AGES

Our objective was to generate an accurate, high-resolution time scale for the past 6 m.y. for Leg 138 sites. Several factors limit the backward extension of this type of time scale. First, the quality of our data deteriorates. It is not yet clear to what extent our composite depth sections are complete representations of the sediment column where the extended core barrel (XCB) was used instead of the APC. Second, both the quality of the GRAPE density data and the fidelity of its relationship to percentage carbonate deteriorates in more lithified sediments. Third, sedimentation rates are not so favorable in the mid-portion of the late Miocene sequence. Fourth, Berger and Loutre (1991) did not claim accuracy for their astronomical reconstructions prior to about 5 Ma and, indeed, it has already been suggested that modifications in the calculations may be required (Berger and Loutre, 1992). Fortunately, the chief basis for tuning is the characteristic modulation of the precession signal by eccentricity, while the most likely modification to the calculated record would be in the timing of the obliquity cycles with respect to the precession cycles.

On the positive side, several of the Leg 138 sites have good magnetostratigraphy, all have good biostratigraphy, and the GRAPE density records show considerable promise. Thus, we have aimed to develop partially tuned age models for the interval between 6 and 10 Ma. Their chief practical utility is that they enable us to propose detailed correlation among sites wherever the GRAPE data permits it; they also enable us to propose calibrated sedimentation rates over intervals that display orbital frequency variability; and finally, they enable us to evaluate the changing response to orbital forcing. We have made some use of bulk sediment $\delta^{13}C$ data (Shackleton and Hall, this volume) as an additional tool for correlation between sites.

Table 14. Ages for reversals in the mid-Pliocene, estimated for Sites 850 and 851.

Event	Hole 850A	Hole 850B	Hole 851B	Hole 851C	Hole 851E	Mean	Event
C2n.1r(t)	3.043	3.048	3.044	N.D.	3.049	3.046	Kaena (t)
C2n.1r(o)	3.133	3.133	3.124	3.132	3.131	3.131	Kaena (o)
C2n.2r(t)	3.224	3.219	3.230	3.222	3.233	3.233[a]	Mammoth (t)
C2n.2r(o)	3.333	3.329	3.327	3.331	3.335	3.331	Mammoth (o)
C2n(o)	3.595	3.596	3.594	3.592	3.591	3.594	Gauss (o)
C3n.1n(t)	N.D.	N.D.	4.194	4.208	4.208	**	Cochiti (t)
C3n.1n(o)	N.D.	N.D.	4.322	N.D.	4.320	**	Cochiti (o)

[a] At C2n.2r(t), the GRAPE density signal is much clearer at Hole 851E than at the other holes, so that we have taken the estimate for that hole, rather than the mean. (t) = termination and (o) = onset. ** See Table 15.

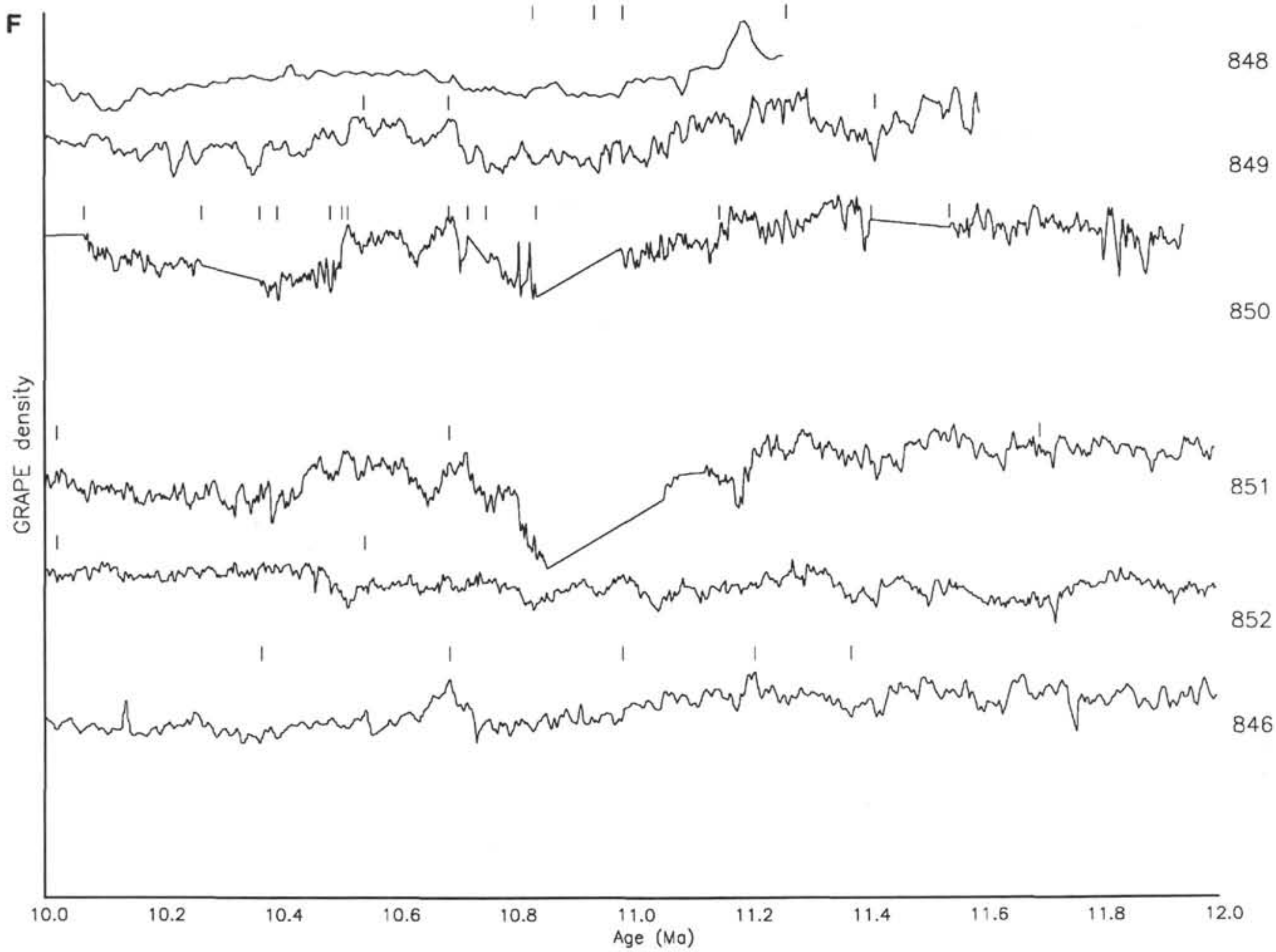

Figure 1 (continued).

Table 15. Ages for reversals in the Gilbert, estimated for Site 852.

Event	Hole 852B	Hole 852C	Hole 852D	Mean	Event
C3n.1n(t)	4.197	4.194	4.194	4.1992[a]	Cochiti (t)
C3n.1n(o)	4.307	N.D.	4.316	4.316[a]	Cochiti (o)
C3n.2n(t)	N.D.	4.480	4.478	4.479	Nunivak (t)
C3n.2n(o)	4.621	4.618	4.631	4.623	Nunivak (o)
C3n.3n(t)	4.780	4.785	4.777	4.781	Sidufjall (t)
C3n.3n(o)	4.882	4.875	4.877	4.878	Sidufjall (o)
C3n.4n(t)	4.980	4.975	4.977	4.977	Thvera (t)
C3n.4n(o)	5.240	5.224	5.231	5.232	Thvera (o)
C3A.1n(t)	5.870	5.892	5.885	5.882	Epoch 5 (t)
C3A.1n(o)	6.106	6.110	N.D.	6.108	
C3A.2n(t)	6.275	6.277	6.283	6.278	

[a] at C3n.1n(o) and (t), the mean is based on Sites 851 and 852. (t) = termination and (o) = onset.

The interval between 6 and 8 Ma is shown in Figure 1D. Between 6 and 7 Ma, several sites show variability that is readily tuned to the insolation record, and some preliminary tuning has been performed. Note that the GRAPE density minimum between 6.5 and 6.6 Ma can be traced from Site 853 with a complete paleomagnetic record, through Site 852 with a similar GRAPE density record, to the extreme represented by Site 850, where this interval is marked by a 20-m-thick sequence of laminated sediment.

In the interval from 8 to 10 Ma shown in Figure 1E, further work will be required to ensure the continuity of the records recovered with the XCB system, but it may be possible ultimately to generate a

Table 16. Ages of the magnetic reversals of the past 6 m.y., according to SBP90, H91, CK92, and this study.

Event	SBP90	H91	CK92	This study	Event
C1n (o)	0.78		0.780		B/M
C1r.1n (t)	0.99		0.984		Jaramillo (t)
C1r.1n (o)	1.07		1.049		Jaramillo (o)
C1r.2n (t)	1.77		1.757		Olduvai (t)
C1r.2n (o)	1.95		1.983		Olduvai (o)
C2An.1n (t)	2.60	2.59/62	2.600		Gauss (t)
C2An.1n (o)		3.04	3.054	3.046	
C2An.2n (t)		3.11	3.127	3.131	
C2An.2n (o)		3.22	3.221	3.233	
C2An.3n (t)		3.33	3.325	3.331	Mammoth (o)
C2An.3n (o)		3.58	3.553	3.594	Gilbert (t)
C3n.1n (t)		4.18	4.033	4.199	Cochiti (t)
C3n.1n (o)		4.29	4.134	4.316	Cochiti (o)
C3n.2n (t)		4.48	4.265	4.479	Nunivak (t)
C3n.2n (o)		4.62	4.432	4.623	Nunivak (o)
C3n.3n (t)		4.80	4.611	4.781	Sidufjall (t)
C3n.3n (o)		4.89	4.694	4.878	Sidufjall (o)
C3n.4n (t)		4.98	4.812	4.977	Thvera (t)
C3n.4n (o)		5.23	5.046	5.232	Thvera (o)
C3An.1n (t)			5.705	5.882[a]	C3A.n1 (t)
C3An.1n (o)			5.946	6.108[a]	C3A.n1 (o)
C3An.2n (t)			6.078	6.278[a]	C3A.n2 (t)

[a] These values are regarded as tentative; we recommend using the figures in Table 17 until a more secure calibration is obtained for events in the late Miocene. (t) = termination; (o) = onset.

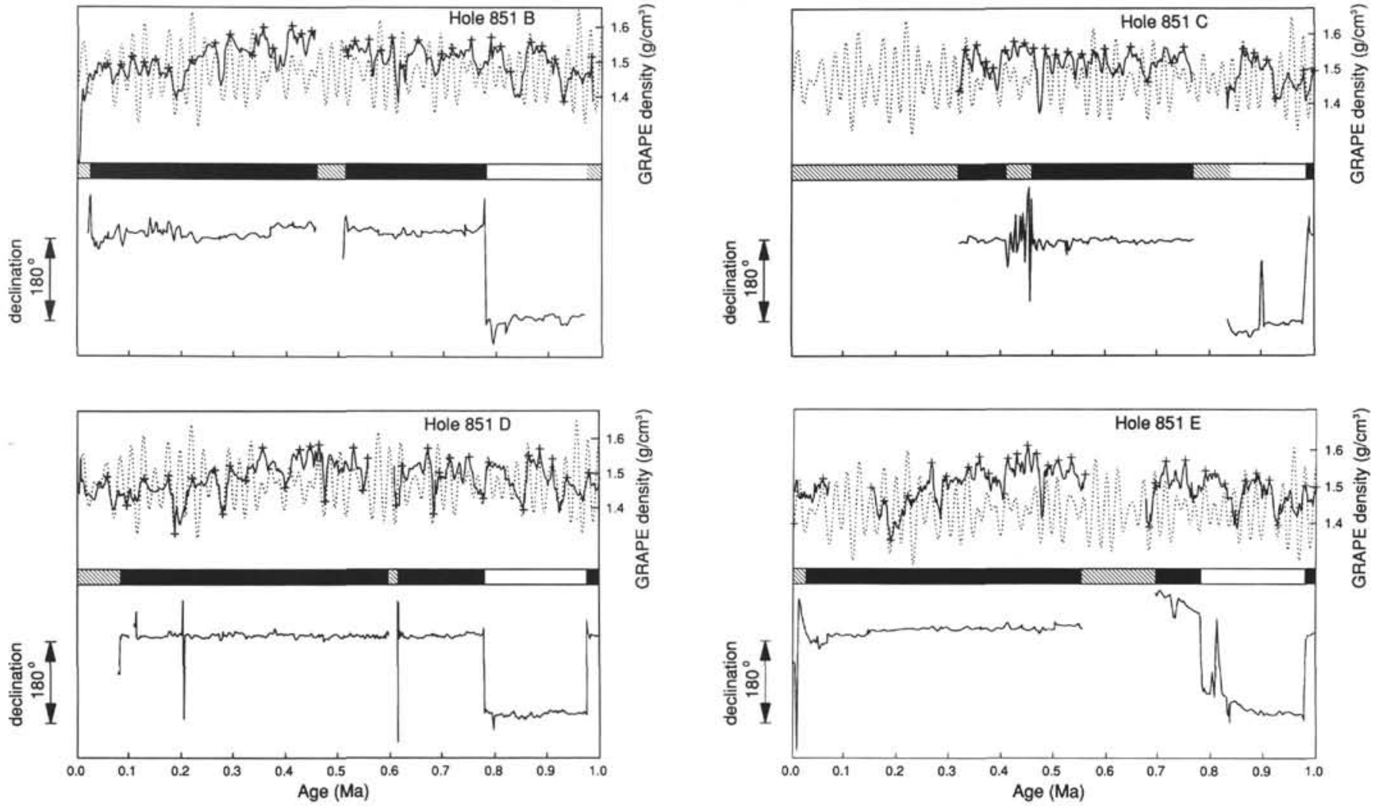

Figure 2. GRAPE density and magnetic declination for Holes 851B, 851C, 851D, and 851E for the interval 0 to 1 Ma, with orbital tuning target. Age control points are marked on the GRAPE density record. Declinations have been rotated arbitrarily for ease of comparison; the original data are shown in the site chapters in Mayer, Pisias, Janecek, et al. (1992).

continuous tuning to 10 Ma. In the meantime, we have made some preliminary correlations to the orbital record so that in correlating a particular maximum in the GRAPE density record from one site to another we use an age corresponding to an insolation maximum. It was on this basis that we adopted the value of 9.639 Ma for C5n.1n (t), which is consistent with the estimate of 9.66 ± 0.05 Ma given by Baksi (1992), while permitting the tentative tuning close to that age shown in Figure 1E.

Beyond 10 Ma, no orbital estimates were available to us, although in fact, the calculations of Berger and Loutre (1991) have been extended back in time (Berger, pers. comm., 1993). We have made some use of GRAPE density as well as biostratigraphy to correlate the other sites to Site 845, for which a good magnetostratigraphy is available to C5AB.n (t) at a recalibrated age of 13.252 Ma. Below that, we have not attempted here to improve on the shipboard age models, which were based exclusively on biostratigraphy. In Tables 1 to 11, we identify those age control points that are based on magnetostratigraphy or biostratigraphy, rather than on GRAPE density.

SEDIMENTATION RATES

The high sediment accumulation rates along the equator are the most obvious geological indication of the characteristics of the physical oceanography of the region, and scientists have long known that the paleoceanographic history could be partly sought simply by examining the history of changing sedimentation rates. The work of van Andel et al. (1975) elegantly exploited and reviewed the material that was available up to the time of DSDP Leg 17. Perhaps the most striking scientific achievement during Leg 138 was the production of the high quality biostratigraphy and magnetostratigraphy that enabled us to generate refined sedimentation rate history (Mayer, Pisias, and Shipboard Scientific Party [1992] and Shackleton and Shipboard Scientific Party [1992]). The main feature of that result was the remarkably high sedimentation rates that prevailed over an interval of about 3 m.y. in the equatorial Pacific Ocean during the early Pliocene and latest Miocene.

Figure 11 shows the sedimentation rate picture that emerges from the more refined time scales developed in this chapter. For each site, sedimentation rate has been estimated over 0.2-m.y. intervals centered at each 0.1 Ma in age (Tables 18 to 28). This presentation effectively damps out any sedimentation rate variability that may be attributed to the result of Milankovitch-scale processes. Both the onset of the interval of enhanced sedimentation rates at about 7.5 Ma and its termination at about 4.5 Ma are surprisingly rapid. We suggest (1) that it is hardly likely that such dramatic changes in the eastern Pacific Ocean could occur without repercussion in other parts of the global climate system and (2) that efforts should be made to identify related changes in other regions with a view to identifying the cause. Certainly, analogous changes have been reported in the equatorial Indian Ocean (Peterson and Backman, 1990) as well as in the western equatorial Pacific (Berger et al., 1993).

SUMMARY

A consistent set of high-resolution age models for the Leg 138 sites is presented; these were provided to the Shipboard Scientific Party for use in preparing other chapters in this volume. For the past 6 m.y., these are fully orbitally tuned, providing a secure, absolute time scale for the seafloor anomaly scale, for the oxygen isotope record, for the seismic stratigraphy of the Pacific Ocean, and, of course, for all those aspects of climatic and oceanographic variability that transfer the astronomical record of varying solar insolation into quasi-cyclic sedimentological variability. For the period prior to 6 Ma, the absolute time calibration becomes less secure, but we have

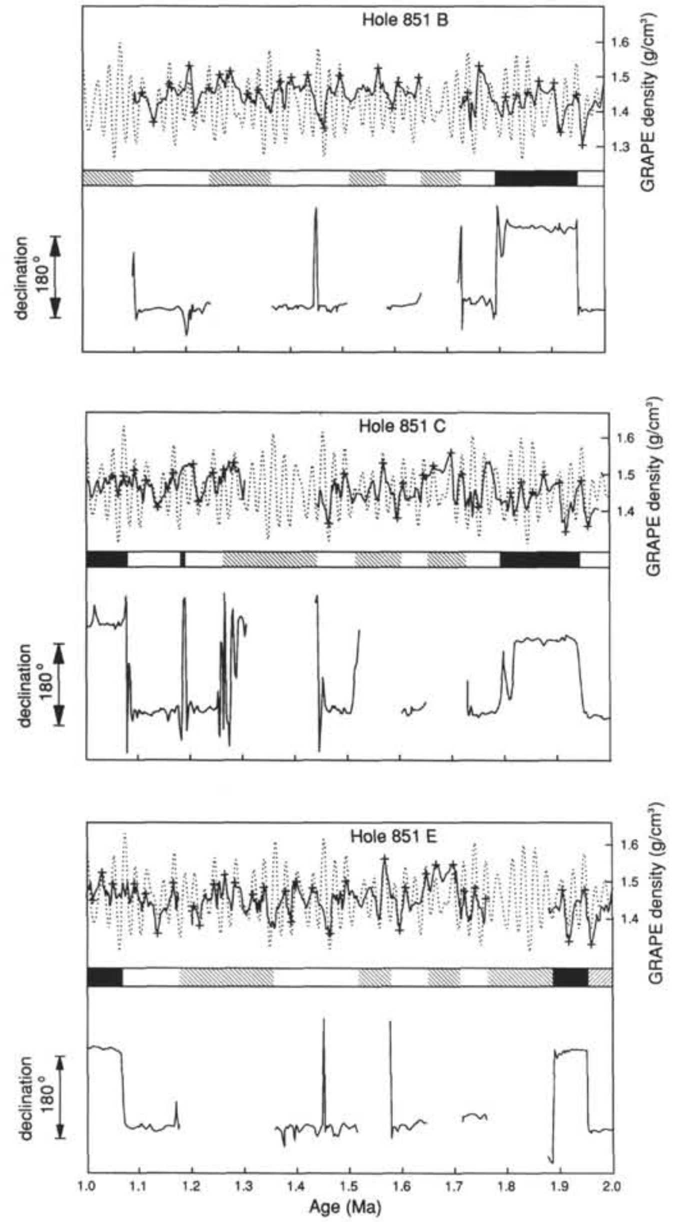

Figure 3. GRAPE density and magnetic declination for Holes 851B, 851C, and 851E for the interval from 1 to 2 Ma, with orbital tuning target. Age control points are marked on the GRAPE density record. Declinations have been rotated arbitrarily for ease of comparison; the original data are shown in the site chapters in Mayer, Pisias, Janecek, et al. (1992).

defined a new magnetic polarity time scale based on astronomical tuning to the base of the Pliocene together with the anomaly distance scale given by CK92 and a new calibration by Baksi (1992) for the young side of C5n.

ACKNOWLEDGMENTS

We thank the crew of *JOIDES Resolution* for enabling the Leg 138 Shipboard Scientific Party to return with such a magnificent legacy of material and our colleagues aboard the ship for sharing nine weeks of exciting, hard work for the benefit of a generation of Pacific-loving paleoceanographers. The labor-intensive job of tuning all the GRAPE density records would have been impossible without the support of NERC through Grant GST/02/554, and we are especially grateful for their contribution to the cost of a Sun SPARCstation as soon as the need for this became apparent. We thank Fritz Hilgen and André Berger for their helpful reviews of the submitted manuscript, and Ted Moore and Jan Backman in particular for valuable discussions at several stages in its progress.

REFERENCES*

Arrhenius, G., 1952. Sediment cores from the east Pacific. *Rep. Swed. Deep-Sea Exped. 1947–1948,* 5:6–227.

Baksi, A.K., 1992. A $^{40}Ar/^{39}Ar$ age for the termination of Chron 5: a new calibration point for the Miocene section of the GPTS. *Eos (Suppl.),* October 27, 1992, 73:630.

Baksi, A.K., and Farrar, E., 1990. Evidence for errors in the geomagnetic polar time-scale at 17–15 Ma: $^{40}Ar/^{39}Ar$ dating of basalts from the Pacific Northwest. *Geophys. Res. Lett.,* 17:1117–1120.

Baksi, A.K., Hsu, V., McWilliams, M.O., and Farrar, E., 1992. $^{40}Ar/^{39}Ar$ dating of the Brunhes-Matuyama geomagnetic field reversal. *Science,* 256:356–357.

Berger, A., 1988. Milankovitch theory and climate. *Rev. Geophys.,* 26:624–657.

Berger, A., and Loutre, M.F., 1991. Insolation values for the climate of the last 10 million years. *Quat. Sci. Rev.,* 10:297–317.

————, 1992. Astronomical solutions for paleoclimate studies over the last 3 million years. *Earth Planet. Sci. Lett.,* 111:369–382.

Berger, A., Loutre, M.F., and Laskar, J., 1992. Stability of the astronomical frequencies over the Earth's history for paleoclimate studies. *Science,* 255:560–566.

Berger, W.H., Leckie, R.M., Janecek, T.R., Stax, R., and Takayama, T., 1993. Neogene carbonate sedimentation on Ontong Java Plateau: highlights and open questions. *In* Berger, W.H., Kroenke, L.W., Mayer, L.A., et al., *Proc. ODP, Sci. Results,* 130: College Station, TX (Ocean Drilling Program), 711–744.

Berggren, W.A., Kent, D.V., and Flynn, J.J., 1985. Jurassic to Paleogene: Part 2. Paleogene geochronology and chronostratigraphy. *In* Snelling, N.J. (Ed.), *The Chronology of the Geological Record.* Geol. Soc. London Mem., 10:141–195.

Berggren, W.A., Kent, D.V., and Van Couvering, J.A., 1985. The Neogene: Part 2. Neogene geochronology and chronostratigraphy. *In* Snelling, N.J. (Ed.), *The Chronology of the Geological Record.* Geol. Soc. London Mem., 10:211–260.

Brüggemann, W., 1992. A minimal cost function method for optimizing the age-depth relation of deep-sea sediment cores. *Paleoceanography,* 7:467–487.

Cande, S.C., and Kent, D.V., 1992. A new geomagnetic polarity time scale for the Late Cretaceous and Cenozoic. *J. Geophys. Res.,* 97:13917–13951.

Farrell, J.W., and Prell, W.L., 1991. Pacific $CaCO_3$ preservation and $\delta^{18}O$ since 4 Ma: paleoceanic and paleoclimatic implications. *Paleoceanography,* 6:485–498.

Glass, B.P., Kent, D.V., Schneider, D.A., and Tauxe, L., 1991. Ivory Coast microtektite strewn field: description and relation to the Jaramillo geomagnetic event. *Earth Planet. Sci. Lett.,* 107:182–196.

Hagelberg, T., 1993. Variability of late Neogene eastern equatorial Pacific carbonate sedimentation and global ice volume on timescales from 10,000 years to 1 million years [Ph.D. thesis]. Oregon State Univ., Corvallis.

Hagelberg, T., Shackleton, N., Pisias, N., and Shipboard Scientific Party, 1992. Development of composite depth sections for Sites 844 through 854. *In* Mayer, L., Pisias, N., Janecek, T., et al., *Proc. ODP, Init. Repts.,* 138 (Pt. 1): College Station, TX (Ocean Drilling Program), 79–85.

Hall, C.M., and Farrell, J.W., 1993. Laser $^{40}Ar/^{39}Ar$ age from Ash D of ODP Site 758: dating the Brunhes-Matuyama reversal and oxygen isotope Stage 19.1. *Eos (Suppl.),* 74:110.

Harland, W.B., 1978. Geochronologic scales. *The Geologic Time Scale.* AAPG, Studies in Geology, 6:9–32.

Harland, W.B., Armstrong, R.L., Cox, A.V., Craig, L.E., Smith, A.G., and Smith, D.G., 1990. *A Geologic Time Scale 1989:* Cambridge (Cambridge Univ. Press).

Hays, J.D., Imbrie, J., and Shackleton, N.J., 1976. Variations in the earth's orbit: pacemaker of the ice ages. *Science,* 194:1121–1132.

* Abbreviations for names of organizations and publication titles in ODP reference lists follow the style given in *Chemical Abstracts Service Source Index* (published by American Chemical Society).

Hays, J.D., Saito, T., Opdyke, N.D., and Burckle, L.R., 1969. Pliocene-Pleistocene sediments of the equatorial Pacific: their paleomagnetic, biostratigraphic, and climatic record. *Geol. Soc. Am. Bull.,* 80:1481–1513.

Heirtzler, J.R., Dickson, G.O., Herron, E.M., Pitman, W.C., III, and Le Pichon, X., 1968. Marine magnetic anomalies, geomagnetic field reversals, and motions of the ocean floor and continents. *J. Geophys. Res.,* 73:2119–2136.

Herbert, T.D., Tauxe, L., and Tarduno, J.A., 1992. A global data base for orbital chronometry of the Plio-Pleistocene timescale. *Eos (Suppl.),* 73:630.

Hilgen, F.J., 1991a. Astronomical calibration of Gauss to Matuyama sapropels in the Mediterranean and implication for the Geomagnetic Polarity Time Scale. *Earth Planet. Sci. Lett.,* 104:226–244.

————, 1991b. Extension of the astronomically calibrated (polarity) time scale to the Miocene-Pliocene boundary. *Earth Planet. Sci. Lett.,* 107:349–368.

Imbrie, J., Hays, J.D., Martinson, D.G., McIntyre, A., Mix, A.C., Morley, J.J., Pisias, N.G., Prell, W.L., and Shackleton, N.J., 1984. The orbital theory of Pleistocene climate: support from a revised chronology of the marine delta $\delta^{18}O$ record. *In* Berger, A., Imbrie, J., Hays, J., Kukla, G., and Saltzman, B. (Eds.), *Milankovitch and Climate* (Pt. 1): Dordrecht (D. Reidel), 269–305.

Imbrie, J., and Imbrie, J.Z., 1980. Modeling the climatic response to orbital variations. *Science,* 207:943–953.

Izett, G.A., and Obradovich, J.D., 1991. Dating of the Matuyama-Brunhes Boundary based on ^{40}Ar-^{39}Ar ages of the Bishop Tuff and Cerro San Luis rhyolite. *Geol. Soc. Am. Abstr. Prog.,* 23:A106.

Keir, R.S., and Berger, W.H., 1985. Late Holocene carbonate dissolution in the Equatorial Pacific: reef growth or neoglaciation? *The Carbon Cycle and Atmospheric CO_2*: Natural Variations Archean to Present. Am. Geophys. Union, Geophys. Monogr., 32:208–219.

Kemp, A.E.S., and Baldauf, J.G., 1993. Vast Neogene laminated diatom mat deposits from the eastern equatorial Pacific Ocean. *Nature,* 362:141–144.

LaBrecque, J.L., Kent, D.V., and Cande, S.C., 1977. Revised magnetic polarity time scale for Late Cretaceous and Cenozoic time. *Geology,* 5:330–335.

Le, J., and Shackleton, N.J., 1992. Carbonate dissolution fluctuations in the western equatorial Pacific during the late Quaternary. *Paleoceanography,* 7:21–42.

Mayer, L.A., 1991. Extraction of high-resolution carbonate data for paleoclimatic reconstruction. *Nature,* 352:148–151.

Mayer, L., Pisias, N., Janecek, T., et al., 1992. *Proc. ODP, Init. Repts.,* 138 (Pts. 1 and 2): College Station, TX (Ocean Drilling Program).

Mayer, L.A., Pisias, N.G., and Shipboard Scientific Party, 1992. High-resolution studies of the eastern Equatorial Pacific. *Eos,* 73:257–262.

McDougall, I., Brown, F.H., Cerling, T.E., and Hillhouse, J.W., 1992. A reappraisal of the geomagnetic polarity time scale to 4 Ma using data from the Turkana Basin, East Africa. *Geophys. Res. Lett.,* 19:2349–2352.

Neeman, B.U., in press. Orbital tuning of paleoclimatic records: a reassessment. *J. Climate.*

Ninkovich, D., and Shackleton, N.J., 1975. Distribution, stratigraphic position and age of ash layer "L," in the Panama Basin region. *Earth Planet. Sci. Lett.,* 27:20–34.

Obradovich, J.D., and Izett, G.A., 1992. The geomagnetic polarity time scale (GPTS) and the astronomical time scale (ATS) now in near accord. *Eos (Suppl.),* 73:630.

Peterson, L.C., and Backman, J., 1990. Late Cenozoic carbonate accumulation and the history of the carbonate compensation depth in the western equatorial Indian Ocean. *In* Duncan, R.A., Backman, J., Peterson, L.C., et al., *Proc. ODP, Sci. Results,* 115: College Station, TX (Ocean Drilling Program), 467–507.

Pisias, N.G., 1983. Geologic time series from deep-sea sediments: time scales and distortion by bioturbation. *Mar. Geol.,* 51:99–113.

Pisias, N.G., and Moore, T.C., Jr., 1981. The evolution of Pleistocene climate: a time series approach. *Earth Planet. Sci. Lett.,* 52:450–458.

Raymo, M.E., Ruddiman, W.F., Backman, J., Clement, B.M., and Martinson, D.G., 1989. Late Pliocene variation in Northern Hemisphere ice sheets and North Atlantic deep water circulation. *Paleoceanography,* 4:413–446.

Ruddiman, W.F., Kidd, R.B., Thomas, E., et al., 1987. *Init. Repts. DSDP,* 94 (Pts. 1 and 2): Washington (U.S. Govt. Printing Office).

Ruddiman, W.F., Raymo, M.E., and McIntyre, A., 1986. Matuyama 41,000-year cycles: North Atlantic and Northern Hemisphere ice sheets. *Earth Planet. Sci. Lett.,* 80:117–129.

Shackleton, N.J., Berger, A., and Peltier, W.R., 1990. An alternative astronomical calibration of the lower Pleistocene timescale based on ODP Site 677. *Trans. R. Soc. Edinburgh, Earth Sci.,* 81:251–261.

Shackleton, N.J., Crowhurst, S., Pisias, N., Hagelberg, T., Schneider, D., Mix, A., and ODP Leg 138 Shipboard Scientific Party, 1992. An astronomically calibrated Pliocene time scale based on Leg 138 GRAPE density records. *GEOMAR Rep.,* 15:260. (Abstract)

Shackleton, N.J., and Opdyke, N.D., 1973. Oxygen isotope and paleomagnetic stratigraphy of equatorial Pacific core V28-238: oxygen isotope temperatures and ice volumes on a 10^5 year and 10^6 year scale. *Quat. Res. N.Y.,* 3:39–55.

Shackleton, N.J., and Shipboard Scientific Party, 1992. Sedimentation rates: toward a GRAPE density stratigraphy for Leg 138 carbonate sections. *In* Mayer, L., Pisias, N., Janecek, T., et al., *Proc. ODP, Init. Repts.,* 138 (Pt. 1): College Station, TX (Ocean Drilling Program), 87–91.

Shipboard Scientific Party, 1992. Explanatory notes. *In* Mayer, L., Pisias, N., Janecek, T., et al., *Proc. ODP, Init. Repts.,* 138 (Pt. 1): College Station, TX (Ocean Drilling Program), 13–42.

Spell, T.L., and McDougall, I., 1992. Revisions to the age of the Brunhes-Matuyama boundary and the Pleistocene geomagnetic timescale. *Geophys. Res. Lett.,* 19:1181–1184.

Tauxe, L., Deino, A.D., Behrensmeyer, A.K., and Potts, R., 1992. Pinning down the Brunhes/Matuyama and upper Jaramillo boundaries: a reconciliation of orbital and isotopic time scales. *Earth Planet. Sci. Lett.,* 109:561–572.

Tiedemann, R., 1992. Astronomic tuning of the high-resolution benthic records from ODP Sites 658 and 659 for the last 5 million years vs. non-linear climate dynamics. *GEOMAR Rep.,* 15:282. (Abstract)

van Andel, T.H., Heath, G.R., and Moore, T.C., Jr., 1975. Cenozoic history and paleoceanography of the central equatorial Pacific Ocean. *Mem.—Geol. Soc. Am.,* 143.

Vincent, E., 1981. Neogene carbonate stratigraphy of Hess Rise (central North Pacific) and paleoceanographic implications. *In* Thiede, J., Vallier, T.L., et al., *Init. Repts. DSDP,* 62: Washington (U.S. Govt. Printing Office), 571–606.

Walter, R.C., Deino, A., Renne, P., and Tauxe, L., 1992. Refining the Plio-Pleistocene GPTS using laser fusion $^{40}Ar/^{39}Ar$ tephrochronology: Case studies from the East African Rift. *Eos (Suppl.),* 73:629. (Abstract)

Walter, R.C., Manega, P.C., Hay, R.L., Drake, R.E., and Curtis, G.H. 1991. Laser-fusion $^{40}Ar/^{39}Ar$ dating of Bed 1, Olduvai Gorge, Tanzania. *Nature,* 354:145–149.

Wilson, D.S., 1993. Confirmation of the astronomical calibration of the magnetic polarity timescale from sea-floor spreading. *Nature,* 364:788–790.

Date of initial receipt: 5 February 1993
Date of acceptance: 27 July 1993
Ms 138SR-106

Table 17. Ages for magnetic anomalies between C3An.1n (t) and C5Bn.1n (t), derived by re-calibrating the distances in CK92 Table 2 with C3An.1n (t) at 5.875 Ma and C5n.1n (t) at 9.639MAMa Ma.

Anomaly study	Berggren et al. (1985)	CK92	This study
C3An.1n (t)	5.35	5.705	5.875
C3An.1n (o)	5.53	5.946	6.122
C3An.2n (t)	5.68	6.078	6.256
C3An.2n (o)	5.89	6.376	6.555
C3Bn (t)	6.37	6.744	6.919
C3Bn (o)	6.50	6.901	7.072
C4n.1n (t)	6.70	7.245	7.406
C4n.1n (o)	6.78	7.376	7.533
C4n.2n (t)	6.85	7.464	7.618
C4n.2n (o)	7.28	7.892	8.027
C4r.1n (t)	7.35	8.047	8.174
C4r.1n (o)	7.41	8.079	8.205
C4An (t)	7.90	8.529	8.631
C4An (o)	8.21	8.861	8.945
C4Ar.1n (t)	8.41	9.069	9.142
C4Ar.1n (o)	8.50	9.149	9.218
C4Ar.2n (t)	8.71	9.428	9.482
C4Ar.2n (o)	8.80	9.491	9.543
C5n.1n (t)	8.92	9.592	9.639
C5n.1n (o)	N.D.	9.735	9.775
C5n.2n (t)	N.D.	9.777	9.815
C5n.2n (o)	10.42	10.834	10.839
C5r.1n (t)	10.54	10.940	10.943
C5r.1n (o)	10.59	10.989	10.991
C5r.2n (t)	11.03	11.378	11.373
C5r.2n (o)	11.09	11.434	11.428
C5An.1n (t)	11.55	11.852	11.841
C5An.1n (o)	11.73	12.000	11.988
C5An.2n (t)	11.86	12.108	12.096
C5An.2n (o)	12.12	12.333	12.320
C5Ar.1n (t)	12.46	12.618	12.605
C5Ar.1n (o)	12.49	12.649	12.637
C5Ar.2n (t)	12.58	12.718	12.705
C5Ar.2n (o)	12.62	12.764	12.752
C5AAn (t)	12.83	12.941	12.929
C5AAn (o)	13.01	13.094	13.083
C5ABn (t)	13.20	12.263	13.252
C5ABn (o)	13.46	13.476	13.466
C5ACn (t)	13.69	13.674	13.666
C5ACn (o)	14.08	14.059	14.053
C5ADn (t)	14.20	14.164	14.159
C5ADn (o)	14.66	14.608	14.607
C5Bn.1n (t)	14.87	14.800	14.800

Note: N.D. = not determined.

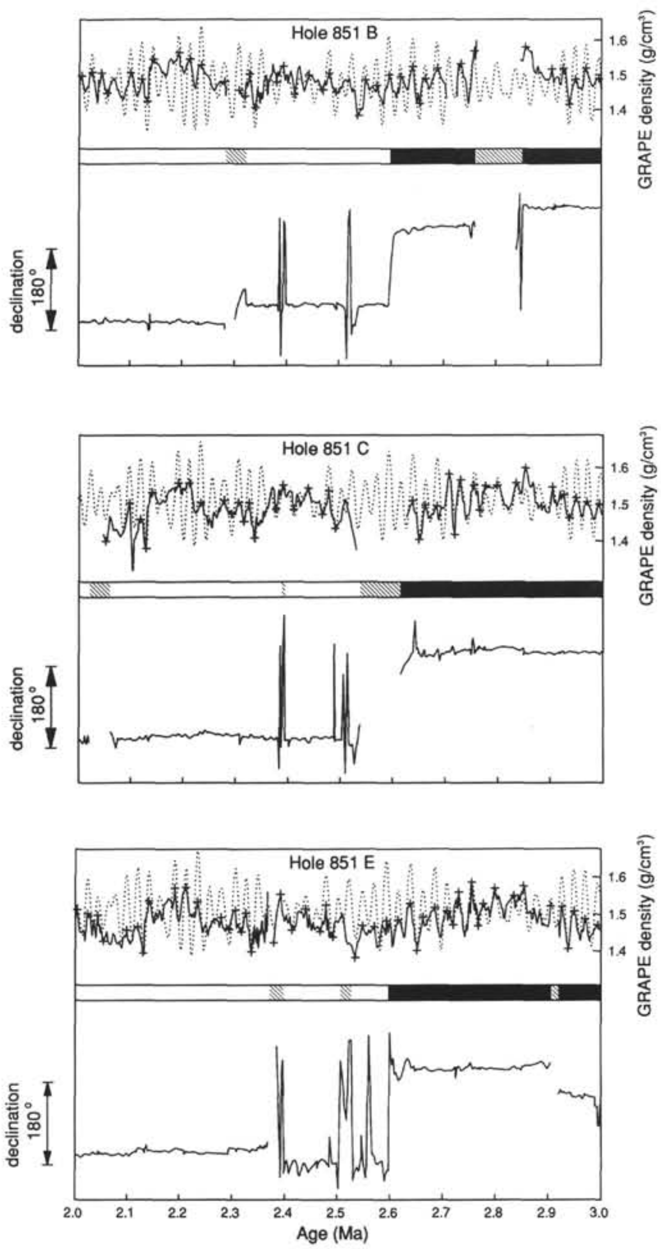

Figure 4. GRAPE density and magnetic declination for Holes 851B, 851C, and 851E for the interval from 2 to 3 Ma, with orbital tuning target. Age control points are marked on the GRAPE density record. Declinations have been rotated arbitrarily for ease of comparison; the original data are shown in the site chapters in Mayer, Pisias, Janecek, et al. (1992).

Table 18. Accumulation rates (mcd scale) estimated in overlapping 0.2 m.y. intervals for Site 844 (from Table 1).

Age (Ma)	Depth (mcd)	Rate (m/m.y.)	Age (Ma)	Depth (mcd)	Rate (m/m.y.)
0.0	0.00		8.5	52.90	6.2
0.1	1.53	12.9	8.6	53.53	7.4
0.2	2.58	11.5	8.8	55.35	9.6
0.3	3.82	12.8	8.9	56.32	8.7
0.4	5.14	14.3	9.0	57.10	7.1
0.5	6.68	15.1	9.1	57.73	7.9
0.6	8.16	12.4	9.2	58.69	8.5
0.7	9.16	10.4	9.3	59.43	6.9
0.8	10.23	9.6	9.4	60.07	7.9
0.9	11.07	8.5	9.5	61.00	10.7
1.0	11.93	9.0	9.6	62.22	10.8
1.1	12.86	8.6	9.7	63.15	10.9
1.2	13.65	7.8	9.8	64.39	12.3
1.3	14.43	7.8	9.9	65.62	12.3
1.4	15.21	7.8	10.0	66.86	11.9
1.5	15.99	7.8	10.1	68.00	11.3
1.6	16.77	7.8	10.2	69.12	11.2
1.7	17.55	7.5	10.3	70.24	11.2
1.9	18.86	5.5	10.4	71.36	11.2
2.0	19.38	5.0	10.5	72.47	12.3
2.1	19.85	4.7	10.6	73.82	14.7
2.2	20.32	4.7	10.7	75.42	18.9
2.3	20.79	4.7	10.8	77.59	21.7
2.4	21.26	4.7	10.9	79.76	22.1
2.5	21.73	4.7	11.0	82.02	26.9
2.6	22.20	4.1	11.1	85.14	31.2
2.7	22.54	3.4	11.2	88.26	31.2
2.8	22.88	3.4	11.3	91.37	32.0
2.9	23.23	3.4	11.4	94.67	35.3
3.0	23.57	3.2	11.5	98.42	37.6
3.1	23.87	3.6	11.6	102.18	37.6
3.2	24.28	3.0	11.7	105.94	37.6
3.3	24.47	2.2	11.8	109.70	37.6
3.4	24.72	3.0	11.9	113.46	37.0
3.5	25.07	3.5	12.0	117.10	32.0
3.6	25.41	3.1	12.1	119.87	27.6
3.7	25.68	2.6	12.2	122.63	27.6
3.8	25.94	2.6	12.3	125.39	27.6
3.9	26.20	2.6	12.4	128.16	27.6
4.0	26.45	2.6	12.5	130.92	27.6
4.1	26.71	2.6	12.6	133.68	33.4
4.2	26.98	3.1	12.7	137.60	42.4
4.3	27.32	3.4	12.8	142.16	45.6
4.4	27.65	3.3	12.9	146.72	43.1
4.5	27.99	3.7	13.0	150.77	39.5
4.6	28.38	3.8	13.1	154.63	38.5
4.7	28.75	3.6	13.2	158.48	37.8
4.8	29.10	3.6	13.3	162.18	36.2
4.9	29.47	4.5	13.4	165.72	35.4
5.0	30.01	5.5	13.5	169.26	35.4
5.1	30.56	5.6	13.6	172.80	35.4
5.2	31.12	5.7	13.7	176.35	35.4
5.3	31.70	5.9	13.8	179.89	35.4
5.4	32.29	5.9	13.9	183.43	35.4
5.5	32.88	5.9	14.0	186.97	35.3
5.6	33.47	5.9	14.1	190.49	34.9
5.7	34.07	5.9	14.2	193.96	34.7
5.8	34.66	6.1	14.3	197.43	34.7
5.9	35.28	6.6	14.4	200.90	14.7
6.0	35.99	7.1	14.5	204.37	34.7
6.1	36.69	7.2	14.6	207.84	34.7
6.2	37.43	6.4	14.7	211.31	34.7
6.3	37.98	4.1	14.8	214.78	34.7
6.4	38.26	2.9	14.9	218.25	36.8
6.5	38.55	3.6	15.0	222.14	41.1
6.6	38.99	5.4	15.1	226.47	43.3
6.7	39.62	6.3	15.2	230.80	43.3
6.8	40.25	6.3	15.3	235.12	43.3
6.9	40.88	5.9	15.4	239.45	43.3
7.0	41.42	5.2	15.5	243.77	43.3
7.1	41.91	4.5	15.7	252.43	43.3
7.2	42.32	4.0	15.8	256.75	42.4
7.3	42.72	4.0	15.9	260.91	41.2
7.4	43.13	6.8	16.0	265.00	40.9
7.5	44.08	8.5	16.1	269.08	40.9
7.6	44.83	9.4	16.2	273.17	40.9
7.7	45.95	11.7	16.3	277.25	40.9
7.8	47.17	12.2	16.4	281.34	40.9
7.9	48.40	12.2	16.5	285.42	40.9
8.0	49.62	10.0	16.6	289.51	40.9
8.1	50.41	7.0	16.7	293.59	40.9
8.2	51.03	6.2	16.8	297.68	40.9
8.3	51.65	6.2	16.9	301.76	40.9
8.4	52.28	6.2	17.0	305.85	

Table 19. Accumulation rates (mcd scale) estimated in overlapping 0.2 m.y. intervals for Site 845 (from Table 2).

Age Ma	Depth (mcd)	Rate m/m.y.	Age Ma	Depth (mcd)	Rate m/m.y.
0.0	0.00		0.0	0.00	
0.1	3.00	30.0	8.4	124.89	20.9
0.2	6.01	30.0	8.5	126.98	20.9
0.3	9.01	30.0	8.6	129.06	21.4
0.4	12.02	25.4	8.7	131.25	22.2
0.5	14.10	20.3	8.8	133.49	22.4
0.6	16.08	19.8	8.9	135.73	20.8
0.7	18.06	19.8	9.0	137.65	17.9
0.8	20.04	19.8	9.1	139.31	17.2
0.9	22.02	19.8	9.2	141.09	16.3
1.0	24.00	19.8	9.3	142.56	14.3
1.1	25.98	19.8	9.4	143.95	15.0
1.2	27.96	19.8	9.5	145.56	16.9
1.3	29.94	19.8	9.6	147.32	16.7
1.4	31.92	19.8	9.7	148.91	16.5
1.5	33.90	19.8	9.8	150.61	15.2
1.6	35.88	19.8	9.9	151.96	13.6
1.7	37.86	19.8	10.0	153.34	13.8
1.8	39.84	19.8	10.1	154.72	13.8
1.9	41.82	17.9	10.2	156.10	13.8
2.0	43.42	12.9	10.3	157.49	13.8
2.1	44.41	9.9	10.4	158.87	13.8
2.2	45.40	9.9	10.5	160.25	13.8
2.3	46.40	9.9	10.6	161.64	13.8
2.4	47.39	9.9	10.7	163.02	13.8
2.5	48.39	9.9	10.8	164.40	12.8
2.6	49.38	9.9	10.9	165.58	12.8
2.7	50.37	9.9	11.0	166.95	16.5
2.8	51.37	9.9	11.1	168.89	19.3
2.9	52.36	9.9	11.2	170.82	19.3
3.0	53.35	10.9	11.3	172.76	20.7
3.1	54.54	11.8	11.4	174.96	22.0
3.2	55.72	11.9	11.5	177.15	20.5
3.3	56.92	11.2	11.6	179.06	19.1
3.4	57.95	9.7	11.7	180.96	19.1
3.5	58.87	9.1	11.8	182.87	20.3
3.6	59.78	9.4	11.9	185.02	22.7
3.7	60.75	9.7	12.0	187.41	26.4
3.8	61.73	9.8	12.1	190.30	28.9
3.9	62.71	9.8	12.2	193.19	28.9
4.0	63.68	9.8	12.3	196.09	28.9
4.1	64.66	9.7	12.4	198.98	28.9
4.2	65.63	8.9	12.5	201.87	28.9
4.3	66.44	9.7	12.6	204.77	30.6
4.4	67.57	11.4	12.7	207.99	32.1
4.5	68.73	10.8	12.8	211.19	32.8
4.6	69.72	10.0	12.9	214.56	32.2
4.7	70.74	9.7	13.0	217.63	30.6
4.8	71.67	7.9	13.1	220.67	33.0
4.9	72.31	9.1	13.2	224.22	31.6
5.0	73.49	11.3	13.3	226.99	23.3
5.1	74.56	10.7	13.4	228.89	19.1
5.2	75.63	13.1	13.5	230.80	19.1
5.3	77.19	16.8	13.6	232.71	19.1
5.4	78.98	17.9	13.7	234.61	19.1
5.5	80.77	17.9	13.8	236.52	19.1
5.6	82.56	17.9	13.9	238.43	19.1
5.7	84.35	17.9	14.0	240.33	19.1
5.8	86.15	17.1	14.1	242.24	19.1
5.9	87.77	13.6	14.2	244.15	19.1
6.0	88.87	11.1	14.3	246.05	19.1
6.1	89.98	14.8	14.4	247.96	19.1
6.2	91.84	17.6	14.5	249.87	19.1
6.3	93.49	13.8	14.6	251.78	19.1
6.4	94.59	11.1	14.7	253.68	19.1
6.5	95.70	11.8	14.8	255.59	19.1
6.6	96.94	13.3	14.9	257.50	19.1
6.7	98.35	14.1	15.0	259.40	19.1
6.8	99.76	14.1	15.1	261.31	19.1
6.9	101.17	13.0	15.2	263.22	19.1
7.0	102.36	12.1	15.3	265.12	19.1
7.1	103.59	13.4	15.4	267.03	19.1
7.2	105.04	14.6	15.5	268.94	19.1
7.3	106.50	14.6	15.6	270.84	19.1
7.4	107.95	15.4	15.7	272.75	19.1
7.5	109.58	14.4	15.8	274.66	31.5
7.6	110.83	15.5	15.9	279.05	49.3
7.7	112.68	19.4	16.0	284.52	54.6
7.8	114.70	20.2	16.1	289.98	54.6
7.9	116.72	20.2	16.2	295.44	54.6
8.0	118.74	15.9	16.3	300.91	54.6
8.1	119.91	10.1	16.4	306.37	
8.2	120.77	14.5			
8.3	122.80	20.6			

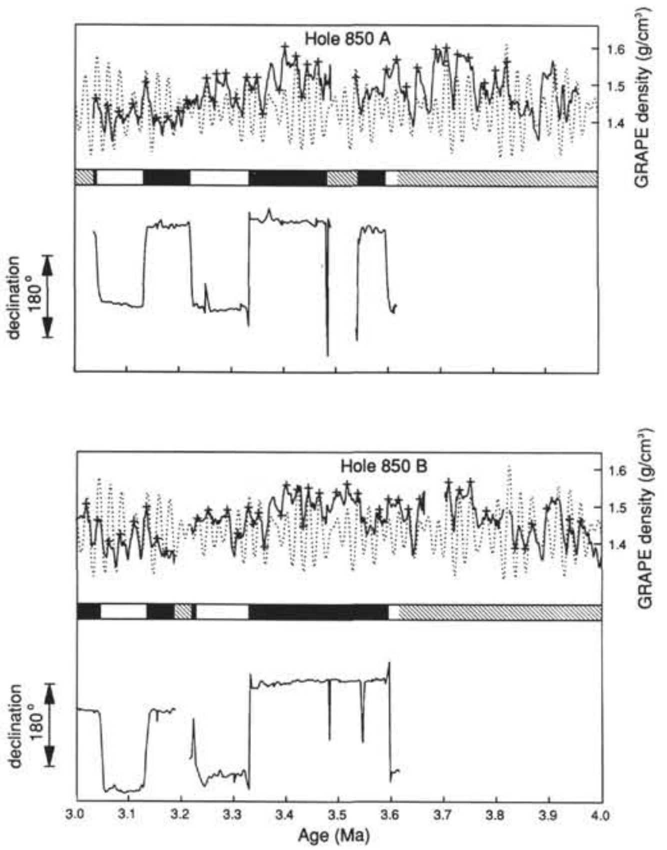

Figure 5. GRAPE density and magnetic declination for Holes 850A and 850B for the interval from 3 to 4 Ma, with orbital tuning target. Age control points are marked on the GRAPE density record. Declinations have been rotated arbitrarily for ease of comparison; the original data are shown in the site chapters in Mayer, Pisias, Janecek, et al. (1992).

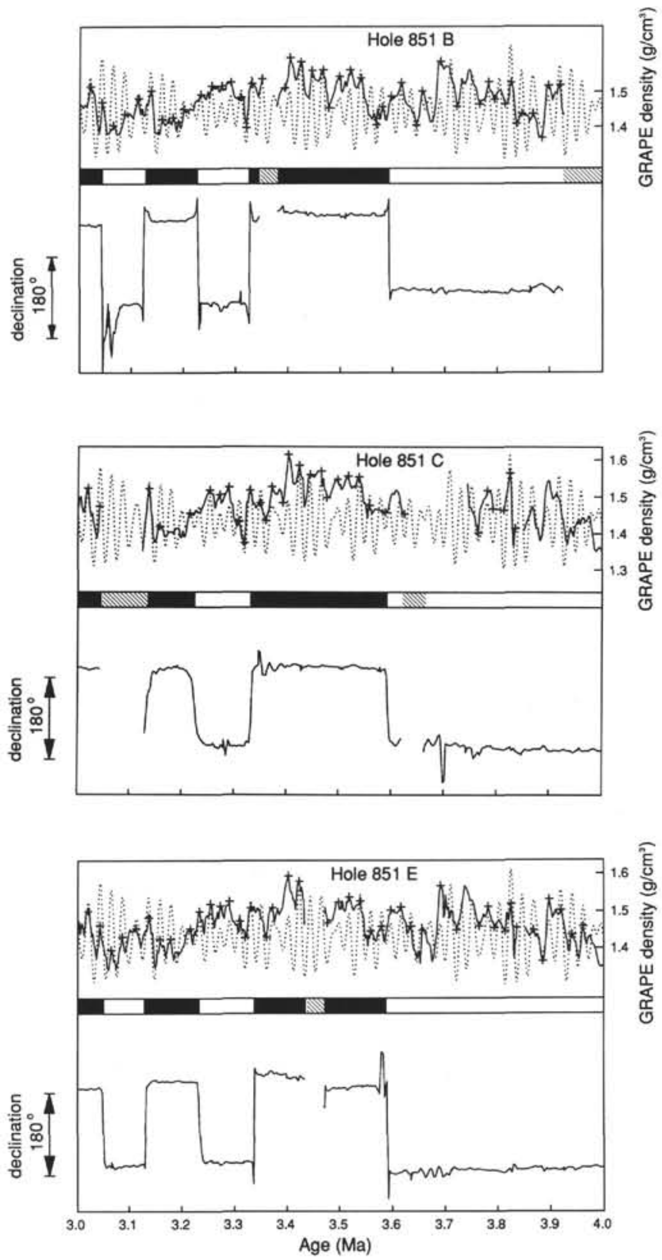

Figure 6. GRAPE density and magnetic declination for Holes 851B, 851C, and 851E for the interval from 3 to 4 Ma, with orbital tuning target. Age control points are marked on the GRAPE density record. Declinations have been rotated arbitrarily for ease of comparison; the original data are shown in the site chapters in Mayer, Pisias, Janecek, et al. (1992).

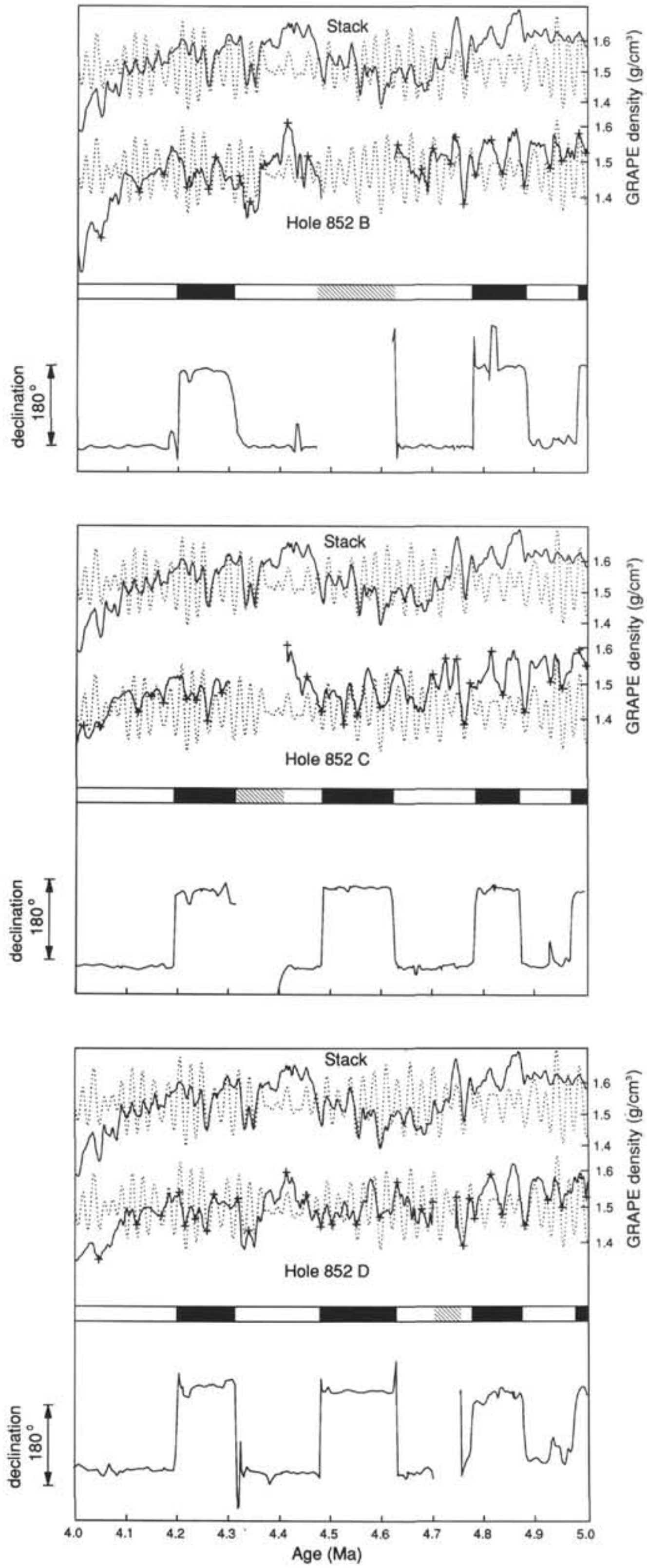

Figure 7. GRAPE density (middle) and magnetic declination (below) for Holes 852B, 852C, and 852D for the interval from 4 to 5 Ma, with orbital tuning target. Age control points are marked on the GRAPE density record. Above: stacked GRAPE density records of Sites 849, 850, and 851 for the same interval. Declinations have been rotated arbitrarily for ease of comparison; the original data are shown in the site chapters in Mayer, Pisias, Janecek, et al. (1992).

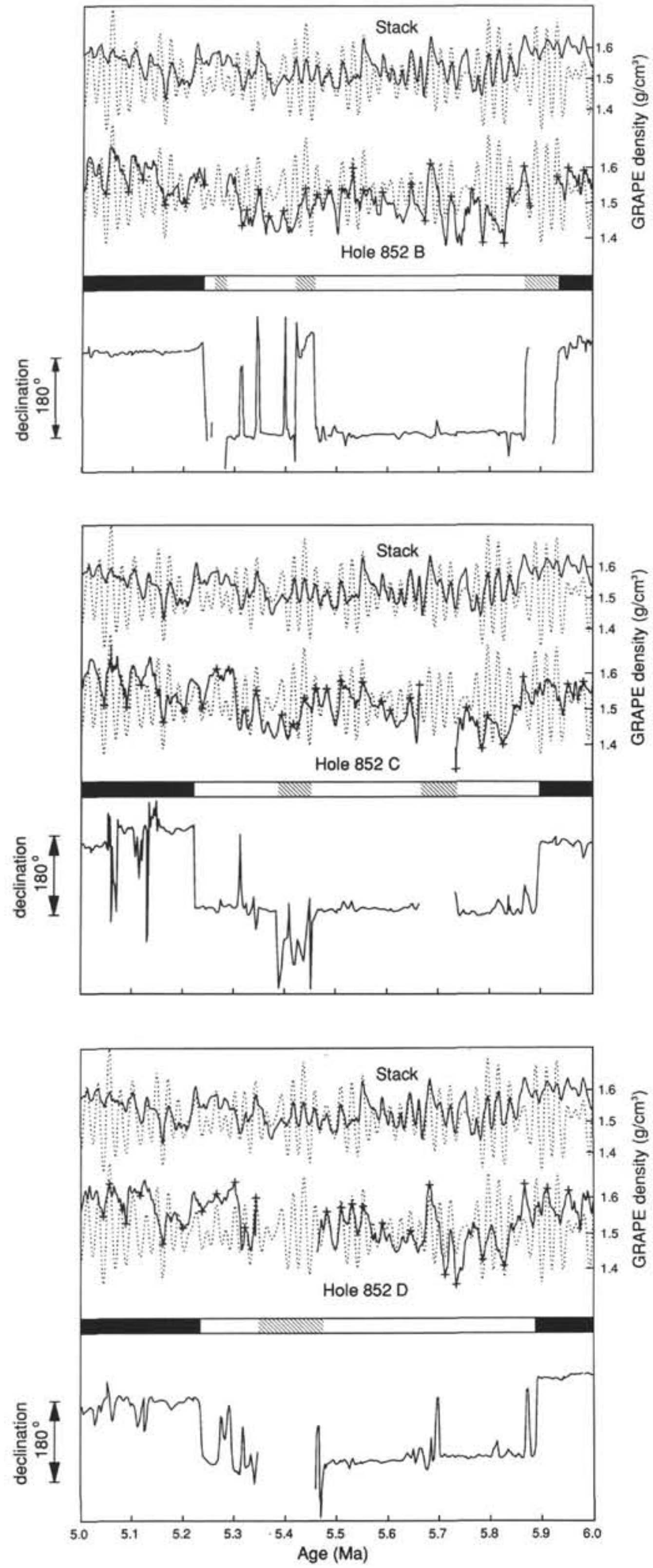

Figure 8. GRAPE density (middle) and magnetic declination (below) for Holes 852B, 852C, and 852D for the interval from 5 to 6 Ma, with orbital tuning target. Age control points are marked on the GRAPE density record. Above: stacked GRAPE density records of Sites 849, 850, and 851 for the same interval. Declinations have been rotated arbitrarily for ease of comparison; the original data are shown in the site chapters in Mayer, Pisias, Janecek, et al. (1992).

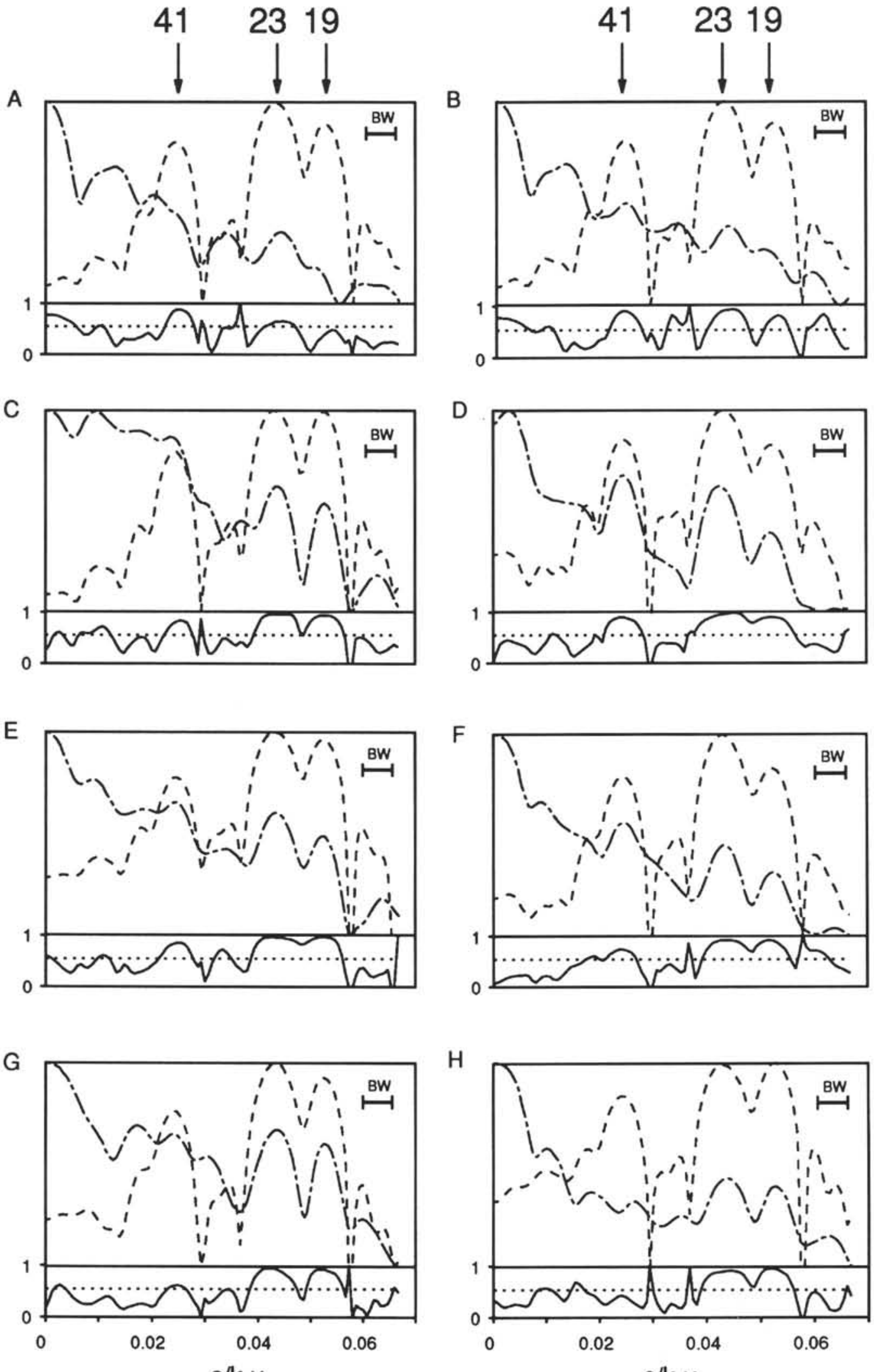

Figure 9. Cross-spectral analysis of average GRAPE density for Sites 849, 850, and 851 vs. summer insolation at 65°N. **A.** 0 to 1 Ma (from Tables 6, 7, and 8). **B.** 0 to 1 Ma (from Table 12). **C.** 1 to 2 Ma. **D.** 2 to 3 Ma. **E.** 3 to 4 Ma. **F.** 4 to 5 Ma. **G.** 5 to 6 Ma. **H.** 6 to 7 Ma. The time series were sampled at 3-k.y. intervals and cross-spectra calculated for 80 lags. Dashed line = insolation spectra; dash-dotted line = GRAPE spectra; solid line = coherency; dotted line = 80% confidence limit for coherency. Arrows at the top of the figure identify prominent peaks in insolation variance associated with obliquity (41 k.y.) and precession (23 and 19 k.y.).

Table 20. Accumulation rates (mcd scale) estimated in overlapping 0.2 m.y. intervals for Site 846 (from Table 3).

Age (Ma)	Depth (mcd)	Rate (m/m.y.)	Age (Ma)	Depth (mcd)	Rate (m/m.y.)	Age (Ma)	Depth (mcd)	Rate (m/m.y.)
0.0	0.00		6.1	249.80	49.2	12.2	374.73	18.0
0.1	4.39	41.5	6.2	253.20	29.6	12.3	376.53	18.0
0.2	8.30	35.8	6.3	255.73	47.5	12.4	378.33	18.0
0.3	11.55	36.0	6.4	262.71	48.0	12.5	380.13	18.0
0.4	15.51	40.1	6.5	265.33	27.7	12.6	381.92	18.0
0.5	19.56	35.4	6.6	268.24	27.2	12.7	383.72	18.0
0.6	22.58	31.6	6.7	270.76	25.2	12.8	385.52	18.0
0.7	25.89	34.5	6.8	273.28	25.2	12.9	387.31	18.0
0.8	29.47	40.4	6.9	275.80	25.2	13.0	389.11	18.0
0.9	33.98	35.6	7.0	278.32	29.4	13.1	390.91	18.0
1.0	36.59	30.9	7.1	281.69	42.2	13.2	392.71	18.0
1.1	40.16	38.0	7.2	286.77	39.9	13.3	394.50	23.4
1.2	44.19	32.5	7.3	289.67	37.8	13.4	397.39	28.5
1.3	46.67	32.2	7.4	294.32	38.7	13.5	400.20	19.1
1.4	50.64	36.3	7.5	297.41	24.7	13.6	401.21	10.1
1.5	53.93	31.9	7.6	299.26	18.4	13.7	402.22	10.1
1.6	57.02	36.2	7.7	301.10	19.4	13.8	403.23	10.1
1.7	61.17	38.4	7.8	303.14	21.0	13.9	404.24	10.1
1.8	64.69	38.9	7.9	305.30	20.7	14.0	405.26	10.1
1.9	68.96	47.0	8.0	307.28	18.0	14.1	406.27	10.1
2.0	74.10	53.1	8.1	308.90	12.2	14.2	407.28	10.1
2.1	79.58	45.6	8.2	309.72	8.1	14.3	408.29	10.1
2.2	83.21	38.6	8.3	310.53	14.9	14.4	409.30	10.1
2.3	87.29	39.7	8.4	312.70	17.8	14.5	410.31	10.1
2.4	91.15	42.8	8.5	314.10	12.6	14.6	411.32	10.1
2.5	95.86	47.9	8.6	315.22	13.3	14.7	412.33	10.1
2.6	100.73	46.2	8.7	316.76	16.6	14.8	413.34	10.1
2.7	105.10	47.4	8.8	318.53	17.7	14.9	414.35	10.1
2.8	110.21	49.4	8.9	320.30	21.5	15.0	415.36	10.1
2.9	114.98	48.1	9.0	322.83	21.3	15.1	416.37	10.1
3.0	119.84	46.6	9.1	324.56	19.0	15.2	417.38	10.1
3.1	124.31	39.8	9.2	326.62	18.2	15.3	418.39	10.1
3.2	127.79	30.2	9.3	328.20	16.0	15.4	419.40	10.1
3.3	130.35	33.4	9.4	329.82	15.1	15.5	420.41	10.1
3.4	134.48	44.3	9.5	331.22	14.2	15.6	421.43	10.1
3.5	139.22	45.7	9.6	332.66	12.9	15.7	422.44	10.1
3.6	143.63	35.9	9.7	333.81	13.9	15.8	423.45	12.1
3.7	146.41	29.0	9.8	335.44	15.1	15.9	424.85	15.1
3.8	149.43	29.0	9.9	336.84	15.2	16.0	426.48	16.2
3.9	152.21	33.9	10.0	338.48	14.7	16.1	428.10	16.2
4.0	156.21	35.3	10.1	339.78	12.9	16.2	429.72	16.2
4.1	159.28	30.1	10.2	341.07	12.9	16.3	431.34	16.2
4.2	162.24	31.6	10.3	342.36	12.5	16.4	432.96	16.2
4.3	165.59	34.9	10.4	343.57	11.1	16.5	434.59	16.2
4.4	169.21	34.3	10.5	344.59	10.1	16.6	436.21	16.2
4.5	172.45	41.6	10.6	345.60	10.6	16.7	437.83	16.2
4.6	177.53	52.2	10.7	346.70	17.2	16.8	439.45	16.2
4.7	182.90	50.0	10.8	349.04	23.3	16.9	441.07	16.2
4.8	187.53	43.4	10.9	351.37	22.9	17.0	442.69	16.2
4.9	191.57	37.4	11.0	353.61	19.3	17.1	444.32	16.2
5.0	195.01	29.1	11.1	355.23	16.2	17.2	445.94	16.2
5.1	197.39	33.7	11.2	356.85	16.8	17.3	447.56	16.2
5.2	201.75	47.0	11.3	358.59	17.6	17.4	449.18	16.2
5.3	206.79	44.6	11.4	360.36	17.8	17.5	450.80	16.2
5.4	210.67	43.5	11.5	362.15	18.0	17.6	452.43	16.2
5.5	215.49	53.1	11.6	363.95	18.0	17.7	454.05	16.2
5.6	221.28	57.0	11.7	365.75	18.0	17.8	455.67	16.2
5.7	226.89	58.9	11.8	367.55	18.0	17.9	457.29	16.2
5.8	233.07	59.7	11.9	369.34	18.0	18.0	458.91	
5.9	238.83	51.4	12.0	371.14	18.0			
6.0	243.36	54.9	12.1	372.94	18.0			

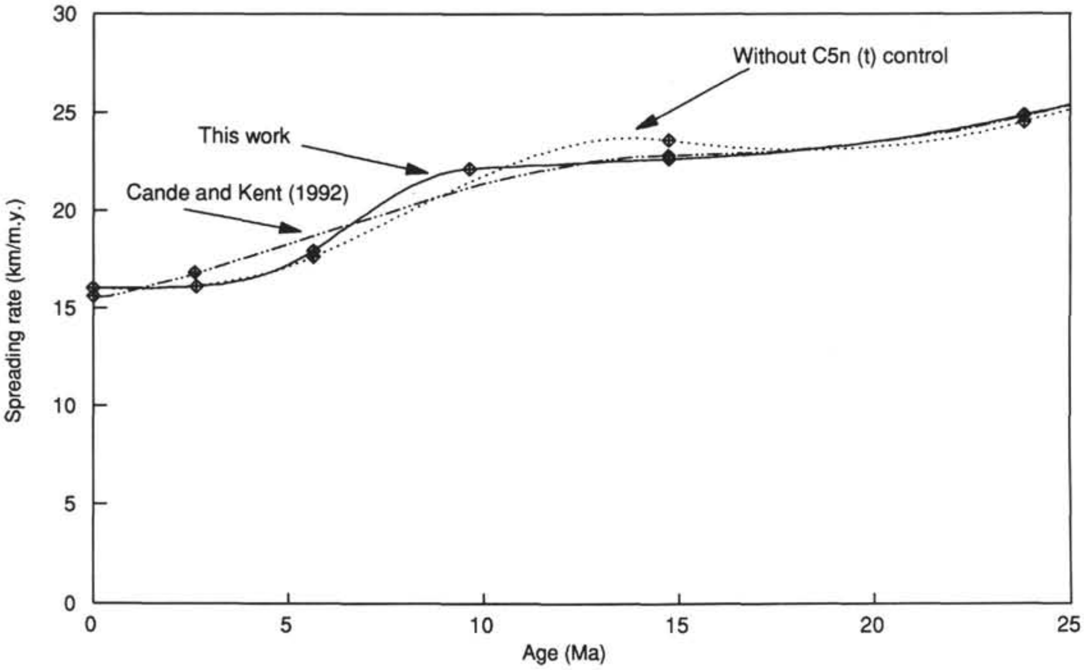

Figure 10. South Atlantic Ocean spreading rates derived by applying a cubic-spline function to the distances in CK92 (Table 2). Line A uses our calibration for C3An (t) in addition to those used in CK92; Line B, our preferred solution, includes an additional calibration at C5n.1n (t).

Table 21. Accumulation rates (mcd scale) estimated in overlapping 0.2 m.y. for Site 847 (from Table 4).

Age (Ma)	Depth (mcd)	Rate (m/m.y.)	Age (Ma)	Depth (mcd)	Rate (m/m.y.)
0.0	0.00		3.5	112.72	28.0
0.1	3.35	35.3	3.6	115.62	29.8
0.2	7.05	33.6	3.7	118.68	29.1
0.3	10.07	32.7	3.8	121.45	27.6
0.4	13.60	32.0	3.9	124.19	25.5
0.5	16.46	25.7	4.0	126.55	23.4
0.6	18.75	26.3	4.1	128.87	23.1
0.7	21.71	29.5	4.3	133.92	31.3
0.8	24.65	30.8	4.4	137.44	31.7
0.9	27.86	28.9	4.5	140.27	43.0
1.0	30.43	29.1	4.6	146.05	77.1
1.1	33.69	34.5	4.7	155.69	66.8
1.2	37.33	36.1	4.8	159.41	53.4
1.3	40.91	37.1	4.9	166.37	50.9
1.4	44.75	34.3	5.0	169.59	36.9
1.5	47.76	29.9	5.1	173.75	39.8
1.6	50.73	28.1	5.2	177.54	39.8
1.7	53.38	33.0	5.3	181.70	39.9
1.8	57.33	42.3	5.4	185.52	37.7
2.0	66.05	41.5	5.5	189.25	40.5
2.1	70.14	34.7	5.6	193.61	48.2
2.2	73.00	29.4	5.7	198.89	45.7
2.3	76.02	30.8	5.8	202.74	41.4
2.4	79.15	35.0	5.9	207.17	40.9
2.5	83.01	35.3	6.0	210.91	50.5
2.6	86.22	31.4	6.1	217.27	64.1
2.7	89.28	31.5	6.2	223.74	64.7
2.8	92.53	30.2	6.3	230.21	58.3
2.9	95.33	29.8	6.4	235.41	52.0
3.0	98.49	28.4	6.5	240.61	52.0
3.1	101.01	27.4	6.6	245.81	52.0
3.2	103.96	30.7	6.7	251.01	
3.3	107.16	30.3			
3.4	110.03	27.8			

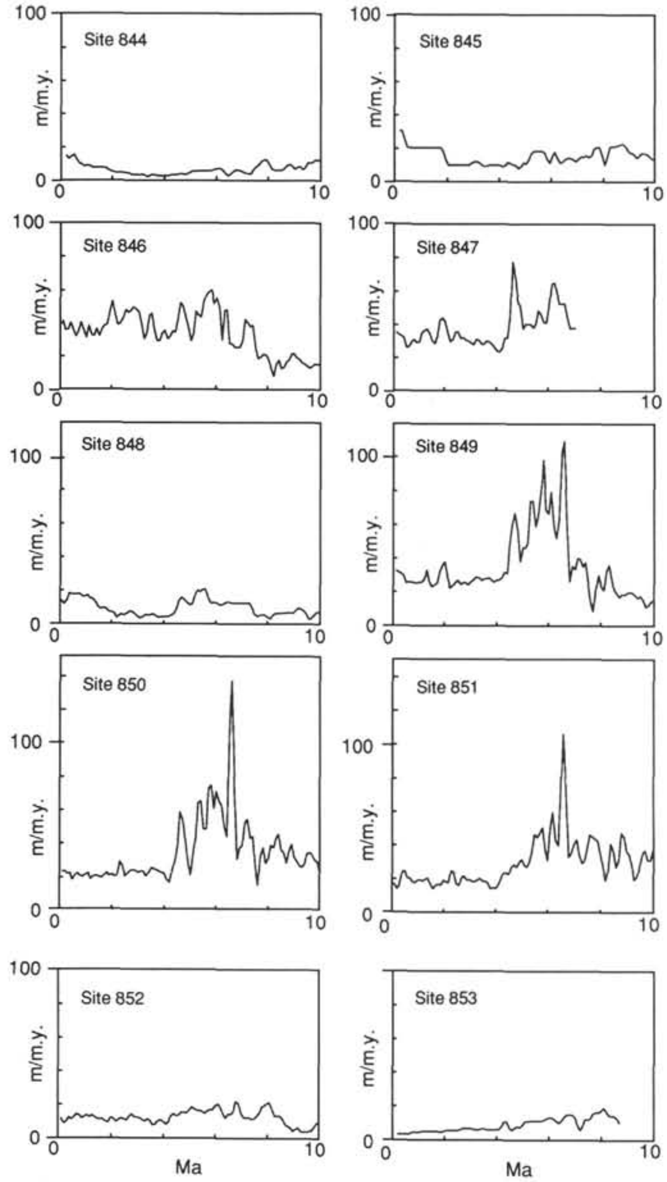

Figure 11. Sedimentation rates from Tables 18 through 28. Estimates are plotted at 0.1-m.y. intervals; each estimate plotted represents the mean for the 0.2-m.y. interval centered on that age, derived by interpolating a depth point every 0.1 Ma from the table. Note that the values given are probably greater than the true in-situ sedimentation rates by about 10%, and somewhat more in the intervals recovered by the XCB (Hagelberg et al., 1992; Fig. 3; Harris et al., this volume).

Table 22. Accumulation rates (mcd scale) estimated in overlapping 0.2 m.y. intervals for Site 848 (from Table 5).

Age Ma	Depth (mcd)	Rate m/m.y.	Age Ma	Depth (mcd)	Rate m/m.y.
0.0	0.00		0.0	0.00	
0.1	1.54	13.8	5.7	60.10	15.7
0.2	2.76	11.8	5.8	61.34	12.4
0.3	3.90	14.2	5.9	62.58	12.4
0.4	5.60	18.3	6.0	63.82	12.4
0.5	7.57	17.8	6.1	65.06	11.8
0.6	9.17	17.6	6.2	66.19	11.3
0.7	11.09	17.9	6.3	67.31	11.9
0.8	12.74	17.9	6.4	68.56	12.8
0.9	14.67	16.5	6.5	69.87	13.0
1.0	16.04	16.4	6.6	71.16	12.6
1.1	17.96	17.0	6.7	72.38	12.3
1.2	19.44	15.0	6.8	73.61	12.3
1.3	20.95	15.0	6.9	74.84	12.3
1.4	22.44	13.1	7.0	76.07	12.3
1.5	23.56	9.9	7.1	77.29	12.3
1.6	24.42	8.8	7.2	78.52	12.3
1.7	25.33	9.4	7.3	79.75	12.3
1.8	26.29	9.2	7.4	80.98	10.0
1.9	27.18	7.2	7.5	81.75	6.1
2.0	27.72	7.1	7.6	82.20	4.6
2.1	28.61	6.4	7.7	82.68	5.0
2.2	29.01	3.7	7.8	83.21	5.3
2.3	29.35	4.9	7.9	83.73	5.3
2.4	29.98	5.9	8.0	84.26	4.1
2.5	30.52	5.4	8.1	84.55	3.0
2.6	31.06	6.3	8.2	84.86	4.8
2.7	31.78	7.4	8.3	85.50	6.3
2.8	32.55	7.2	8.4	86.13	6.3
2.9	33.22	5.8	8.5	86.77	6.3
3.0	33.71	4.3	8.6	87.40	6.5
3.1	34.08	3.5	8.7	88.06	6.6
3.2	34.41	4.0	8.8	88.73	6.7
3.3	34.88	5.2	8.9	89.40	6.7
3.4	35.46	5.0	9.0	90.06	6.6
3.5	35.88	5.2	9.1	90.72	8.3
3.6	36.50	5.8	9.2	91.72	9.6
3.7	37.04	4.7	9.3	92.65	8.9
3.8	37.44	3.9	9.4	93.50	8.3
3.9	37.82	4.0	9.5	94.32	5.9
4.0	38.24	4.1	9.6	94.69	3.2
4.1	38.64	4.3	9.7	94.95	3.2
4.2	39.10	4.3	9.8	95.32	5.3
4.3	39.50	5.0	9.9	96.01	7.1
4.4	40.10	6.3	10.0	96.74	7.2
4.5	40.77	9.1	10.1	97.46	7.2
4.6	41.92	14.1	10.2	98.18	7.2
4.7	43.58	15.8	10.3	98.90	7.2
4.8	45.08	14.3	10.4	99.63	7.2
4.9	46.43	12.6	10.5	100.35	7.2
5.0	47.59	11.2	10.6	101.07	7.2
5.1	48.68	11.9	10.7	101.80	7.2
5.2	49.97	16.8	10.8	102.52	6.6
5.3	52.04	20.3	10.9	103.12	6.0
5.4	54.04	19.4	11.0	103.71	6.4
5.5	55.92	20.8	11.1	104.41	7.0
5.6	58.20	20.9	11.2	105.11	

Table 23. Accumulation rates (mcd scale) estimated in overlapping 0.2 m.y. intervals for Site 849 (from Table 6).

Age (Ma)	Depth (mcd)	Rate (m/m.y.)	Age (Ma)	Depth (mcd)	Rate (m/m.y.)
0.0	0.02		5.6	189.91	65.5
0.1	3.12	32.9	5.7	196.45	79.7
0.2	6.61	32.2	5.8	205.84	98.6
0.3	9.55	31.1	5.9	216.16	69.2
0.4	12.83	30.1	6.0	219.69	66.6
0.5	15.56	25.7	6.1	229.49	79.7
0.6	17.96	26.2	6.2	235.62	59.1
0.7	20.81	26.1	6.3	241.32	52.3
0.8	23.19	25.7	6.4	246.09	63.7
0.9	25.95	25.5	6.5	254.05	102.3
1.0	28.28	26.0	6.6	266.55	109.6
1.1	31.15	25.9	6.7	275.96	58.1
1.2	33.46	28.0	6.8	278.16	26.3
1.3	36.75	33.1	6.9	281.22	35.8
1.4	40.08	26.1	7.0	285.32	33.6
1.5	41.97	23.1	7.1	287.94	40.5
1.6	44.71	24.4	7.2	293.41	39.9
1.7	46.85	25.6	7.3	295.91	35.2
1.8	49.82	32.3	7.4	300.45	38.1
1.9	53.31	36.4	7.5	303.53	26.8
2.0	57.10	38.1	7.6	305.81	14.2
2.1	60.93	29.4	7.7	306.37	8.6
2.2	62.99	22.4	7.8	307.54	21.4
2.3	65.42	23.8	7.9	310.64	29.9
2.4	67.75	25.9	8.0	313.51	23.4
2.5	70.59	27.3	8.1	315.33	21.4
2.6	73.21	24.8	8.2	317.79	32.3
2.7	75.55	25.8	8.3	321.79	36.5
2.8	78.36	25.7	8.4	325.08	26.7
2.9	80.69	24.5	8.5	327.14	21.8
3.0	83.25	26.2	8.6	329.43	19.1
3.1	85.93	27.3	8.7	330.95	17.1
3.2	88.72	29.1	8.8	332.85	18.8
3.3	91.76	28.7	8.9	334.71	18.5
3.4	94.46	27.2	9.0	336.55	19.7
3.5	97.21	27.9	9.1	338.64	20.1
3.6	100.04	28.1	9.2	340.57	19.7
3.7	102.82	28.6	9.3	342.59	18.0
3.8	105.76	27.3	9.4	344.18	16.5
3.9	108.28	26.2	9.5	345.88	17.5
4.0	111.00	27.2	9.6	347.68	15.2
4.1	113.73	27.4	9.7	348.92	11.2
4.2	116.48	28.9	9.8	349.93	12.1
4.3	119.50	32.0	9.9	351.34	14.5
4.4	122.89	31.4	10.0	352.82	14.9
4.5	125.79	49.2	10.1	354.31	14.9
4.6	132.72	60.0	10.2	355.80	14.9
4.7	137.78	67.2	10.3	357.29	14.9
4.8	146.17	57.0	10.4	358.77	14.9
4.9	149.18	38.5	10.5	360.26	17.0
5.0	153.86	47.0	10.6	362.18	21.3
5.1	158.57	46.5	10.7	364.52	25.9
5.2	163.17	49.4	10.8	367.37	28.4
5.3	168.45	74.3	10.9	370.21	28.4
5.4	178.02	74.5	11.0	373.05	28.4
5.5	183.35	59.5	11.1	375.89	

Table 24. Accumulation rates (mcd scale) estimated in overlapping 0.2 m.y. intervals in Site 850 (from Table 7).

Age (Ma)	Depth (mcd)	Rate (m/m.y.)	Age (Ma)	Depth (mcd)	Rate (m/m.y.)
0.0	0.00		6.1	177.62	64.3
0.1	1.85	22.0	6.2	183.10	61.7
0.2	4.41	22.2	6.3	189.95	49.1
0.3	6.29	20.8	6.4	192.91	42.5
0.4	8.57	20.9	6.5	198.45	106.0
0.5	10.47	17.1	6.6	214.12	135.4
0.6	11.99	19.8	6.7	225.53	69.6
0.7	14.44	20.9	6.8	228.03	29.2
0.8	16.17	19.5	6.9	231.38	35.6
0.9	18.34	18.9	7.0	235.15	37.7
1.0	19.95	20.2	7.1	238.92	51.4
1.1	22.37	20.9	7.2	245.43	53.4
1.2	24.13	17.5	7.3	249.60	41.6
1.3	25.87	19.2	7.4	253.75	42.6
1.4	27.97	19.4	7.5	258.12	26.1
1.5	29.75	19.1	7.6	258.96	14.3
1.6	31.80	18.1	7.7	260.98	31.3
1.7	33.38	19.5	7.8	265.23	35.8
1.8	35.70	21.4	7.9	268.13	26.9
1.9	37.65	19.6	8.0	270.62	30.4
2.0	39.62	20.4	8.1	274.21	37.8
2.1	41.73	19.1	8.2	278.17	36.2
2.2	43.44	19.5	8.3	281.46	41.7
2.3	45.63	27.7	8.4	286.51	44.3
2.4	48.98	25.8	8.5	290.32	34.9
2.5	50.78	19.2	8.6	293.49	33.4
2.6	52.83	21.0	8.7	297.01	27.3
2.7	54.99	22.7	8.8	298.96	34.0
2.8	57.37	22.9	8.9	303.82	38.3
2.9	59.56	22.4	9.0	306.62	30.9
3.0	61.85	21.5	9.1	310.00	28.6
3.1	63.86	22.2	9.2	312.34	26.0
3.2	66.29	22.0	9.3	315.20	24.9
3.3	68.26	19.1	9.4	317.31	26.8
3.4	70.11	21.5	9.5	320.56	32.5
3.5	72.57	24.5	9.6	323.82	33.3
3.6	75.00	23.5	9.7	327.22	32.2
3.7	77.26	22.9	9.8	330.27	29.4
3.8	79.57	22.1	9.9	333.10	27.9
3.9	81.69	21.4	10.0	335.85	21.7
4.0	83.86	20.8	10.1	337.43	31.7
4.1	85.85	17.4	10.2	342.18	40.7
4.2	87.34	15.8	10.3	345.57	24.1
4.3	89.00	23.4	10.4	347.01	27.2
4.4	92.02	28.3	10.5	351.01	60.5
4.5	94.66	37.0	10.6	359.10	63.8
4.6	99.41	57.4	10.7	363.77	37.0
4.7	106.15	52.5	10.8	366.51	35.1
4.8	109.90	40.8	10.9	370.79	44.9
4.9	114.30	26.5	11.0	375.48	46.9
5.0	115.20	19.8	11.1	380.17	45.7
5.1	118.26	33.7	11.2	384.63	43.1
5.2	121.93	42.2	11.3	388.80	41.7
5.3	126.70	63.2	11.4	392.97	24.9
5.4	134.57	64.1	11.5	393.77	13.5
5.5	139.53	47.3	11.6	395.67	26.1
5.6	144.04	46.9	11.7	399.00	33.3
5.7	148.90	71.6	11.8	402.32	33.3
5.8	158.37	73.6	11.9	405.65	
5.9	163.63	59.4			
6.0	170.25	70.0			

Table 25. Accumulation rates (mcd scale) estimated in overlapping 0.2 m.y. intervals for Site 851 (from Table 8).

Age (Ma)	Depth (mcd)	Rate (m/m.y.)	Age (Ma)	Depth (mcd)	Rate (m/m.y.)
0.0	1.40		6.1	139.10	50.1
0.1	3.43	17.3	6.2	145.74	59.5
0.2	4.86	13.9	6.3	151.01	42.7
0.3	6.22	15.9	6.4	154.29	39.5
0.4	8.05	19.3	6.5	158.90	74.7
0.5	10.09	17.2	6.6	169.23	106.4
0.6	11.49	18.3	6.7	180.18	70.4
0.7	13.74	20.6	6.8	183.31	32.9
0.8	15.61	18.2	6.9	186.76	35.0
0.9	17.37	17.6	7.0	190.30	40.0
1.0	19.13	19.1	7.1	194.75	43.0
1.1	21.18	19.4	7.2	198.91	34.3
1.2	23.01	18.5	7.3	201.60	29.2
1.3	24.89	19.6	7.4	204.75	30.5
1.4	26.94	19.9	7.5	207.70	37.2
1.5	28.88	16.9	7.6	212.19	46.1
1.6	30.31	13.9	7.7	216.92	45.0
1.7	31.66	16.2	7.8	221.20	43.3
1.8	33.55	16.5	7.9	225.58	42.4
1.9	34.96	16.1	8.0	229.68	34.3
2.0	36.76	19.1	8.1	232.43	27.4
2.1	38.78	18.2	8.2	235.17	19.1
2.2	40.40	17.6	8.3	236.25	25.3
2.3	42.30	24.7	8.4	240.24	40.6
2.4	45.34	23.8	8.5	244.38	35.9
2.5	47.07	16.8	8.6	247.42	26.8
2.6	48.70	16.0	8.7	249.74	31.3
2.7	50.26	20.3	8.8	253.69	47.0
2.8	52.76	21.7	8.9	259.14	44.7
2.9	54.61	19.3	9.0	262.63	36.1
3.0	56.62	19.6	9.1	266.36	34.5
3.1	58.53	18.5	9.2	269.53	27.5
3.2	60.31	18.2	9.3	271.86	19.5
3.3	62.17	19.2	9.4	273.44	21.3
3.4	64.16	19.9	9.5	276.13	27.7
3.5	66.16	18.6	9.6	278.98	34.9
3.6	67.87	18.8	9.7	283.11	36.6
3.7	69.91	17.5	9.8	286.31	31.1
3.8	71.38	14.4	9.9	289.33	30.6
3.9	72.79	14.7	10.0	292.43	36.3
4.0	74.32	14.3	10.1	296.59	43.5
4.1	75.66	15.7	10.2	301.13	45.4
4.2	77.47	19.6	10.3	305.68	45.4
4.3	79.58	23.0	10.4	310.22	45.4
4.4	82.06	23.6	10.5	314.76	45.4
4.5	84.31	22.5	10.6	319.30	45.4
4.6	86.56	26.8	10.7	323.83	44.4
4.7	89.68	28.4	10.8	328.18	43.5
4.8	92.25	26.8	10.9	332.52	43.5
4.9	95.03	29.6	11.0	336.87	43.5
5.0	98.16	31.7	11.1	341.22	43.5
5.1	101.37	27.8	11.2	345.56	40.0
5.2	103.73	26.8	11.3	349.21	36.0
5.3	106.73	29.7	11.4	352.77	33.2
5.4	109.66	36.5	11.5	355.85	30.2
5.5	114.02	46.2	11.6	358.80	29.6
5.6	118.90	44.3	11.7	361.76	29.6
5.7	122.88	46.6	11.8	364.72	29.6
5.8	128.22	50.3	11.9	367.67	29.6
5.9	132.94	37.5	12.0	370.63	
6.0	135.71	30.8			

Table 26. Accumulation rates (mcd scale) estimated in overlapping 0.2 m.y. intervals for Site 852 (from Table 9).

Age (Ma)	Depth (mcd)	Rate (m/m.y.)	Age (Ma)	Depth (mcd)	Rate (m/m.y.)
0.0	0.00		5.5	66.08	15.3
0.1	1.27	11.5	5.6	67.54	14.4
0.2	2.29	8.9	5.7	68.96	15.9
0.3	3.06	9.4	5.8	70.72	16.5
0.4	4.16	12.1	5.9	72.27	16.4
0.5	5.48	11.3	6.0	74.00	18.8
0.6	6.42	11.9	6.1	76.03	19.9
0.7	7.87	14.1	6.2	77.99	17.8
0.8	9.23	13.4	6.3	79.59	14.0
0.9	10.55	11.6	6.4	80.79	11.8
1.0	11.56	12.6	6.5	81.95	13.9
1.1	13.07	13.3	6.6	83.57	14.0
1.2	14.21	12.3	6.7	84.75	15.2
1.3	15.53	13.3	6.8	86.61	21.4
1.4	16.87	12.0	6.9	89.03	20.1
1.5	17.93	11.0	7.0	90.64	14.1
1.6	19.08	11.1	7.1	91.85	12.1
1.7	20.18	10.9	7.2	93.06	12.1
1.8	21.27	9.7	7.3	94.27	12.1
1.9	22.12	9.1	7.4	95.48	10.9
2.0	23.09	11.8	7.5	96.45	11.4
2.1	24.48	11.6	7.6	97.75	12.7
2.2	25.41	9.4	7.7	98.99	14.8
2.3	26.35	10.5	7.8	100.70	18.1
2.4	27.52	11.7	7.9	102.61	19.1
2.5	28.69	11.0	8.0	104.52	20.3
2.6	29.72	10.3	8.1	106.67	20.7
2.7	30.76	12.7	8.2	108.66	16.5
2.8	32.27	14.0	8.3	109.98	13.1
2.9	33.56	12.4	8.4	111.29	13.1
3.0	34.76	12.0	8.5	112.60	13.1
3.1	35.95	11.8	8.6	113.91	11.2
3.2	37.13	10.5	8.7	114.83	8.2
3.3	38.05	9.8	8.9	116.28	6.2
3.4	39.09	10.9	9.0	116.80	4.4
3.5	40.24	10.1	9.1	117.15	5.6
3.6	41.11	7.7	9.2	117.91	6.2
3.7	41.77	8.3	9.3	118.39	4.2
3.8	42.77	10.0	9.4	118.75	3.8
3.9	43.78	10.5	9.5	119.15	4.0
4.0	44.87	9.7	9.6	119.54	4.0
4.1	45.72	8.1	9.7	119.96	4.5
4.2	46.48	9.2	9.8	120.44	6.6
4.3	47.56	12.9	9.9	121.28	8.8
4.4	49.06	14.3	10.0	122.20	9.5
4.5	50.42	13.0	10.1	123.17	9.8
4.6	51.67	13.6	10.2	124.16	9.9
4.7	53.14	15.3	10.3	125.15	9.9
4.8	54.72	15.0	10.4	126.14	9.9
4.9	56.14	14.7	10.5	127.13	8.8
5.0	57.66	16.5	10.6	127.90	4.7
5.1	59.43	18.0	10.7	128.08	1.7
5.2	61.25	17.0	10.8	128.25	
5.3	62.83	16.1			
5.4	64.48	16.2			

Table 27. Accumulation rates (mcd scale) estimated in overlapping 0.2 m.y. intervals for Site 853 (from Table 10).

Age (Ma)	Depth (mcd)	Rate (m/m.y.)	Age (Ma)	Depth (mcd)	Rate (m/m.y.)
0.0	0.22		4.4	24.57	10.7
0.1	0.55	3.3	4.5	25.48	7.0
0.2	0.88	3.3	4.6	25.98	5.9
0.3	1.20	3.3	4.7	26.66	7.1
0.4	1.53	3.3	4.8	27.40	7.9
0.5	1.86	3.3	4.9	28.25	7.7
0.6	2.20	3.5	5.0	28.93	8.7
0.7	2.56	4.2	5.1	29.99	10.7
0.8	3.04	4.5	5.2	31.07	10.9
0.9	3.46	4.3	5.3	32.17	11.1
1.0	3.89	4.4	5.4	33.28	11.1
1.1	4.34	4.8	5.5	34.39	11.1
1.2	4.86	5.2	5.6	35.51	11.1
1.3	5.38	5.2	5.7	36.62	11.1
1.4	5.89	5.2	5.8	37.73	11.4
1.5	6.41	5.2	5.9	38.90	12.3
1.6	6.92	5.2	6.0	40.20	13.1
1.7	7.44	5.0	6.1	41.51	13.1
1.8	7.93	4.6	6.2	42.82	12.4
1.9	8.36	4.6	6.3	43.99	10.8
2.0	8.85	5.2	6.4	44.99	10.0
2.1	9.40	5.6	6.5	45.98	11.1
2.2	9.96	5.6	6.6	47.20	13.5
2.3	10.51	5.6	6.7	48.67	14.7
2.4	11.07	5.6	6.8	50.15	14.7
2.5	11.62	5.6	6.9	51.62	14.7
2.6	12.18	6.1	7.0	53.10	13.5
2.7	12.85	6.7	7.1	54.32	9.0
2.8	13.52	6.7	7.2	54.89	5.7
2.9	14.20	6.7	7.3	55.46	8.2
3.0	14.87	6.8	7.4	56.52	11.9
3.1	15.55	6.7	7.5	57.85	11.8
3.2	16.20	6.0	7.6	58.88	12.5
3.3	16.76	6.0	7.7	60.36	15.4
3.4	17.39	6.6	7.8	61.96	16.0
3.5	18.07	6.7	7.9	63.56	16.0
3.6	18.74	6.4	8.0	65.17	17.2
3.7	19.35	6.1	8.1	67.00	18.7
3.8	19.96	6.0	8.2	68.91	16.7
3.9	20.56	6.0	8.3	70.34	14.2
4.0	21.16	6.0	8.4	71.75	14.1
4.1	21.77	6.2	8.5	73.16	14.1
4.2	22.41	7.9	8.6	74.57	
4.3	23.34	10.8			

Table 28. Accumulation rates (mcd scale) estimated in overlapping 0.2 m.y. intervals for Site 954 (from Table 11).

Age (Ma)	Depth (mcd)	Rate (m/m.y.)	Age (Ma)	Depth (mcd)	Rate (m/m.y.)
0.0	0.00		4.8	19.71	0.2
0.1	0.52	5.2	4.9	19.73	0.2
0.2	1.05	5.2	5.0	19.75	0.2
0.3	1.57	5.2	5.1	19.77	0.2
0.4	2.09	5.2	5.2	19.79	0.2
0.5	2.62	5.2	5.3	19.81	0.2
0.6	3.14	5.2	5.4	19.83	0.2
0.7	3.66	5.3	5.5	19.85	0.2
0.8	4.20	5.7	5.6	19.87	0.2
0.9	4.81	6.0	5.7	19.89	0.2
1.0	5.41	6.1	5.8	19.91	0.8
1.1	6.03	6.5	5.9	20.05	3.1
1.2	6.71	6.8	6.0	20.53	4.8
1.3	7.39	6.8	6.1	21.00	5.2
1.4	8.08	6.8	6.2	21.58	5.3
1.5	8.76	6.8	6.3	22.07	4.4
1.6	9.45	6.8	6.4	22.45	3.7
1.7	10.13	6.5	6.5	22.82	4.3
1.8	10.76	5.5	6.6	23.31	5.5
2.0	11.88	7.2	6.7	23.92	6.2
2.1	12.68	8.0	6.8	24.54	6.2
2.2	13.48	8.0	6.9	25.15	9.7
2.3	14.28	8.0	7.0	26.49	13.4
2.4	15.08	8.0	7.1	27.83	11.4
2.5	15.88	8.0	7.2	28.78	9.4
2.6	16.68	5.1	7.3	29.72	9.4
2.7	16.90	5.2	7.4	30.66	12.3
2.8	17.12	2.2	7.5	32.18	12.3
2.9	17.34	2.2	7.6	33.12	11.8
3.0	17.56	2.1	7.7	34.54	15.1
3.1	17.76	1.8	7.8	36.14	16.0
3.2	17.92	1.6	7.9	37.75	16.0
3.3	18.08	2.2	8.0	39.35	15.1
3.4	18.36	3.1	8.1	40.76	14.3
3.5	18.70	3.4	8.2	42.21	9.4
3.6	19.04	3.3	8.3	42.63	3.8
3.7	19.37	2.3	8.4	42.98	3.5
3.8	19.51	0.8	8.5	43.32	3.5
3.9	19.53	0.2	8.6	43.67	4.1
4.0	19.55	0.2	8.7	44.14	4.9
4.1	19.57	0.2	8.9	45.17	5.3
4.3	19.61	0.2	9.0	45.72	5.7
4.4	19.63	0.2	9.1	46.30	7.1
4.5	19.65	0.2	9.2	47.15	7.5
4.3	19.61	0.2	9.3	47.80	6.2
4.4	19.63	0.2	9.4	48.38	6.2
4.5	19.65	0.2	9.5	49.04	6.5
4.6	19.67	0.2	9.6	49.67	
4.7	19.69	0.2			